

ผลของกระบวนการขึ้นรูปและคุณสมบัติของการเผาต่อค่าสัมประสิทธิ์การขยายตัวเนื่อง
จากความร้อนของเนื้อดินเซรามิก



นายคชินท์ สายอินทวงศ์

สถาบันวิทยบริการ

จุฬาลงกรณ์มหาวิทยาลัย

วิทยานิพนธ์นี้เป็นส่วนหนึ่งของการศึกษาตามหลักสูตรปริญญาวิทยาศาสตรดุษฎีบัณฑิต

สาขาวิชาวัสดุศาสตร์ ภาควิชาวัสดุศาสตร์

คณะวิทยาศาสตร์ จุฬาลงกรณ์มหาวิทยาลัย

ปีการศึกษา 2550

ลิขสิทธิ์ของจุฬาลงกรณ์มหาวิทยาลัย

EFFECTS OF FORMING PROCESS AND FIRING TEMPERATURE ON THERMAL EXPANSION
COEFFICIENT OF CERAMIC BODIES



Mr. Kachin Saiintawong

สถาบันวิทยบริการ
จุฬาลงกรณ์มหาวิทยาลัย
A Dissertation Submitted in Partial Fulfillment of the Requirements
for the Degree of Doctor of Philosophy Program in Materials Science

Department of Materials Science

Faculty of Science

Chulalongkorn University

Academic year 2007

Copyright of Chulalongkorn University

Thesis Title EFFECTS OF FORMING PROCESS AND FIRING TEMPERATURE ON
THERMAL EXPANSION COEFFICIENT OF CERAMIC BODIES


By Mr. Kachin Saiintawong

Field of Study Materials Science


Thesis Advisor Assistant Professor Sirithan Jiemsirilers, Ph.D.

Thesis Co-advisor Associate Professor Supatra Jinawath, Ph.D.

Accepted by the Faculty of Science, Chulalongkorn University in Partial Fulfillment of the
Requirements for the Doctoral Degree

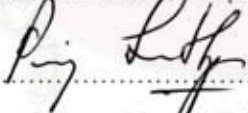
 Dean of the Faculty of Science
(Professor Supot Hannongbua, Ph.D.)


THESIS COMMITTEE

 Chairman
(Associate Professor Saowaroj Chuayjuljit)


 Thesis Advisor
(Assistant Professor Sirithan Jiemsirilers, Ph.D.)

 Thesis Co-advisor
(Associate Professor Supatra Jinawath, Ph.D.)

 External Member
(Prinya Sainamthip, Ph.D.)

 External Member
(Pitak Laoratanakul, Ph.D.)

 Member
(Associate Professor Danai Arayaphong)

 Member
(Thanakorn Wasanapiampong, Ph.D.)

กชันทน์ สายอินทวงศ์ : ผลของกระบวนการขึ้นรูปและอุณหภูมิของการเผาต่อค่าสัมประสิทธิ์การขยายตัว
 เนื่องจากความร้อนของเนื้อดินเซรามิกชนิดต่างๆ (EFFECTS OF FORMING PROCESS AND
 FIRING TEMPERATURE ON THERMAL EXPANSION COEFFICIENT OF CERAMIC
 BODIES) อ. ที่ปรึกษา ศศ.ดร.ศิริธันว์ เจียมศิริเลิศ., อ.ที่ปรึกษาร่วม : รศ.ดร.สุพัตรา จินาวัฒน์
 185 หน้า.

งานวิจัยนี้ได้ทำการศึกษาผลของกระบวนการขึ้นรูปต่างๆ ได้แก่การอัดด้วยความดัน การรีด และการหล่อแบบ ต่อค่าสัมประสิทธิ์การขยายตัวเนื่องจากความร้อนของเนื้อดินเซรามิกชนิดต่างๆ ได้แก่ เนื้อดินปอร์ซเลน เนื้อดินนิเทรียส ไชน่า เนื้อดินสโตนแวร์ เนื้อดินเออร์เทนแวร์และเนื้อดินเทอร์ราคอตตาโดยการปรับเปลี่ยค่าตัวแปรของการขึ้นรูป และทำการเผาชิ้นงานที่อุณหภูมิต่างๆกันขึ้นกับชนิดของเนื้อดินตั้งแต่ 950- 1250 องศาเซลเซียส จากนั้นทดสอบสมบัติของชิ้นงานหลังเผา ได้แก่ การหดตัวหลังเผา ความหนาแน่น การดูดซึมน้ำ ความแข็งแรงหลังเผา องค์ประกอบของเฟส โครงสร้างจุลภาค และค่าสัมประสิทธิ์การขยายตัวเนื่องจากความร้อน และเปรียบเทียบค่าที่ได้กับค่าจากการคำนวณ

การตรวจสอบและวิเคราะห์ผลพบว่า กระบวนการขึ้นรูปที่แตกต่างกันรวมทั้งตัวแปรในการขึ้นรูปที่แตกต่างกันจะส่งผลต่อสมบัติทางกายภาพทั้งการหดตัว การดูดซึมน้ำ ความหนาแน่นและความแข็งแรงหลังเผา นอกจากนี้จะทำให้โครงสร้างจุลภาคมีความแตกต่างกันรวมทั้งส่งผลต่อค่าสัมประสิทธิ์การขยายตัวเนื่องจากความร้อน ซึ่งในเนื้อดินแต่ละชนิดนั้นมีผลที่เหมือนกันคือถ้าชิ้นงานหลังเผามีค่าความหนาแน่นสูงก็จะมีค่าสัมประสิทธิ์การขยายตัวเนื่องจากความร้อนสูงตามไปด้วย ซึ่งกระบวนการขึ้นรูปที่ทำให้ชิ้นงานมีความหนาแน่นสูงที่สุดนั้นคือการอัดที่แรงดันสูงและการขึ้นรูปด้วยการรีด

ค่าความหนาแน่นของชิ้นงานหลังเผากับค่าสัมประสิทธิ์การขยายตัวเนื่องจากความร้อนสามารถนำมาหาความสัมพันธ์และสร้างเป็นสมการเพื่อใช้ค่าความหนาแน่นของชิ้นงานหลังเผามาคำนวณเพื่อประมาณค่าสัมประสิทธิ์การขยายตัวเนื่องจากความร้อน

ภาควิชา.....วัสดุศาสตร์.....
 สาขาวิชา.....วัสดุศาสตร์.....
 ปีการศึกษา.....2550.....

ลายมือชื่อนิสิต.....
 ลายมือชื่ออาจารย์ที่ปรึกษา.....
 ลายมือชื่ออาจารย์ที่ปรึกษาร่วม.....

4773802823 : MAJOR MATERIALS SCIENCE

KEY WORD: THERMAL EXPANSION COEFFICIENT/ MULLITE/ GLASSY PHASE/ FORMING PROCESS

KACHIN SAIINTAWONG: EFFECTS OF FORMING PROCESS AND FIRING TEMPERATURE ON THERMAL EXPANSION COEFFICIENT OF CERAMIC BODIES.

THESIS ADVISOR: ASST. PROF. SIRITHAN JIEMSIRILERS, Ph.D.,

THESIS COADVISOR : ASSOC. PROF. SUPATRA JINAWATH, Ph.D, 185 pp.

The objective of this research is to study the effects of forming process on the physical properties of ceramic body after firing. The body is used in this research are porcelain, vitreous china, stoneware, earthenware, and terracotta. The specimens were formed by pressing, extruding, and slip casting and fired at 950- 1250 °C depending on types of body. The following properties: firing shrinkage, bulk density, water absorption, modulus of rupture (MOR), phase composition, microstructure and thermal expansion coefficient of the fired bodies were investigated.


Based on the experimental results, it was found that the physical properties of fired specimens in each ceramic body were depended on forming process and its parameters. The crystal phases of fired specimens from different forming processes determined by XRD were the same but morphologies of crystals and pores were significantly different.

Thermal expansion coefficient can be estimated from bulk density of fired specimens. At the same firing temperature, the specimen with high bulk density has higher thermal expansion coefficient than lower bulk density specimen. Forming process has strong effect on densification of the specimen and related to the difference of thermal expansion as well. The specimens formed by extrusion obtained almost equivalent bulk density and physical properties as 150 bar pressed specimens. Empirical models were developed based on measured data which related bulk density and thermal expansion. The experimental data were compared to the predicted data of the models.

Department..... Materials Science.....

Field of study..... Materials Science.....

Academic year2007.....

Student's signature 

Advisor's signature 

Co-advisor's signature..... 

Acknowledgements

I would like to express sincere thanks to Assistance Professor Dr. Sirithan Jiemsililers for support knowledge, the way to do experiment, idea and helping to anything.

The extend many thanks to Associate Professor Dr. Supatra Jinawath for many recommendation and proof the publishing paper.

I would like to thank Siamese Merchandise Company, The Siam ceramic group Industry Company, Siam sanitary ware Industry Company, Power Insulator Company to support body for this research.

I would like to acknowledge Mr. Masaaki Tada for help and support characterization for SEM image analysis.

My thanks are also extended all teachers in materials science department for knowledge and helpful comments.

Finally, I would like to express my gratitude to my family for their loves, understanding and encouragement.



สถาบันวิทยบริการ
จุฬาลงกรณ์มหาวิทยาลัย

Content

	Page
ABSTRACT (in Thai).....	iv
ABSTRACT (in English).....	v
ACKNOWLEDGEMENTS.....	vi
CONTENTS.....	vii
LIST OF TABLES.....	xi
LIST OF FIGURES.....	xii
CHAPTER I INTRODUCTION.....	1
CHAPTER II LITERATURE REVIEW.....	3
2.1 Thermal expansion.....	3
2.2 Thermal expansion, measurement by thermal dilatometric analysis (TDA).....	13
2.3 Additional information on TDA.....	16
2.3.1 Vertical Dilatometer.....	18
2.3.2 Percent Length Change (PLC) and Coefficient of Thermal Expansion (COE).....	19
2.3.3 Temperature range.....	19
2.3.4 Thermal Cycle.....	20
2.3.5 Heat-up Rate.....	20
2.3.6 Sample Size.....	21
2.3.7 Atmospheres.....	22
2.4 Thermal expansion profile.....	22
2.5 Glaze-body interface.....	24
2.6 Glaze fit.....	26
2.7 Glaze stress.....	30
2.8 Differential thermal expansion.....	34
2.9 Glaze-body reaction (Buffer layer).....	39
2.10 crazing test.....	43

2.11 Defect of ceramic product from thermal expansion coefficient.....	45
2.12 Forming process.....	50
2.12.1 Extrusion.....	50
2.12.2 Slip casting.....	53
2.12.3 Pressing.....	56
CHAPTER III EXPERIMENTAL PROCEDURE.....	59
3.1 Raw materials and characterization.....	60
3.1.1 Raw materials.....	60
3.1.2 Raw materials characterization.....	60
3.1.3 Raw materials preparation and parameter for forming.....	61
3.2 Forming process.....	63
3.2.1 Dry pressing.....	63
3.2.2 Extruding.....	64
3.2.3 Slip casting.....	65
3.3 Drying and Firing process.....	66
3.4 Characterization of fired specimens.....	67
3.4.1 Shrinkage.....	67
3.4.2 Water absorption.....	67
3.4.3 Bulk density.....	68
3.4.4 Bending strength.....	69
3.4.5 Phase analysis.....	69
3.4.6 Microstructure examination.....	70
3.4.7 Thermal expansion coefficient.....	70
CHAPTER IV EXPERIMENTAL RESULTS AND DISCUSSION.....	73
4.1 Raw material characterization.....	73

	Page
4.1.1 Particle size determination.....	73
4.1.2 Chemical composition of starting materials analyzed by X-Ray Fluorescence.....	74
4.1.3 Calculation of thermal expansion coefficient by percentage of oxide in the body formula.....	74
4.1.4 Rheology of body slip.....	75
4.2 Characterization of fired specimens.....	76
4.2.1 Porcelain body.....	76
4.2.1.1 Shrinkage.....	76
4.2.1.2 %Water absorption.....	78
4.2.1.3 Bulk density.....	79
4.2.1.4 Bending strength.....	80
4.2.1.5 Phase analysis by X-Ray diffraction (XRD).....	81
4.2.1.6 Microstructure examination by Scanning electron microscope (SEM).....	83
4.2.1.7 Thermal expansion coefficient.....	87
4.2.2 Vitreous china body.....	90
4.2.2.1 Shrinkage.....	90
4.2.2.2 %Water absorption.....	91
4.2.2.3 Bulk density.....	92
4.2.2.4 Bending strength.....	93
4.2.2.5 Phase analysis by X-Ray diffraction (XRD).....	95
4.2.2.6 Microstructure examination by Scanning electron microscope (SEM).....	97
4.2.2.7 Thermal expansion coefficient.....	99
4.2.3 Stone ware body.....	102
4.2.3.1 Shrinkage.....	102
4.2.3.2 %Water absorption.....	103
4.2.3.3 Bulk density.....	105
4.2.3.4 Bending strength.....	106

	Page
4.2.3.5 Microstructure examination by Scanning electron microscope (SEM).....	108
4.2.3.5 Thermal expansion coefficient.....	109
4.2.4 Earthenware body.....	111
4.2.4.1 Shrinkage.....	111
4.2.4.2 %Water absorption.....	112
4.2.4.3 Bulk density.....	113
4.2.4.4 Bending strength.....	114
4.2.4.5 Microstructure examination by Scanning electron microscope (SEM).....	115
4.2.4.6 Thermal expansion coefficient.....	118
4.2.5 Terracotta body.....	121
4.2.5.1 Shrinkage.....	121
4.2.5.2 %Water absorption.....	122
4.2.5.3 Bulk density.....	123
4.2.5.4 Bending strength.....	124
4.2.5.5 Thermal expansion coefficient.....	125
4.3 The relationship between bulk density and thermal expansion coefficient of each body formula.....	128
4.3.1 Porcelain body.....	128
4.3.2 Vitreous china body.....	131
4.3.3 Stoneware body.....	133
4.3.4 Earthenware body.....	135
4.3.5 Terracotta body.....	138
CHAPTER V CONCLUSIONS.....	140
CHAPTER VI FUTURE WORK.....	142
REFERENCES.....	143
APPENDICES.....	148
VITA.....	185

LISTS OF TABLES

	Page
Table 2.1 Thermal expansions.....	5
Table 2.2 Thermal expansion versus Melting Temperature.....	10
Table 2.3 Thermal expansion of selected uniaxial crystal.....	12
Table 2.4 Practical glaze-body system.....	36
Table 2.5 Glaze-body differential expansions.....	37
Table 3.1 Type of bodies.....	60
Table 3.2 Parameter for each forming process.....	66
Table 3.3 Dimension of specimens.....	66
Table 3.4 Firing temperature for all kind of products.....	67
Table 4.1 Average particle size and standard deviation of Raw materials.....	73
Table 4.2 Oxide content of ceramic bodies analyzed by X-RAY fluorescence.....	74
Table 4.3 Thermal expansion coefficient of oxide in body.....	74
Table 4.4 The calculation value of thermal expansion Coefficient of every body formula.....	75

สถาบันวิทยบริการ
จุฬาลงกรณ์มหาวิทยาลัย

LISTS OF FIGURES

	Page
Fig2.1 Schematic drawing showing the origin of thermal expansion.....	4
Fig2.2 Interatomic distance.....	6
Fig 2.3 Thermal expansion of common structure materials.....	7
Fig 2.4 Thermal expansion coefficient of closed-packed binary compounds and glass.....	7
Fig 2.5 Schematic of different kind of thermal expansion coefficient.....	8
Fig 2.6 Thermal expansion of ZnO.....	11
Fig 2.7 show a fused silica tube and fused silica rod of dilatometer.....	14
Fig 2.8 show graph between temperature and linear expansion.....	15
Fig 2.9 show the concept of a dilatometer.....	17
Fig 2.10 show a horizontal dilatometer.....	17
Fig 2.11 shows vertical dilatometer.....	18
Fig2.12 Thermal expansion(a) normally cooled glaze bar b) rapidly cooled glaze bar	24
Fig 2.13 show cause of peeling problem.....	27
Fig 2.14 show defect of peeling on terra cotta body.....	27
Fig 2.15 show cause of crazing problem.....	29
Fig 2.16 show crazing glaze.....	30
Fig. 2.17 Thermal expansion curves repositioned to demonstrate glaze-body fit.....	37
Fig. 2.18 show pug mill for mixing clay-water.....	50
Fig. 2.19 show honey diaphragm in vacuum chamber of extruder.....	51
Fig. 2.20 show wire equipment for cutting clay from extrusion.....	52
Fig. 2.21 show the extruder with central core for produced hollow product.....	52
Fig. 2.22 working mould for sanitary ware.....	54
Fig 2.23 High pressure casting machine.....	56
Fig 2.24 Cycle of pressing process.....	57
Fig 2.25 Upper and lower punch of pressing machine for cordierite kiln furniture.....	57
Fig 2.26 Grid inside the charger for sharing powder into the cavity mould.....	58
Fig.3.1 Dry pan mill.....	62
Fig.3.2 Hydraulic pressing machine.....	64

Fig.3.3 Extrusion machine.....	65
Fig.3.4 Mould for slip casting.....	65
Fig.3.5 Dilatometer.....	70
Fig.3.6 Sample and thermal couple.....	71
Fig.3.7 Flow chart of the preparing of body in different forming process.....	72
Fig 4.1 Relationship between viscosity of body slip and %solid content in various body formula (using spindle no.4).....	75
Fig 4.2 Relationship between %shrinkage and forming process in various firing temperature of porcelain body.....	77
Fig 4.3 Relationship between %water absorption and forming process in various firing temperature of porcelain body.....	78
Fig 4.4 Relationship between Bulk density and various forming process in various firing temperature of porcelain body.....	79
Fig 4.5 Relationship between bending strength and various forming process in various firing temperature of porcelain body.....	80
Fig 4.6 XRD pattern of porcelain forming by pressing at 150 psi and firing in various temperature.....	81
Fig 4.7 XRD pattern of porcelain body firing at 1250 °C in various forming process....	82
Fig 4.8 SEM images of sintered porcelain body forming by pressing at 150 psi (Firing at 1250 °C) at 500X.....	83
Fig 4.9 SEM images of sintered porcelain body forming by casting at 40% water Content (Firing at 1250 °C) at 500X.....	83
Fig 4.10 SEM images of sintered porcelain body forming by extruding (Firing at 1250 °C) at 500X.....	83
Fig.4.11 SEM image and EDS graphs of sintered porcelain body at 1250 °C formed by different forming process at 10,000X.....	85
Fig 4.12 Relationship between thermal expansion coefficient and various forming process in various firing temperature of porcelain body (range of temperature 20-500 °C).....	87

Fig 4.13 Relationship between thermal expansion coefficient and various forming process in various firing temperature of porcelain body (range of temperature 500-600 °C).....	88
Fig 4.14 Relationship between %shrinkage and forming process in various firing temperature of vitreous china body.....	90
Fig 4.15 Relationship between %water absorption and forming process in various firing temperature of vitreous china body.....	91
Fig 4.16 Relationship between Bulk density and various forming process in various firing temperature of vitreous china body.....	92
Fig 4.17 Relationship between bending strength and forming process in various firing temperature of vitreous china body.....	93
Fig 4.18 XRD pattern of vitreous china forming by pressing at 150 psi and firing in various temperature.....	95
Fig 4.19 XRD pattern of vitreous china body firing at 1250 °C in various forming Process.....	96
Fig.4.20 SEM image and EDS graphs of sintered vitreous china body at 1250 °C formed by different forming process at 5,000X.....	97
Fig 4.21 Relationship between thermal expansion coefficient and forming process in various firing temperature of vitreous china body (range of temperature 20-500 °C)....	99
Fig 4.22 Relationship between thermal expansion coefficient and forming process in various firing temperature of vitreous china body (range of temperature 500-600 °C).....	100
Fig 4.23 Relationship between %shrinkage and forming process in various firing temperature of stoneware body.....	102
Fig 4.24 Relationship between %water absorption and forming process in various firing temperature of stoneware body.....	103
Fig 4.25 show over firing of stoneware body.....	104
Fig 4.26 Relationship between Bulk density and various forming process in various firing temperature of stoneware body.....	105
Fig 4.27 Relationship between bending strength and forming process in various firing temperature of stoneware body.....	106

Fig.4.28 SEM image and EDS graphs of sintered stoneware body at 1150 °C by various forming process at 5000X.....	107
Fig 4.29 Relationship between thermal expansion coefficient and various forming process in various firing temperature of stoneware body (range of temperature 20-500 °C).....	109
Fig 4.30 Relationship between thermal expansion coefficient and various forming process in various firing temperature of stoneware body (range of temperature 500-600 °C).....	110
Fig 4.31 Relationship between %shrinkage and forming process in various firing temperature of earthenware body.....	111
Fig 4.32 Relationship between water absorption and forming process in various firing temperature of earthenware body.....	112
Fig 4.33 Relationship between bulk density and forming process in various firing temperature of earthenware body.....	113
Fig 4.34 Relationship between bending strength and forming process in various firing temperature of earthenware body.....	114
Fig 4.35 SEM images of sintered earthen ware body forming by extruding (Firing at 1150 °C) at 500X.....	115
Fig 4.36 SEM images of sintered earthen ware body forming by pressing at 150 psi (Firing at 1150 °C) at 500X.....	115
Fig 4.37 SEM images of sintered earthen ware body forming by casting with 40%solid (Firing at 1150 °C) at 500X.....	115
Fig.4.38 SEM image and EDS graphs of sintered earthenware body at 1250 °C formed by different forming process at 2500X.....	117
Fig 4.39 Relationship between thermal expansion coefficient and forming process in various firing temperature of earthenware body (range of temperature 20-500 °C)...	118
Fig 4.40 Relationship between thermal expansion coefficient and forming process in various firing temperature of earthenware body (range of temperature 500-600 °C)..	119
Fig 4.41 Relationship between %shrinkage and forming process in various firing temperature of terracotta body.....	121

Fig 4.42 Relationship between water absorption and forming process in various firing temperature of terracotta body.....	122
Fig 4.43 Relationship between bulk density and forming process in various firing temperature of terracotta body.....	123
Fig 4.44 Relationship between bending strength and forming process in various firing temperature of terracotta body.....	124
Fig 4.45 Relationship between thermal expansion coefficient and forming process in various firing temperature of terracotta body (range of temperature 20-500 °C).....	125
Fig 4.46 Relationship between thermal expansion coefficient and forming process in various firing temperature of terracotta body (range of temperature 500-600 °C)....	126
Fig 4.47 Scatter diagram of bulk density and thermal expansion coefficient of porcelain body firing at 1250 °C.....	128
Fig 4.48 Multiple regression analysis between bulk density and thermal expansion coefficient of porcelain body firing at 1250 °C.....	128
Fig 4.49 Scatter diagram of bulk density and thermal expansion coefficient of porcelain body firing at 1200 °C.....	129
Fig 4.50 Multiple regression analysis between bulk density and thermal expansion coefficient of porcelain body firing at 1200 °C.....	129
Fig 4.51 Multiple regression analysis between bulk density and thermal expansion coefficient of porcelain body firing at 1150 °C.....	130
Fig 4.52 Scatter diagram of bulk density and thermal expansion coefficient of vitreous china body firing at 1250 °C.....	131
Fig 4.53 Multiple regression analysis between bulk density and thermal expansion coefficient of vitreous china body firing at 1250 °C.....	132
Fig 4.54 Multiple regression analysis between bulk density and thermal expansion coefficient of vitreous china body firing at 1200 °C.....	132
Fig 4.55 Multiple regression analysis between bulk density and thermal expansion coefficient of stoneware body firing at 1200 °C.....	133
Fig 4.56 Multiple regression analysis between bulk density and thermal expansion coefficient of stoneware body firing at 1150 °C.....	133

Fig 4.57 Multiple regression analysis between bulk density and thermal expansion coefficient of stoneware body firing at 1100 °C.....	134
Fig 4.58 Scatter diagram of bulk density and thermal expansion coefficient of earthenware body firing at 1150 °C.....	135
Fig 4.59 Multiple regression analysis between bulk density and thermal expansion coefficient of earthenware body firing at 1150 °C.....	135
Fig 4.60 Multiple regression analysis between bulk density and thermal expansion coefficient of earthenware body firing at 1100 °C.....	136
Fig 4.61 Multiple regression analysis between bulk density and thermal expansion coefficient of earthenware body firing at 1050 °C.....	136
Fig 4.62 Scatter diagram of bulk density and thermal expansion coefficient of terracotta body firing at 1050 °C.....	138
Fig 4.63 Multiple regression analysis between bulk density and thermal expansion coefficient of terracotta body firing at 1050 °C.....	138

CHAPTER I

INTRODUCTION

Thermal expansion is a property that important for material science. This property is evaluated by thermal expansion coefficient. Over small temperature ranges. When heat is added to most materials, the average amplitude of the atoms' vibration within the material increases (1). This is increases the separation between the atoms causing the material to expand. If the temperature change, ΔT , is such that the material does not go through a phase change, then it can be shown that the change in the object length, ΔL , is given by the equation the linear nature of thermal expansion leads to expansion relationships for length, area, and volume in terms of the linear, area or volume expansion coefficient.

Thermal expansion coefficient of materials are useful for select the material in suitable application such as we choose low thermal expansion material for kiln furniture products in order to improve thermal properties such as thermal shock resistance, creep resistance, spalling resistance. We are select clay body and glaze fit together for traditional ceramic such as ceramic tile, sanitary ware, ceramic roof tile, table ware, electrical insulator.

When thermal expansion coefficient of body and glaze will be mismatch is cause of defect on ceramic product such as peeling, crazing, delay crazing, thermal shock. Therefore ceramist must study about the factor which is effect to thermal expansion coefficient.

The objectives of this research are

1. To study the mechanism of sintering in different kinds of ceramic body and different forming processes
2. To study the effect of forming processes on thermal expansion coefficient of ceramic product
3. To study the effect of firing temperature on thermal expansion coefficient of ceramic product
4. To study the relationship between microstructure of body that various forming process and thermal expansion coefficient

Targets of this research are

1. Know why and know how in term of thermal expansion mechanism in different ceramic products
2. The relationship between firing temperature and thermal expansion coefficient
3. Know how the effect of microstructure on thermal expansion

Research approaches

- Choose a forming process to produce ceramic products in order to study the relation between process and thermal expansion behavior.
- Select body in 4 type of ceramic product in different ceramic producer in Thailand by using porcelain body from electrical insulator, vitreous china body from sanitary ware, stone ware from floor tile, earthen ware from wall tile, terracotta from flower pot to study the relation between body formula in different forming process with thermal expansion behavior
- Study the factor in various forming process to be effect with thermal expansion coefficient
- Vary firing temperature in each kind of body in order to study the relation of thermal expansion and firing temperature
- Study the microstructure of the body and thermal expansion coefficient

CHAPTER II

LITERATURE REVIEW

When any material goes through temperature changes, its internal energy also changes. This change affects to several properties of interest for material researcher and engineer. Various thermal behaviors are direct consequences of the atomic energies within a material among these are: [1] thermal expansions, [2] heat capacities, and [3] thermal conductivities (2).

The significant material properties related to thermal behaviors are including:

- (1) Thermal expansion coefficient of materials
- (2) Glaze fit, glaze stress and glaze-body interface
- (3) Craze resistance
- (4) Thermal shock resistance
- (5) Thermal stresses, with attendant spalling and relaxation of stresses
- (6) High-temperature deformation that involves anelastic behaviors, creep, and viscous flow (3).

2.1 Thermal Expansion

Thermal expansion coefficients of selected materials are given in Table 2.1. The volume changes which accompany with temperature changes can be explained by an energy with in Fig. 2.1, which indicates the basis for structural dilatation. Three conclusions may be drawn.

(1) Expansion occurs because the energy trough for interatomic spacing is asymmetrical.

(2) The thermal expansion coefficient is greater at higher temperatures.

(3) The energy trough is deeper and more symmetrical for materials which melt at high temperatures. As a result, there is a relationship between melting temperature and thermal expansion.

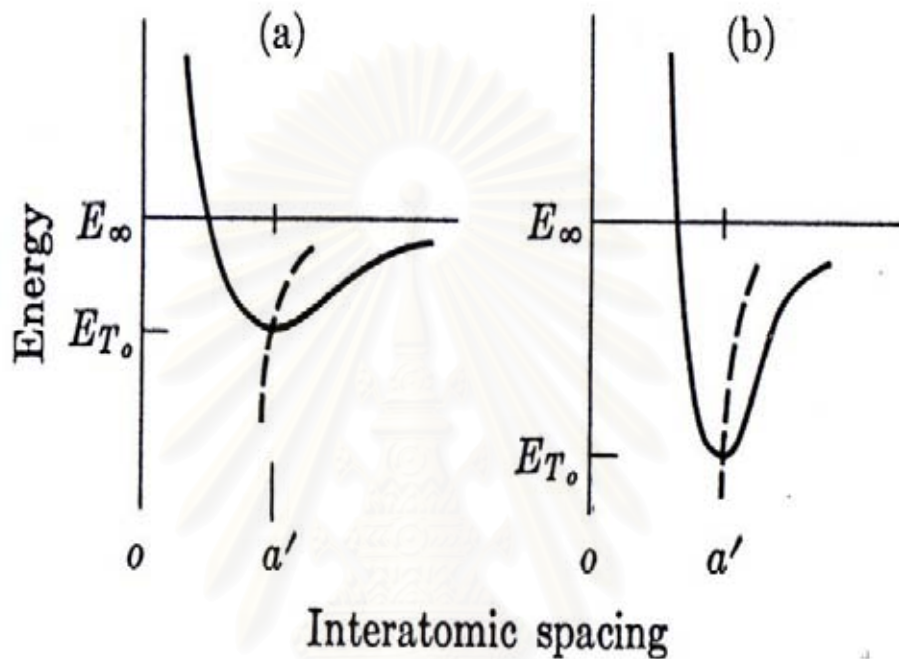


Fig2.1 Schematic drawing showing the origin of thermal expansion (a) Weakly bonded structures. (b) Strongly bonded structure (2)

There is two other concerning of thermal expansion that is not as evident from previous considerations:

(4) Densely packed phases, such as ionic crystals, have greater thermal expansion than phases with more open structures, such as glasses (2).

(5) The thermal expansion varies with the symmetry of the crystalline phase.

Table 2.1 Thermal expansion (4)

Material : polycrystals	Thermal expansion coefficient : 20 to 1000°C-mean temperature*, $\times 10^{-6}$ cm/cm/°C
Cordierite ($\text{Mg}_2\text{Al}_4\text{Si}_5\text{O}_{18}$)	2
Corundum (Al_2O_3)	9
Periclase (MgO)	14
Quartz (SiO_2)(20-400°C)	17
Spinel (MgAl_2O_4)	9
Zircon (ZrSiO_4)	4
Fused silica	0.6
Mullite	5.5
Vitreous china ware	4.0
Zircon porcelain	3.68
Stone ware	4.75
High tension porcelain	5.30
Semi-vitreous dinner ware	5.80
Steatite	6.20

* The coefficient at 20°C is somewhat less than the above figures. Linear expansion generally increases with temperature.

The asymmetry of the energy trough for interatomic spacing derives directly from the fact that the attractive and repulsive forces, expressed as functions of interatomic distance, show different variations from coulombic forces of attraction between charged atoms are classified as ionic solids which is found in many ceramic materials.

The net coulombic attraction within an ionic solid may be represented by the upper curve of Fig 2.2.

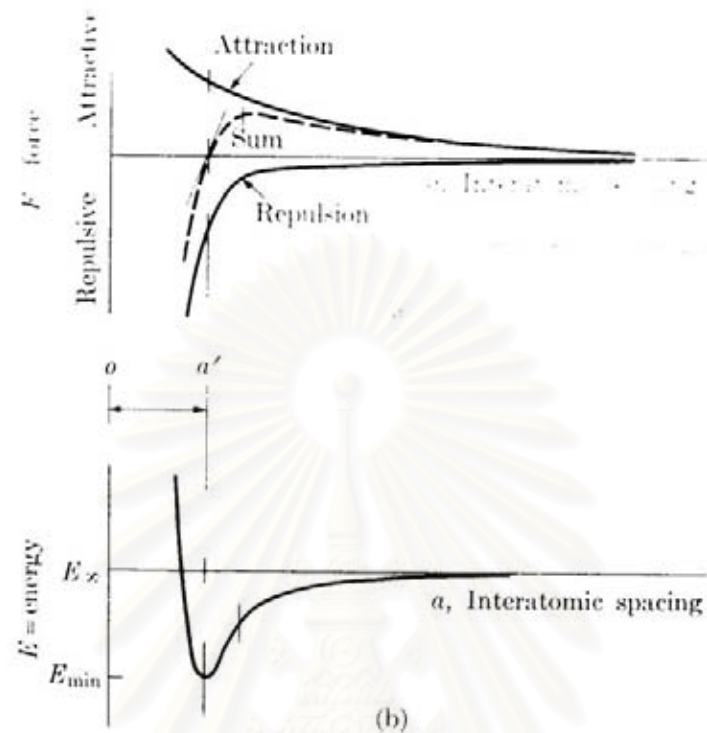


Fig2.2 Interatomic distance (a) The equilibrium spacing o-a' is the distance at which the attractive forces equal the repulsive forces. (b) The lowest potential energy occurs at distance o-a' (2)

As the positive and negative ions are brought closer together, energy is released. Not until the electron shells around the ions begin to interact are the net coulombic forces of attraction balanced by those of repulsion (lower curve of Fig 2.2a), the net coulombic attractive energy in ionic crystals increases as a function of $1/\alpha$, while the electronic repulsive energy decreases as a function of $1/\alpha^n$, where n is approximately 9. Thus the mean interatomic spacing increases with increasing thermal energy.

The linear coefficient of thermal expansion α_l may be expressed as

$$\alpha_l = (d\ell/\ell) (1/dT), \quad (2-1)$$

where $d\bar{l}/\bar{l}$ has dimensionless units such as in./in. or cm/cm. As shown in Fig. 2.1, the slope of the curve of the mean interatomic spacing changes at higher energies. Hence, the linear coefficient of thermal expansion is a function of temperature (Fig. 2.3). The relationship is can be written as shown in equation 2.2

$$\alpha_t = \alpha + bT + cT^2, \quad (2-2)$$

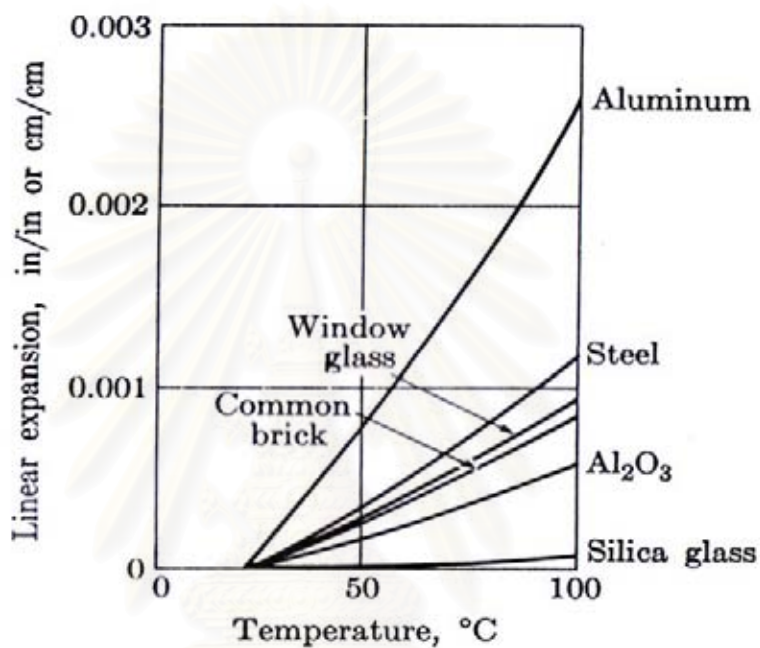


Fig 2.3 Thermal expansion of common structure materials (5)

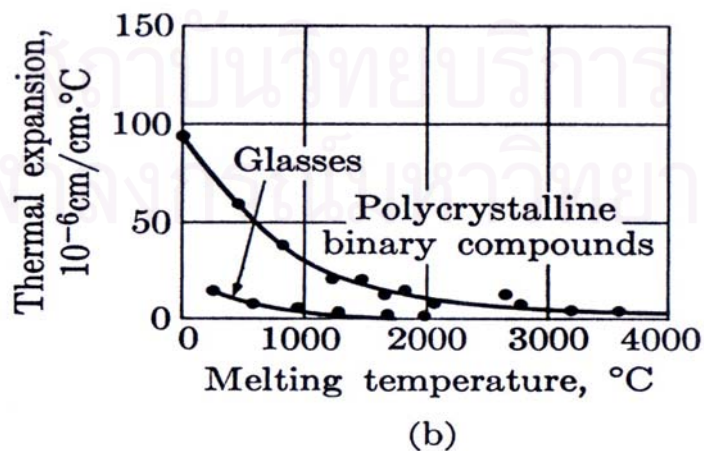


Fig 2.4 Thermal expansion coefficient of closed-packed binary compounds and glass

is generally an empirical equation of experimental data. Theoretical derivations are possible, but require numerous assumptions.

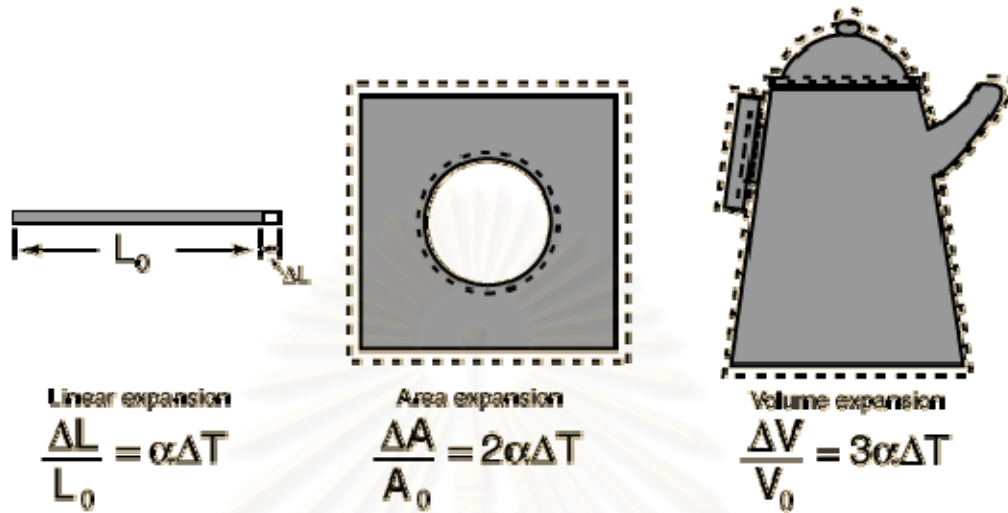


Fig 2.5 Schematic of different kind of thermal expansion coefficient

The coefficient of linear expansion, α is expressed as the fractional increase in length when the temperature of the specimen is raised by 1°C . The relationship is :

$$l_t = l_0 (1 + \alpha t) \quad (2-3)$$

where l_0 is the length at 0°C

l_t is the length at $t^\circ\text{C}$

The coefficient of cubical (volume) expansion is three times of the linear coefficient for isotropic materials. The values for the transformation temperature, T_f and the dilatometric softening point are recorded on the curve (6).

Percentage linear expansion. The percentage linear expansion between room temperature t_1 and a higher temperature t_2 is obtained from the equation :

$$\text{Percentage expansion} = \frac{(\text{Expansion at } t_2 - \text{Expansion at } t_1) \times 100}{\text{Length } l_1} \quad (2-4) (7)$$

The correlation between thermal expansion and melting temperature is indicated in Table 2.2 and Fig. 2.3. This correlation could be predicted, since materials with high melting temperatures require more thermal energy to overcome the greater attractive forces present within these materials. But the correlation in Table 2.2 is not perfect, which indicates that factors other than those just cited are also present. One such factor is the structure of the phases: If the structure has a low atomic packing factor providing internal voids interatomic expansion can occur with small overall dimensional changes. Examples are the glasses and those crystals which have low atomic coordination numbers and therefore lower thermal expansions (Table 2.2).

Anisotropic structures have an asymmetrical distribution of interatomic bonds. Therefore, phases which do not have cubic (or amorphous) structures have anisotropic thermal expansions. This is illustrated in Fig. 2.6 for zincite (ZnO). Zincite, in common with wurtzite (ZnS), has a hexagonal structure

สถาบันวิทยบริการ
จุฬาลงกรณ์มหาวิทยาลัย

Table 2.2 Thermal expansion versus melting temperature (2)

Materials	Thermal expansion, cm/cm/°C at 0°C	Melting temperature, °C
I. Polycrystalline binary compounds		
H ₂ O	90 x 10 ⁻⁶	0
CsCl	54	646
NaCl	40	800
PbS	20	1120
CaF ₂	20	1330
Fe ₂ O ₃	9	1560
SiO ₂	12	1710
Al ₂ O ₃	8	2050
ZrO ₂	10	2700
MgO	9	2800
TiC	7	3190
Graphite	5	>3500
II. Glasses and amorphous Materials		
Bismuth	11	271
Antimony	9	630
Arsenic	5	>1000
Pyrex	3	~1400
Vycor (96%SiO ₂)	0.5	~1550
Fused silica	0.3	1710

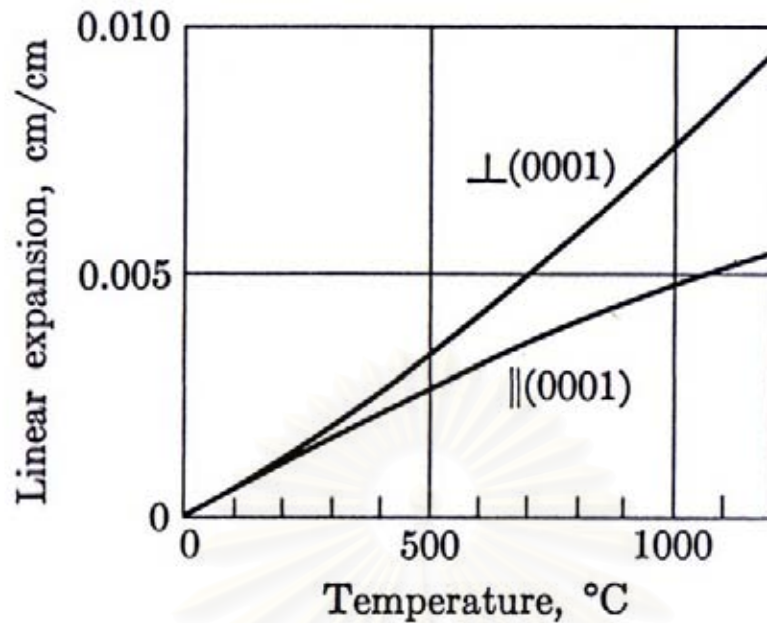


Fig 2.6 Thermal expansion of ZnO. The anisotropic expansion derives from the hexagonal structure (8).

The variation in thermal expansion of zincite derives from the fact that, as temperature increases, thermal vibrations produce greater dilatation perpendicular to the stacking planes than parallel to the planes. Also, let us not that the interatomic forces between these planes are more easily ruptured by normal and shear stresses; thus mechanical weakness can arise in these areas.

Table 2.3 shows the variation of thermal expansion for a few selected hexagonal and tetragonal crystals. The negative value for calcite (CaCO_3) is not unique among ceramic phases; however, it does require explanation. Calcite's characteristic of high thermal expansion in the direction of weaker interatomic forces produces a contraction in perpendicular directions. Thus, although there is a negative linear coefficient, it should be noted that the volume expansion α_v of Calcite, for small temperature changes, is still positive:

$$\alpha_v = (1 + \alpha_x)(1 + \alpha_y)(1 + \alpha_z) - 1, \quad (2-5a)$$

or

$$\alpha_v \approx \alpha_x + \alpha_y + \alpha_z \quad (2-5b)$$

Table 2.3 Thermal expansion of selected uniaxial crystal (8)

Phase	Thermal expansion, cm/cm/°C, at 0°C	
	(0001) or (001)	⊥ (0001) or (001)
Zincite (ZnO)	6×10^{-6}	5×10^{-6}
Quartz (SiO ₂)	14	9
Calcite (CaCO ₃)	-6	25
Zircon (ZrSiO ₄)	4	6
Rutile (TiO ₂)	7	8

There are rare cases where the volume thermal expansion can be negative. But in each case, these apparent anomalies result from a change in atomic coordination from open to close packing. The change of ferrite (body-centered-cubic iron) to austenite (face-centered-cubic iron) (9) at 910°C (1670°F) is such a case: Here, the change in coordination number from 8 to 12 actually produces a phase change. Another example, in which the changes in internal structure are more subtle than those in iron, is the contraction of water between 0°C and 4°C.

The densification of molecular packing that occurs when ice changes to water is continued to give this small contraction. Other examples with small negative expansions are some of the lithium aluminosilicates that are used for electrical insulating purposes (10). Here experiment has not yet defined the structural changes responsible, but it is known that these changes are related to atomic packing.

Cycling of temperature produces thermal growth (or thermal ratcheting) in materials with anisotropic expansions if the differential changes in dimensions introduce cracking or permanent deformation. The microcracks thus formed produce a slight porosity which is not removable on the return cycle. Because of a gradual increase in bulk volume, succeeding cycles aggravate the situation.

2.2 Thermal Expansion, Measurement by Thermal Dilatometric Analysis (TDA)

Of the common methods of measuring coefficients of thermal expansion the dilatometric technique is the one chosen by most industrial glaze users. Commercially available dilatometers operating automatically measure a complete expansion curve over the whole temperature range from room temperature to softening point. Not only coefficient of Thermal Expansion (COE) and softening point dilatometric measurement are indicated glass transition temperature, Curie point, crystalline transformation, phase transition, shrinkage, warping, bloating, sintering rate, isothermal creep, and stress relaxation. The test results are a graph of the TDA signal (converted to percent length change) on the Y-axis plotted versus the sample temperature in °C on the X-axis. The most popular apparatus available was originally devised by the British Ceramic Research Association (11). Although at first it was manually operated, the apparatus can be fully automated. The specimen both of body and glaze is heated at a controlled rate of 5-10 °C min⁻¹ in a fused silica tube furnace. A fused silica window acts as a stop such that the specimen lies centrally in the heating zone.



Fig 2.7 show a fused silica tube and fused silica rod of dilatometer

The glaze test pieces are prepared by pouring the glaze suspension into a refractory mould lined with bat wash or by pressing a rod from the dry glaze powder. Optimum dimensions for the bar are 15 mm x 15 mm x 75 mm. The unfired specimen is melted on the same time-temperature schedule for which the glaze has been designed, followed by an annealing cycle. After firing, the specimen is freed from the bat wash and ground, with coplanar ends, to size. Its length should be measured to ± 0.1 mm.

The body test pieces are prepared by forming in different process such as pressing, casting, and extruding and firing at production temperature. Cutting to the bar same dimension as glaze test pieces.

With the specimen in position, the silica push rod is moved up to it, the gauge set firmly against this and the dial zeroed. Each test is done at room temperature and in the manually-operated apparatus the expansion recorded at intervals of 30°C until the transformation temperature is reached. From T_f onwards the expansion is recorded every 5°C until the dial gauge registers its first reverse reading as the glaze reaches its softening point M_f . To these readings is added the quartz correction for that length of sample, giving the corrected expansion. In the automatic instrument the recorder can be

adjusted to give a print-out of a silica corrected percentage thermal expansion curve (11).

The expansion at any temperature t recorded on the gauge is the increase in length of the specimen, plus the expansion of the silica push rod in the furnace minus the expansion of the outer silica sheath. The expansion of the specimen is the reading on the dial plus the expansion of an equivalent length of fused silica rod. This correction is small and is obtained following dilatometric measurements on a material of known expansion (the calibration standard is usually an alumina bar).

Results can be recorded either as a graph, as a percentage expansion up to a fixed temperature or a coefficient of linear expansion.

1. A typical curve taken from a recorder on an automatic instrument is shown in Fig. 2.8.

2. From the gradient of the straight section can be calculated the coefficient of thermal expansion.

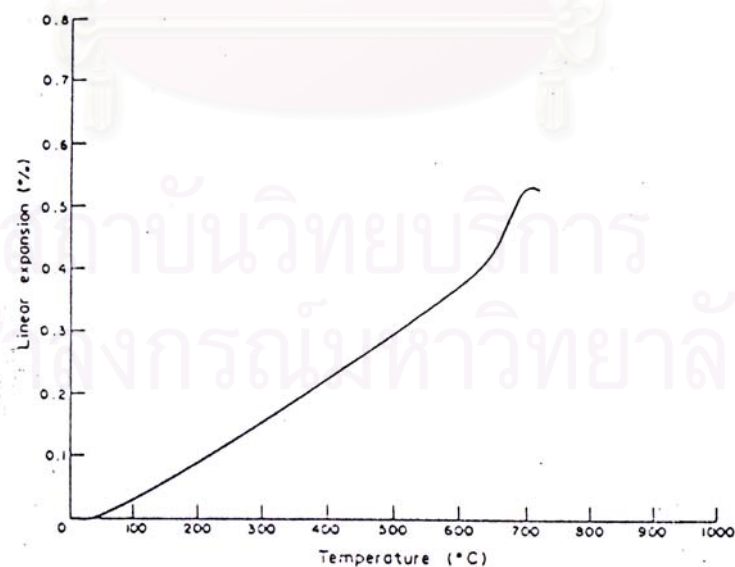


Fig 2.8 show graph between temperature and linear expansion

By custom in the U.K. ceramics industry the percentage linear expansion is calculated between room temperature t_1 at 20°C and the higher temperature t_2 at 500°C . As a mean of routine control, when the expansion of a batch is being compared with that of the standard, comparison of the percentage, linear expansion from $20 - 500^\circ\text{C}$ is usually adequate (12). However, as will be explained shortly, the use of such expansion figures can lead to problems in assessing glaze fit between body and glaze.

2.3 Additional Information on TDA

All materials expand and contract as a function of temperature. For two materials to adhere to each other, such as glass to metal seals, metalizations to substrates, and glazes to bodies, their respective thermal expansion characteristics must be known, matched, and controlled. Thermal Dilatometric Analysis (TDA), often called Dilatometry, measures the amount of dimensional change of a material (ceramics, glasses, metals, composites, carbon/graphite, minerals, plastics, and others) during a controlled thermal cycle. Dilatometry measures the normal expansion and contraction of a material, including its reversible phase changes. This procedure also measures the irreversible changes in length that are the result of decompositions, phase transformations, and other chemical reactions, and helps to identify the temperature ranges of those events and reactions. Such testing is helpful when trying to control the thermal expansion characteristics of various lots of materials, and in determining drying and firing schedules (13).

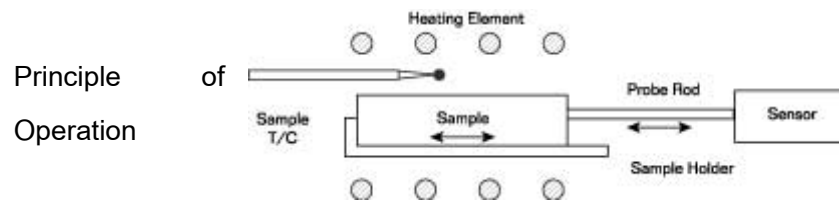


Fig 2.9 show the concept of a dilatometer (14)

Fig 2.9 shows the concepts of a dilatometer. A sample specimen is placed between the end of the sample holder and the end of the movable probe rod, and the furnace is heated according to a pre-programmed thermal cycle. As the sample temperature changes (as recorded by the sample thermocouple), the sample expands (pushing against the probe rod) or shrinks (pulling away from the probe rod). The probe rod transmits the amount of sample movement to an electronic displacement sensor located outside of the heated chamber. The displacement sensor generates an electronic signal corresponding to the positive or negative change in sample length and continuously sends the signal to the computer. The computer converts the signal to the percent of length change (%DL) and saves it along with the elapsed time and the sample temperature. The basic TDA curve is generated by plotting the percent of length change (%DL) on the Y-axis against the sample temperature (15).

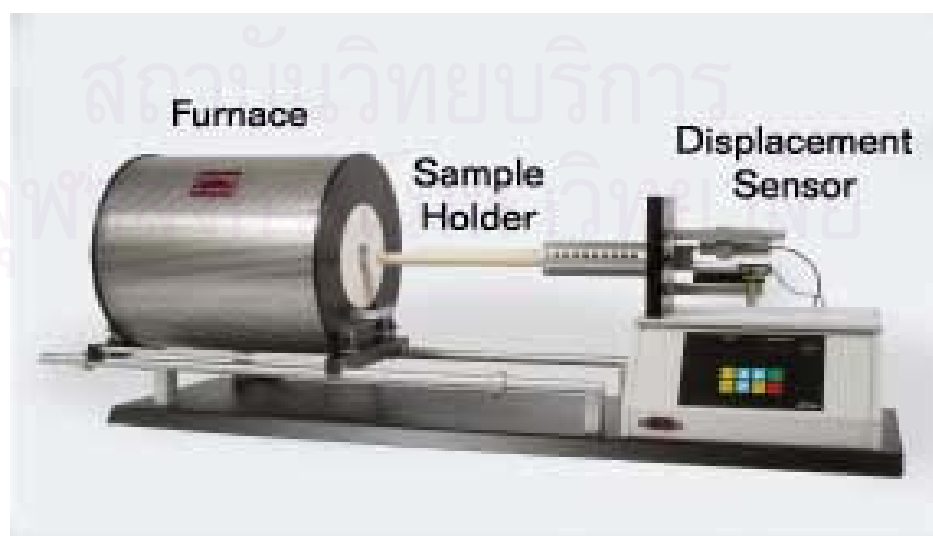


Fig 2.10 show a horizontal dilatometer

Fig 2.10 shows a horizontal dilatometer with the furnace moved away to expose the sample holder, and a close-up view of the sample holder. Fig 2.7 shows how the sample is positioned between the end of the sample holder and the probe rod. After positioning the sample in the sample holder, the furnace is moved horizontally to surround the sample and sample holder. The probe rod extends from the end of the sample, through the sample holder tube, and connects to the displacement sensor assembly outside the furnace. The probe rod is spring loaded outside the furnace to keep it in constant contact with the sample, even when shrinking. The main advantage of the horizontal system is the uniform temperature zone for the sample. Most dilatometer tests are performed with a horizontal unit (16).

2.3.1 Vertical Dilatometer

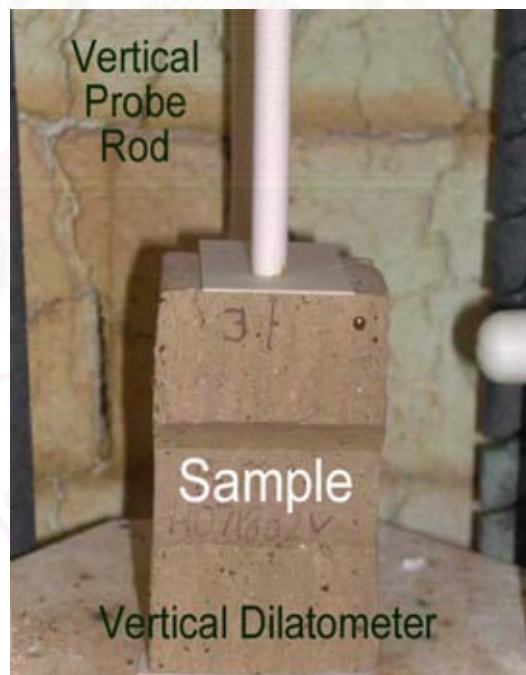


Fig 2.11 shows vertical dilatometer (17)

For larger samples, such as structural clay bodies, a vertical dilatometer is used. The sample is placed into the furnace and the vertical probe rod is lowered to contact the sample (as shown in Fig 2.11). The furnace is heated according to the pre-programmed thermal cycle. As the sample temperature changes, the sample expands, pushing up on the probe rod, or shrinks, pulling away from the probe rod. The probe rod is vertically suspended and counterweighted so that gravity keeps it in constant contact with the sample (18). The probe rod transmits the amount of sample movement to the electronic displacement sensor located overhead and outside the furnace.

2.3.2 Percent Length Change (PLC) and Coefficient of Thermal Expansion (COE)

Percent Linear Change (PLC) is the amount of expansion or shrinkage expressed in percentage of an initial length. A standard TDA curve is usually the PLC on the Y-axis and the temperature on the X-axis. The thick, black line in the graph below is a typical TDA curve of glass.

2.3.3 Temperature Range

The temperature range for a dilatometer is determined by the type of heating element or heating system used. The standard Orton dilatometers are made for one of the following temperature ranges:

- -170°C to +300°C (Cryogenic cooling chamber and Ni-chrome Heating Element with Fused Quartz Sample Holder and Probe Rod)
- Room Temperature to 1,000°C (Kanthal Heating Element with Fused Quartz Sample Holder and Probe Rod)

- Room Temperature to 1,200°C (Kanthal Heating Element with High Alumina Sample Holder and Probe Rod)
- Room Temperature to 1,600°C (Silicon Carbide or Platinum Heating Element with High Alumina Sample Holder and Probe Rod)
- Room Temperature to 1,700°C (Molybdenum Disilicide Heating Element with High Alumina Sample Holder and Probe Rod)¹⁹

2.3.4 Thermal Cycle

The most commonly used thermal cycle for dilatometry is a simple, controlled heat-up rate of 3-5 °C per minute from ambient temperature to the maximum temperature, then the test is terminated. For testing materials that experience irreversible reactions or when quartz transitions are critical, the thermal cycle can be extended to include a cool down segment. For developing firing schedules or examining what happens during a certain firing schedule, the dilatometer can be programmed to follow an actual production schedule that contains multiple ramps and soaks. The Orton dilatometer can be programmed for simple cycles, or up to a 20 segment thermal cycle.

2.3.5 Heat-up Rate

A sample does not absorb heat instantaneously, so it does not expand or shrink instantaneously. Since a finite amount of time is required for a sample to come to an equilibrium temperature and expansion/shrinkage condition, some thermal expansion measurements are made by holding the furnace temperature constant until the sample reaches an equilibrium temperature and length. These static condition (isothermal) tests take a lot of time, and are generally performed at only a few temperatures. To save time and generate more information over a broader range of temperatures, most thermal

expansion measurements are taken while the sample is being heated during a dynamic heat up. The thermal conductivity, size, and geometry of the sample will influence how quickly the sample can absorb heat and change length. With fast heat up rates, there is a tendency for the sample temperature to lag behind the furnace temperature, and the corresponding change in length to lag as well. With slow heat up rates, the amount of thermal lag and length change lag are much less, but the tests can be very long. Over the years the common industrial practice has evolved to a compromise rate of 3°C per minute. This keeps the amount of lag to a minimum and the testing time practical. The important factor is to be consistent in the heat up rate used, and to be consistent with the sample size and geometry.

2.3.6 Sample Size

The maximum sample size for the horizontal dilatometer is 2" long by 3/8" diameter or square. Samples longer than 2" will extend beyond the isothermal zone, and larger diameter samples will not fit into the sample holder. The ends of samples must be flat, parallel, and perpendicular to the length axis. The ultimate sample length depends upon the total amount of expansion or the total amount of shrinkage expected. The displacement sensor on the standard Orton dilatometer has a total linear movement of 5.0 millimeters (0.200 inches). Orton prefers to use only the center half of this range, so total sample movement (expansion or shrinkage) is 2.5 millimeters (0.100 inches). Consequently, low expansion/shrinkage samples should be long, and high expansion/shrinkage samples can be shorter. The following table shows the maximum percent expansion / shrinkage of different length samples.

2.3.7 Atmospheres

Tests are normally performed in ambient air. By adding the controlled atmosphere option to the Orton dilatometer, inert and reducing atmospheres, as well as vacuums are possible. There are several concerns when running tests in controlled atmospheres:

- The atmosphere tube surrounding the sample is a thermal barrier, and creates a larger thermal lag between the heating elements and the sample. Faster heating rates create an even larger thermal lag. Slower heating rates may be desirable.
- Flowing a gas over the sample will cool the sample, and create an even greater thermal lag between the sample and the heating elements. Flow rates should be as low as possible to minimize this effect.
- Reducing atmospheres, such as hydrogen, will significantly degrade platinum thermocouples at elevated temperatures. Small amounts of moisture with the hydrogen will increase the rate of platinum degradation. Using dry hydrogen will reduce the moisture attack. Using a surrogate gas, such as dry helium, may be reducing enough, and will retard platinum deterioration. A last alternative is to use a shielded thermocouple to totally avoid platinum degradation. However, a shielded thermocouple introduces another thermal lag into the test.
- A vacuum is an excellent thermal barrier to heat transfer. There is no gas for conduction and convection. Radiation does not become an effective heat transfer mechanism until elevated temperatures (20).

2.4 Thermal Expansion Profile

It is rare that have a fully - formed vitreous glaze on a ceramic substrate during the rising part of the glost heating cycle. As an aid to understanding events therefore consider the glaze-body relationship while cooling ; that is, as the glaze contracts. When

assigning values to the differential thermal expansion it must consider the thermal expansion properties of the glaze as a fully-formed material.

There have seen earlier that as the temperature of a fired glaze rises there are usually associated changes in dimension which, in the majority of vitreous compositions taken to a limiting temperature, are reversible. This is seen in the characteristic thermal expansion curve of a glaze taken to its softening point (but not beyond).

For most glazes in general ceramic use, the dimensional change from near room temperature up to a point near 500°C is positive and linear and remains so to the transformation range. From this zone the glass expands at a greater rate until a point is reached where the specimen apparently contracts.

The several fixed points on the thermal expansion curve of a glaze are determined by its composition and by the heat treatment used. Glazes which have crystallized, or devitrified, can have different fixed points from their glassy parent. Silica glass -ceramics have zero thermal expansion.

Figure 2.12 shows typical percentage linear expansion curves on the same leadless glaze specimen bars which have been (a) cooled slowly and (b) cooled rapidly from the glost temperature. Some $20 - 50^{\circ}\text{C}$ above temperature T_g the curve develops a negative slope due solely to the experimental technique. When the viscosity falls to about 10^7 poise the glaze bar softens to a point where it cannot act as a rigid bar; consequently, it deforms under the small force used to keep the measuring gauge in

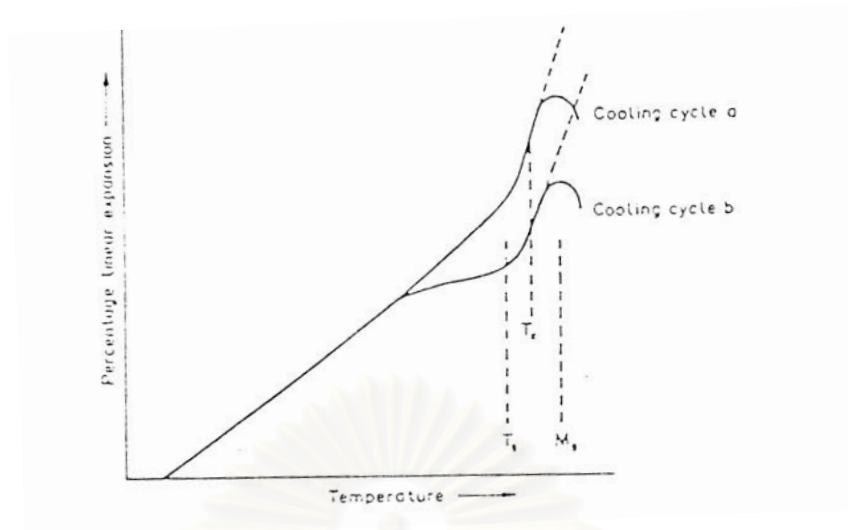


Fig2.12 Thermal expansion (a) normally cooled glaze bar (b) rapidly cooled glaze bar.

contact with the specimen. This temperature is identified as the (dilatometric) softening point, M_i

Again it is emphasized that the specimen bar upon which the thermal expansion is determined must be prepared in the same heating cycle which the glaze follows in the glost fire.

On the curve (Fig. 2.12) of the thermal expansion of the typical leadless glaze, the fixed points which are relevant to the question of glaze fit are :

- (a) The dilatometric softening point, M_i ,
- (b) The set point, T_x
- (c) The transformation temperature, T_t (or transition temperature)

2.5 Glaze-Body Interface

In considering the development of stress between glaze and body which have different thermal expansions, it has been convenient to think of it as a two-part-body-

glaze system. Although this is a useful simplification, in practice any problem of crazing or peeling needs to consider the two modes in which the composition of the glaze. (And, therefore, its thermal expansion) can change during firing.

1. Fluxes can be lost from the surface by volatilization.
2. The glaze might dissolve some of the substrate and form a layer of intermediate composition.

In many instances there is sufficient time at the elevated temperature of the glaze fire for an interaction between glaze and substrate to produce an interlayer or buffer zone. When molten, the glaze attacks and dissolved elements into the glaze occur slowly, forming a compositional gradient. The dissolved body material may diffuse through the total thickness of the glaze to the outer surface. As the glazed unit cools, crystallization in the interfacial zone is initiated, and layers whose coefficient of thermal expansion is different from that of either glaze or body, develop. The evidence for such a compositional gradient can be found in an examination of changes in refractive index across the glaze from surface to body (21).

Factors controlling the development of this zone will be:

1. The composition of the body.
2. The composition of the glaze.
3. The glaze thickness.
4. Glaze application such as spraying, dipping, water fall, double disc etc.
5. The maximum temperature reached and whether there is any soaking period during the firing cycle.
6. Where the production technique includes single-or double-firing.
7. The composition of engobe if the product must be used engobe for make a good color or protect water mark from the body (22).

Therefore thermal expansion coefficient of Engobe must be concern to control interface between glaze and body.

The in-service behavior of the ware is affected by the extent and properties of this buffer zone. Trials to test the crazing of glazes fired at different temperatures, for different lengths of time or on non-standard bodies from those normally used, are misleading.

2.6 Glaze Fit

The substrate-glaze system is constrained by the ability of the glaze technologist to prepare meltable compositions falling within a narrow band of available thermal expansions. There is a lower limit to the coefficient of thermal expansion above which all practical glaze must exist. The thermal expansion of a glaze is an additive property depending upon the composition, each component contributing to the total expansion by a factor characteristic of the element. Such factors can be used to calculate a value for the coefficient of thermal expansion, although the figure so obtained is not accurate. In particular, the use of these factors for crystal-containing glazes can lead to marked discrepancies between the actual and the calculated figures. The use of such factors is useful when there is a need to modify glazes which have failed in service.

Stress in the glaze layer develops as a result of a differential thermal expansion between the glaze and the body as they cool from the setting temperature down to room temperature. The magnitude and sign of this stress determines whether the glaze on the ware will craze, will be serviceable or will peel (23).

If that consider, in Fig. 2.13, a ceramic body coated with glaze at the glost temperature with the glaze-forming reactions complete, the two components have the same dimension, and any size change in the ceramic has been accommodated by

viscous flow in the glaze. As the ware moves through the cooling cycle the glaze begins to solidify until a temperature is reached where the two parts, solid glaze and body, are rigidly bonded.

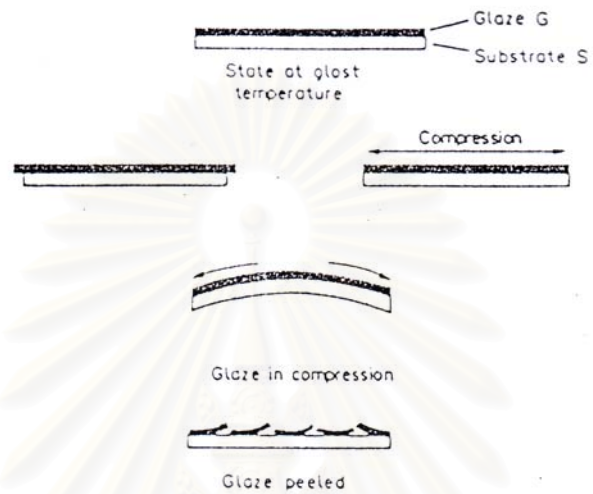


Fig 2.13 show cause of peeling problem (19)



Fig 2.14 show defect of peeling on terra cotta body

At this point the effect of any difference in the linear coefficients of thermal expansion of the glaze, α_g and of the body, α_b will become apparent. The dilatometer test ensures the coefficient on heating, although the stress in glaze-body or glaze to a limiting temperature matches the contraction in magnitude and is often called reversible thermal expansion. (Heating an unfired body in a dilatometer results in an irreversible thermal expansion measurement).

There can consider firstly the effect of different coefficients, ignoring for the moment a consideration of the shape of the expansion curves and any possible after-expansion of the body.

1. *Assuming equality of coefficient $\alpha_g = \alpha_b$.* Both glaze G and body B will contract in unison and no strain will be generated.

2. *Assuming $\alpha_b > \alpha_g$.* If the two layers were not constrained by their interfacial adhesion they would contract at different rates. The action of sealing the two together obliges them to be equal in length and stress develops in both components. With further cooling the body will try to contract the greater amount, but at the end of the cooling cycle the final lengths must be equal. As a consequence the glaze will be compressed and the substrate will be permanently stressed in tension. The tensile stress exerted by the glaze might be great enough to bend the body if only one side is glazed. For wall tiles to be flat after glazing it might be necessary for them to be given an initial reverse curvature (24).

When the difference between the thermal contractions of a body is much higher than that of the glaze, excessive compression is generated in the glaze. This can be greater than the strength of adhesion between glaze and substrate and there is then stress-relieving fracture at the interface known as peeling.

The strength of the body or the interfacial layer has an important bearing on the development of peeling. A thin or weak substrate can shatter if it is subjected to stress beyond its strength.

3. Assuming $\alpha_g > \alpha_b$. As cooling continues, the glaze, which has the higher coefficient of thermal contraction will try to contract the more. Again the final lengths of the two parts must be equal so the glaze will compress the body and thus must carry a balancing tensile stress. If its tensile strength is adequate, and the glaze is free from flaw, it might be able to withstand the stress. Unfortunately glass is less able to withstand tensile forces than compressive force and even when α_g is only slightly greater than α_b , the glaze fails in tension with crazing being the result. The elasticity of the glaze and the presence of flaws, as well as the coefficient of thermal expansion have an important bearing on the occurrence of crazing as show in Fig. 2.15.

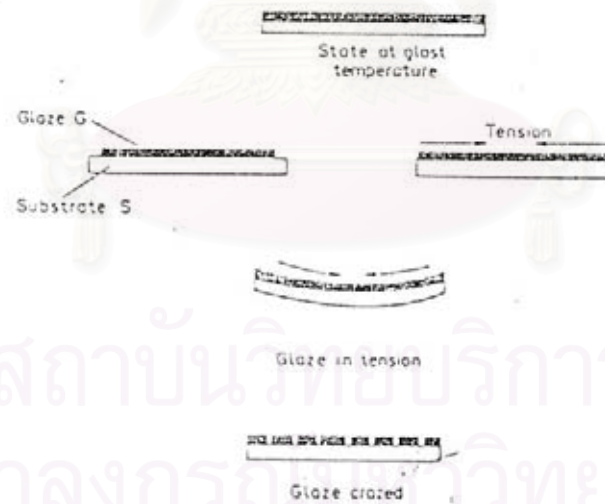


Fig 2.15 show cause of crazing problem (19).



Fig 2.16 show crazing glaze

The induced compressive stress might be great enough to bend the substrate if glazed only on one side. A weak body might shatter rather than respond to this degree of stress.

2.7 Glaze Stress

The ability of glazed ware to resist delayed crazing is related to the degree of glaze compression. When in compression, glaze increase the mechanical strength and the thermal shock-resistance of the ware. When the stress in the glaze approaches zero, the body strength is reduced. Excessive compression can lead to glaze peeling, but there are other reasons which can account for this effect and knowledge of the stress in the glaze can be useful in identifying and correcting the fault. Several methods have therefore been developed for assessing the magnitude and sign of stress in glaze.

Some are subjective, as is the simple impact test. When the ware is sharply struck by a metal point, the development of concentric cracks around the impact

suggests that the glaze is in compression. If the cracks are star-shaped the glaze is probably in tension.

Ring test. This method gives either a qualitative or quantitative assessment of glaze stress. For the test, hollow cylindrical rings 50 mm (2 in) diameters are glazed on the outside only. They are fired at the glaze temperature. When cooled, datum lines are marked in one edge of the ring from which measurements are taken.

The ring is cut between the marks with a diamond saw or apply force to generate any stress in the system (body and glaze) becomes obvious by movement.

If the glaze is in tension the gap opens, but if it is in compression the gap closes. From these changes in dimension a value for the maximum stress can be calculated. Unglazed blank rings are given a similar treatment and act as standards for the behavior of the substrate.

The test can be used to measure the effect of moisture expansion.

Tuning fork test. The basis of the test has been long established. Once control is exercised over the preparation of the test specimens the method produces a good laboratory tool for studying the development of glaze stress. A test piece is fabricated from two pieces of body, fixed at their base with slip to a third piece of the same body. After biscuit firing the fork is sprayed with a uniform coating of glaze on the outer faces. It is fired according to the glaze schedule and cool down. Movement in the tines of the fork is a measure of the magnitude of the stress inherent in the glaze and this movement can be measured by a telescope fitted with a micrometer eyepiece. A stress development curve can be obtained for the glaze by shutting off the furnace at the maximum temperature and recording the reading of the deflection of the tines against temperature (11).

Microscope method. Optical techniques can determine the type of strain which exists in glaze on its base. Transparent glazes, free from undissolved mill additions or pigment grains, are particularly suited to such methods. It is an advantage if the glaze is applied thickly.

When glass is strained it becomes doubly refracting and if viewed in polarized light between crossed Nicol prisms it shows interference fringes and colours. Strain-free glass is isotropic.

A section about 0.5 mm thick is cut through the glaze and body at right angles to the glaze surface. This is thicker than a thin section cut for mineralogical examination. The surfaces are finely ground with great care to avoid chipping the edges. The glaze face can be protected by resin.

It is mounted on a microscope slide and a cover slip cemented over it using extra resin to protect the glaze. The section is viewed with a sensitive tint plate mounted in the microscope such that the glaze surface is parallel with the slow direction. With glaze in compression the section appears yellow. With glaze in tension the section appears blue (25).

The strength of this color depends upon the path length of the light through the glaze (i.e. its thickness) and the amount of strain in it. With a known glaze thickness and using a quartz wedge, the amount of the strain can be measured.

The difficulties in precisely defining the setting point of a glaze, and with it deducing from two separate expansion curves the fit of glaze and body, can be avoided by directly measuring glaze-body fit with a tensometer. This instrument has a horizontal tube furnace closed at one end. At this end there is a support for the test specimen whilst at the opposite end of the instrument, and in the line of axis, there is a system for measuring small movements. A pyrometer is accurately positioned over the centre of the

sample to register the standard rate of temperature rises. The apparatus can be used up to 1,300°C (26).

Specimen bars are cast with a trapezoidal cross-section to a uniform weight and size from the subject body. This might be biscuit fired before receiving a precisely positioned uniform (but partial) coating of glaze. The specimen is clamped in the furnace. Differences in thermal expansion between glaze and body cause the bar to deflect from the zero data. The deflection is recorded. A series of mirror deflections is recorded as stress is induced during the cooling cycle.

The setting point of the glaze is given by the point at which the deflection changes from compression to tension.

The test can be carried out as an imitation of the once fired process to determine the effect of glaze on clay bodies. There is a risk of error from possible residual stresses in the body. Autoclave tests on the same combination of glaze and body can confirm the interpretation of the tensometer test results. For routine control of glaze, a stock of standard body is retained (27).

The effect of changes in firing schedules on the glaze-body interactions can be measured by this method.

The curvature caused by dissimilar thermal expansivity can be measured by transducer. In this method using the cross-over temperature (where the glaze goes into compression on the cooling cycle) rather than the strain-point temperature, leads to correlation between theoretical and practical values of stress-induced camber.

A simple instrument measures glaze fit by recording the differential curvature between glazed and biscuit bars. The instrument consists of a three-sided frame with pins for registering precisely the test ceramic bar. A dial gauge passes through the frame to measure the changes in curvature. The differences in curvature of the bar

before and after glaze firing is a measure of the glaze fit. Convexity on the glazed side implies compressive stress in the glaze. Concavity on the glaze side implies tension in the glaze. A modification to this technique measure the change in curvature of a glazed specimen when the glaze is ground away (28).

2.8 Differential Thermal Expansion, Δ , and Crazing Resistance

In order to study the relationship between the expansion characteristics of glaze and the crazing resistance it must to compare the percentage thermal expansion values of glaze and substrate at 500°C. According to the magnitude and sign of the differential, the liability to crazing or peeling can be forecast to some degree.

While the glaze is above its softening point stress will be relieved, but as the glaze-body composite cools down a new condition develops from temperature T_x onwards. At T_x , the glaze behaves as a solid and any stress induced in the glaze from this temperature down will remain. Continued cooling from T_x creates strain in the glaze-body system of a value proportional to the differential contraction between glaze and body to room temperature.

Unfortunately, there is no agreed single position of T_x on the thermal expansion curve. The temperature at which a glaze becomes rigid enough to accept strain has been fixed variously.

The transformation temperature is difficult to define precisely from the expansion graph and a compromise is made by recording the intercept of the produced lines of the two principle parts of the expansion graph. Provided that the same convention is always used by the glaze technologist in the same circumstances, then a meaningful picture will exist for stress development in the glaze-body composite. It is proposed that we consider

$$T_x = \frac{M_I + T_I}{2}$$

T_x Set point

M_I Dilatometric softening point

T_I Transformation temperature

The curves of the expansion of glaze and body are drawn to the same scale and considered in conjunction. The graph is moved for the glaze along the ordinate axis over the body graph until the set point T_x of the glaze coincides with a point at the same temperature on the body curve. Depending upon the thermal expansion of the glaze, which is the gradient of the graph, the origin of the glaze curve is displaced by an amount Δ , the contraction mismatch. Any alternative glaze with different thermal expansion characteristics or with a different value of T_x will have a different contraction mismatch.

The behavior of three glazes on the same body can be examined as examples of this. The set point of each glaze, T_x (where it is assumed the glaze accepts stress), is said to be the half-way point between the transformation temperature T_x and the softening point M_x . In any one family of glazes this temperature will not vary greatly.

For Table 2.4 show typical glaze thermal expansion coefficient using for each kind of ceramic body.

สถาบันวิทยบริการ
จุฬาลงกรณ์มหาวิทยาลัย

Table 2.4 Practical Glaze-Body system (29),(30)

Body	Biscuit fired(°C)	Glaze	Glaze firing temperature (°C)	COEglazex10 ⁻⁶ C ⁻¹
Porcelain	1000	Clear, Lead free	1350	5.0
Bone china	1235	Clear, Medium lead	1020-1100	8.5-10.0
Hotel china	1250	High frit content	1050	6.0-7.0
Sanitary ware	Single fire	Opaque, Lead free	1250	6.0-7.0
Stoneware	1000	Lead free	1230	6.5
Semi-vitreous	1250	Lead free, High frit	1050	7.0
Wall tile	1100	High frit	980-1060	7.0-8.0
Floor tile	Single fire	Need engobe	1150-1180	6.0-7.0
Earthenware	1100-1150	High frit	980-1080	7.0-8.0
Brick	950-1120 /Single fire	High lead, High frit	950-1120	5.5-7.5

Normal Expansion Glaze

Combined in Fig 2.17 are the curves for the percentage thermal expansion of an earthenware body and of a leadless glaze designed for this body and known to give good service. using the ordinate lines as a guide, the marked set point on the glaze curve is superimposed on the body curve. It is noticed at once that the origins of the curves, being displaced and on the same scale, differ by an amount 0.X %, characteristic of this combination at room temperature. The difference Δ between the

two origins as they cut the ordinate are given in Table 2.5 where the figure is compared with the differences in percentage expansion at 500°C.

Table 2.5 Glaze-Body Differential Expansions (11)

	%Linear exp. At 500 °C	By difference at 500 °C Δ	By set point Δ at room temp.	Type of glaze
Earthenware body	0.34			
Glaze A	0.30	+0.04	+0.03	Normal expansion
Glaze B	0.235	+0.105	+0.10	Low expansion
Glaze C	0.355	-0.015	-0.075	High expansion

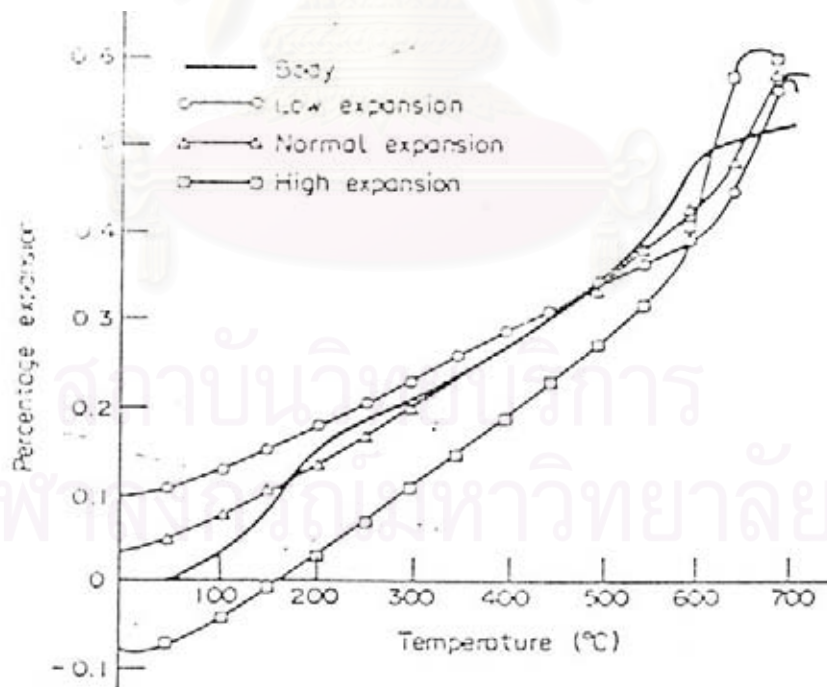


Fig. 2.17 Thermal expansion curves repositioned to demonstrate glaze-body fit.

Low Expansion Glaze

Normally a glaze with these properties would be used on an oven-to-table body having a lower expansion than the chosen earthenware body. Again the set point has been calculated and marked on the glaze expansion graph. Using the ordinate line as a guide, the glaze curve is moved over the body curve until the set point of the glaze coincides with the same temperature on the body graph. Like the case above, the origin of the glaze curve is displaced from the origin of the body curve and by a greater amount than shown by the glaze with an average thermal expansion.

High Expansion Glaze

Using this technique with the curve of a high expansion glaze, the absence of any compressive stress at room temperature can be forecast.

Practice has determined general guide lines needed for protection against eventual crazing. For more practical purposes an adequate margin of safety is given if the percentage linear expansion of the body exceeds that of the glaze by an amount between 0.02 % and 0.06 %.

For vitreous bodies the differential Δ lies in the range 0.02 - 0.04 %.

For porous bodies the differential Δ lies in the range 0.04 - 0.06 %.

Crystalline Glazes

Assuming that the glaze at the peak firing temperature is wholly glassy, then as the glaze passes through a deliberately lengthened cooling cycle, crystals form progressively.

As crystallization proceeds, phases develop (for example of zircon, alumina, spinel, wollastonite and zinc silicate), which have different thermal expansions from that of the parent glassy glaze. The expansion of these phases can be either higher or lower than the parent depending upon the composition of the crystal phases. Crystallization will alter the composition of the residual glass will progressively alter. The effect these changes can have on the thermal expansion of the crystalline glaze can be either:

(a) A counterbalancing of a high expansion phase and a low expansion phase having little resultant effect on the coefficient, or

(b) An imbalance of the phases leading to a coefficient greatly different from that of the parent glaze.

Unfortunately the eventual effect cannot be accurately predicted.

Again it is emphasized that glaze specimens for thermal expansion measurement must be prepared according to the production glaze firing cycle (31).

2.9 Glaze-Body Reactions (Buffer Layer)

Generally, there is a variety of formula for any glaze composition for any glaze effect. For any fritted glaze there can be a combination of low-temperature borax frit, lead bisilicate, feldspar and china clay or it could be a combination of lead borosilicate frit, feldspar and clay. The rapidity with which the frits lose viscosity and gain in reactivity will be different in each case.

Once a liquid phase forms, attack on the body substrate begins, leading to the formation of intermediate compositions which could be either vitreous or crystalline (32). The mechanism of this corrosion is similar to acid-base reactions in aqueous solution. There is subsequent diffusion of chemical species from the body into the glaze and from

the glaze into the body. A well-developed reaction zone develops and influences the ability of the glaze to resist imposed stresses. Once the zone is formed the reactions slow down.

These intermediate compositions can be expected to have different viscosity and surface tension and consequently have different powers to release bubbles. The same glaze fired on a variety of bodies can give quite different surface qualities because of this factor. The difference can be attributed to porosity in the body, in some instances.

During slow-cooling, crystals form which can extend from the unreacted body into the glaze. Fast cooling prevents crystal growth and the interface can only be seen as an amorphous layer. Mechanical strength of the ware can be affected by the magnitude of this crystal layer and by whether it retains an adequate bond with the body. The reaction zone can comprise 25 % of the total original glaze thickness.

Evidence of this crystal layer can be seen in the cross-section of a glaze-body interface. A fully-fritted, low-solubility glaze, compounded from a lead borosilicate frit (ground with 10 % clay) fired onto bone china shows three distinct layers when scanned by electron microscopy. There is an intermediate composition between glaze and body which can be seen in the illustration of a transverse polished section of this system. The boundaries are sharp. Element distribution images can be prepared for the same area. show the relative concentration and distribution of silicon, aluminium, phosphorus and lead through the body-buffer-glaze interface.

The density of the white dots indicates the abundance of a particular element. It is evident that there is more phosphorus in the body (as the component calcium phosphate) than in the glaze and that the crystalline interface resembles more the body

itself for phosphorus content. Diffusion of lead from the glaze into the body is very evident (33).

The nature of the body composition is significant in the way it influences subsidiary glaze reactions, such as the manner in which it affects the bubble population. High-quality gloss cannot be developed in a glaze either still containing, or which has recently contained, much bubble. Bodies containing materials processed by hydrocyclone generally have been found to give a glaze with an improved surface. The quality of glaze is related to the size and amount of free silica in the body and by inference to how many large free silica grains or crystals occur at the glaze-body interface. Bodies with the lowest amount of free silica give the best glaze appearance. Consequently a glaze fired on bone china gives a better finish than when the same composition is used on earthenware.

During maturation of any glaze the amount of bubbles present is not so very different, but what distinguishes glazes with poor surfaces from those with good surfaces is the amount of bubbles they retain after firing. Those bubbles which remain are often associated with edges and points of free silica crystalline material.

Dissolved surface components in the body will include iron impurities and other coloring ions (if present) and as these enter the glaze structure the colored zone is enlarged, magnifying the impact of the original specks or contamination. Fluid lead glazes can become uniformly colored cream through the overall solution of a high iron (terra-cotta) body (34).

Green spot is a fault seen in the glazing of fireclay products. The spots, frequently intensely colored, are caused by the presence in the clay surface of a copper containing impurity (CuFeS_2) which subsequently dissolves in the glaze during the glost fire. Zircon opaque glazes in reacting with the body are modified by the dissolved

elements, often to such an extent that the intermediate layer between glaze and body is transparent.

Analysis by an energy dispersive X-ray technique is used to examine the behavior of the special glazes which coat electro-ceramic substrates. The insulating properties of the glaze must not be modified by unwanted ion migration and compositions can be designed to reduce such ionic to a minimum.

Migration of aluminium and lead ions on firing a single ground lead borosilicate composition (70 % PbO, 20 % B₂O₃ 10 % SiO₂) on a 96 % alumina substrate has been demonstrated. Examination of the glaze and body to 6 μm on either side of the glaze-body interface on a sample fired at 800°C for 10 min was carried out by energy dispersive analysis/ scanning electron microscopy. This revealed that the PbO content (wt %) within the glaze at 2 μm from the interface was 70 % but fell to approximately 40 % at the apparent interface. On the body side of this apparent interface. PbO was detected falling from 40 % at the interface to zero at 2 μm within the body. The Al₂O₃ content was found to fall from the 96 % present in the body at 2 μm from the interface to 60% at the interface and then to level out at approximately 20% at a distance of 2 μm within the glaze from the interface. This Al₂O₃ level was retained from 2 to 6 μm from the interface within the glaze (35).

The fired glazed thickness was reported as being 11 μm . Such findings demonstrate that the interaction of a thick film glass with the substrate can affect the properties of the as fired composition compared with that expected from the theoretical glass composition.

Knowledge of the manner in which ions migrate can be used to explain some aspects of the surface behavior of a glaze. Under favorable circumstances some body ions can move across the thickness of the glaze. Following a change in the flux

component of a ceramic body, glazed normally with a potassium-free composition, and applied lithographic decoration did not sink into the glaze surface to the degree expected (this would have an adverse effect on the durability of the decoration.) Subsequent analysis showed that K^+ ions from the body had replaced Na^+ ions in the surface layers of the glaze to a degree which modified the glaze viscosity at the decorating temperature thus preventing flow (36).

2.10 crazing Test

Three methods of assessing crazing potential are used.

1. Immersion in a steam autoclave,
2. Heating in air and quenching the water.
3. Heating in steam and quenching in water.

Moisture expansion takes place in porous bodies, rapidly at first on newly fired gloss ware but then at a decreasing rate. If this expansion equals the value of the differential thermal expansion Δ , the compression in the glaze will be nullified. When it exceeds Δ crazing will occur as the induced stress overcomes the tensile strength of the glaze. The main practical test for crazing resistance imitates in the short term this long-term behavior. Steam under pressure accelerates the moisture expansion of porous ceramic bodies and, in a few hours, test moisture expansions equivalent to years of service can be reproduced.

In the standard test, six specimens of the glazed ware are repeatedly subjected to an atmosphere of steam, in an autoclave. In the autoclave the ware can be subjected to steam at high pressure (340 kN m^{-2}) for hourly periods (37). To make the body accessible to the steam three small scars (about 6 cm^2) are ground in the glaze to penetrate the glaze-body interface. After each cycle the ware is examined for signs of

crazing by rubbing the glaze with a pad soaked in methylene blue dye solution. That which is uncrazed is put through a repeat cycle until a maximum of 16 cycles is reached. Each piece should be exposed only to steam and not to water. With this test thermal shock is avoided.

The number and description of the specimens failing after each cycle is recorded. Service conditions are variable and the differences in the properties of any type of glazed ware are many. There is no direct equivalence between any test attainment and a period of freedom from crazing, but regular crazing tests are valuable.

The differential expansion, Δ , was deduced for conditions at room temperature, but there is a valid argument for deducing Δ at the temperature reached by the ware in the crazing pot, i.e. at 40 psi. This is at 142°C.

Heating in air avoids the effect of moisture expansion and the test results are influenced rather by the shape, thickness and overall dimensions of the pieces and upon the magnitude of the temperature drop on quenching. Because this is a critical feature, variations in the time between removing the ware from the oven and quenching and the speed of quenching are sources of error.

A test was developed which relates thermal shock results to actual working conditions and possible life span in service. Initially the test piece is heated to 120°C in an electric oven, then plunged into cold water at 20°C. If no crazing can be detected the cycle is repeated but with an increase in the temperature of 10°C. Each heating is gradual to ensure the article reaches the required temperature. Successive temperature rises and cold water quenches are made until the glaze crazes.

Criteria were established relating the crazing temperatures to the probable life in service.

Quenching limit of 120°C - possible crazing in a few days.

Quenching limit of 180°C - ware uncrazed for 2 years (38).

This test is not often used because its results are difficult to assess. With moisture expansion and thermal shock combined in one test the factor causing crazing cannot be stated (39).

2.11 Defect of Ceramic Product From Thermal Expansion Coefficient

Defect of ceramic products are related to thermal expansion of glaze and body mainly is crazing and peeling. Crazing is due to a thermal expansion mismatch between body and glaze. As a piece of ware is heated and cooled during normal use, it expands and contracts. An incompatible body and glaze usually means the glaze either immediately or eventually fails by crazing or peeling (shivering). Thus since glaze and clay are inseparably joined they must be expansion-compatible, no amount of covering over this incompatibility is going to make it disappear. It may well lengthen the time before crazing starts but it will not change the fact that it will happen. If crazing is the result of an expansion mismatch between body and glaze, then the only real solution is to adjust the expansion of one or both. If a suggested solution does not accommodate this, then are treating the symptoms and not the cause. In middle-fire and high-fire where glaze and interface development is good, the appearance of crazing suggests a huge incompatibility, not a small one. Strength tests have demonstrated up to a threefold difference in the strength of glaze test bars between high and low expansion versions of a glaze without visible crazing to suggest a problem. This means that by the time crazing shows up, there are already unreleased stresses that result in a big strength problem. To fix it, a significant change is needed, one that not only fixing the crazing phenomenon but that restores the fired strength of the body/glaze compatible. The bottom line is that crazing is best solved on the oxide level for the glaze and the

material level for the body. That means body testing and glaze chemistry are involved in any real solution.

The solution to solve the problem of crazing and peeling

1. Apply a thinner glaze coat. Either a glaze fits or it does not. Putting it on thinner does not change that. It could be argued that a greater percentage of the total glaze thickness is a part of the clay-glaze interface on a stoneware piece and thus a better fit result. Still, either it fits or it does not and if it doesn't then every time the glaze gets applied too thick it is going to craze. Also, glazing thinner might appear to prevent crazing, but time and delayed crazing will be the true indicator of whether the glaze really fits or not.
2. Add increasing amounts of silica. It is true that this does work in some cases of slight crazing. In more serious cases, it is surprising how much must be added to reduce expansion to any degree. Yes, silica is a low expansion oxide, but if the glaze is full of high expansion fluxes like sodium and potassium adding silica is a little like adding white paint to dilute the color of black. Additions of silica are often inappropriate for other reasons. The amount of silica in a glaze is a critical player in its appearance and surface texture; what is there is usually what is required. Adding enough to simply hide out-of-the-kiln crazing does not deal with the deeper fit problems, these weaken the ware and will eventually craze it anyway. Adding more can introduce unwanted gloss, higher melting temperatures, and change in surface character. Since mattes, which usually maintain a critical balance of these very factors, are the ones that often craze, adding silica is not a solution. In addition, highly melted special-purpose glazes typically depend on low silica for their unique character. The glossy glazes will tolerate silica additions, but

again, to put enough in to solve the problem will normally detrimentally affect melting.

3. Firing to correct cone over a longer time. The contention here is that the clay will tighten and have a better interface with the glaze; this better interface will produce a better the fit. But a better interface for a crazing glaze does not mean a better fit, it means a forced fit. Firing to improve the clay-glaze interface to solve a clay-glaze expansion mismatch is misdirected. If the expansion is wrong, then this is what should be changed. The interface is conceptually the glue that holds the glaze on. This approach is like saying; If they are not compatible, then glue them together more strongly. Surely, it is best to make them more compatible. Again, time will be the true test of compatibility.
4. Fire higher, if glaze can take it, and they might fit better, we are trying to do is change the range shrinkage of either the clay body, the glaze, or both in order to bring the glaze under slight compression'. Firing a glaze higher on the chance that it might fit better is not really a methodical approach. Incompatibilities do not normally just go away. Firing higher is likely to introduce new problems with vitrified bodies or visual differences in the glaze. In fact, firing higher could enable the feldspar to take more body quartz into glass solution, reducing the body expansion and making crazing worse. Firing higher will work in one situation: An under fired body will absorb water and the moisture expansion will craze the glaze, firing it higher will make it less absorbent (40).
5. Add increments of 5% silica to the clay body. It remains crystalline. True, adding coarser sizes of high-expansion silica has the effect of compressing the glaze (by virtue of its 1% contraction going down through quartz inversion). However, it is not the whole matrix that contracts; rather it is each of those little independent

crystals. If temperature gradients exist in the cooling ware, waves of stress wave through it. On the other hand, if the body is not vitreous and very fine silica is added, the extra will accelerate cristobalite formation (because of the lack of glass development to arrest the conversion). The result could be ware likely to crack or craze due to the 3% expansion associated with repeated heating of a cristobalite body through 220°C during common use. Many bodies are already optimized to have the maximum practical silica. Adding more has to be done at the expense of other materials in the mix. If the clay component is reduced, the body will be less plastic; if the feldspar is cut back, the result will likely be a less vitreous and weaker material. Adjusting body expansion is a complex process that must consider glass development, the size and availability of quartz, and the types of clay minerals employed. At any rate, it is not usually practical to adjust the body because most people use prepared clays.

6. Slow cool the glaze kiln, do not open it until it is below 200 °C. If the glaze can barely withstand a normal cool cycle after firing, then how will it take the thermal punishment of the dish washer or the normal hot-cold shocks of everyday use? It is possible that a glaze under tension can be eased down and may well appear to be fine when the kiln is opened. But the first thermal stresses it undergoes in use will reveal what the slow cool temporarily covered up⁴¹.
7. Biscuit higher if low fire glaze is not fitting. Making a glaze fit on a low temperature body where there is a lack of clay-glaze interface is much more difficult. Band-aid approaches just would not work, the thermal expansion of the clay and glaze must match closely. It is true that crazing will be evident at low-fire with a much smaller difference between clay and glaze expansions than with stoneware. Thus smaller changes have a bigger effect. It is true that firing higher can change a clay body's

expansion. However, the above approach will only work if the increased temperature lowers the expansion and if the glaze firing is lower than the bisque. However, adjusting low fire glazes with boron sourcing materials (i.e. frits) is much more practical. Low expansion frits, specifically targeted as additions to reduce crazing, are available.

8. Change to a frit of lower expansion. This suggestion goes in the right direction as it proposes to change the expansion. However, few frits are used in stoneware glazes (the few that are normally there for a very specific purpose). Thus simply changing to a frit of different chemistry and lower expansion is likely to mean altered glaze properties unless you know the implications. In lower fire glazes, this approach is much more common since many boron frits are quite balanced, almost stand-alone glazes by themselves.

Rather than thinking of crazing as something that is caused by something else, it is better to think of crazing as evidence that a body and glaze are not expansion-compatible. Viewing crazing as a material level problem might be fine for certain highly fritted low temperature glazes, but it does not work for stoneware glazes. It is oxides of high expansion that cause crazing, not materials. That why crazing is a problem that is much more effectively solved on the oxide or formula level using simple calculations (e.g. substituting fluxing oxides of lower expansion for those with higher expansion).

2.12 Forming Process

2.12.1 Extrusion

Extrusion forming of ceramics is accomplished by compacting a plastic mass in a high-pressure chamber (Cylinder) and forcing the mass to flow out of the chamber through a specially shaped die orifice. The cross-section of the extruded column (often called the pug) takes the shape of the die. Parts of desired length are formed by cutting the extruded column with rotating knives or stiff wires. Obviously, only shapes having a constant cross-section can be formed by extrusion.

The stiff mud forming of most building brick and much refractory brick is accomplished by extrusion, using a clay-water mass of fairly high yield point. Clay and tempering water are continuously fed into a pug mill attached to the extruder (Fig 2.18).



Fig. 2.18 show pug mill for mixing clay-water

The pug mill cuts and kneads the material to temper it and moves it forward through a shredder into the extruder proper (sometimes called the press). The extruder

consists of the auger that moves the tempered mixture consecutively through two sealed chambers. The first or de-airing chamber uses a vacuum to remove air from the shredded clay. The de-airing step is a critical one (Fig. 2.19).



Fig. 2.19 show honey diaphragm in vacuum chamber of extruder.

Since the presence of air pockets in the extruded column would lead to delamination and cracking of the ware. The de-aired clay is then passed by the auger into the second or compacting chamber where the shreds are reconsolidated into a dense plastic mass. The forming die is at the end of the compacting chamber and the auger pushes the plastic mass out through the die where it can be cut to length by a wire cutter shown in Fig. 2.20



Fig. 2.20 show wire equipment for cutting clay from extrusion

Hollow shapes such as structural tile, flue tile, drain tile, sewer pipe, and some model of electrical insulator can be formed by extruding stiff mud through a special die that contains a central structure made up a solid core suspended by thin radial support within the entrance from the compacting chamber (Fig. 2.21)



Fig. 2.21 show the extruder with central core for produced hollow product.

Extrusion is often used as a preliminary step to other plastic forming procedures. This is especially true of porcelain mineral mixtures that are generally blunged with excess water or grinding in ball mill, and then filter-pressed to the proper moisture content for plastic forming, and then extruded and wire cut into short slugs (sometimes called blanks) that can be fed to other forming machines.

Nonplastic high-yield-point ceramic mixes are usually extruded from a vertical or horizontal piston press rather than with an auger (42). These materials can sometimes be extruded at low pressure, but high-pressure extrusion reduces the amount of binder and moisture required during extrusion and yields a denser and more uniform final product. A common practice in plasticizing nonclay ceramic mixes is to first blend the various dry ceramic raw materials together in a sigma-blade, muller mixer, dry-pan mill or wet-pan mill.

For high-pressure extrusions, the moisture content is usually reduced to the point where the material tends to form granules about $\frac{1}{4}$ inch in diameter in the mixer. These granules are easy to pour into the extrusion press. Extrusion press capable of exerting more than 100 tons are commercially available.

2.12.2 Slip Casting

A slip is slurry of very fine ceramic materials suspended in water (or occasionally another liquid) and generally having the consistency of thick cream. If such a slip is poured into a porous plaster mould, the mould will draw water from the slurry and will build up a deposit of ceramic particles on the mould wall. In this manner a ceramic green ware can be formed having an outer configuration that reproduces the inner configuration of the plaster mould.

Wall buildup during slip casting continues as long as any slip remains in the mould. However, the rate of buildup drops off with time, because water can be removed from the slip only by passing through the thickening cast wall. If a hollow cast is desired, the excess slip is poured or drained out of the mould after the required wall thickness has been achieved, and for this reason the operation is sometimes called drain casting.

It is also possible to cast solid objects of small cross-section if a large enough slip reservoir is designed into the mould. Some product such as sanitary ware can be has drain casting and solid casting in the same pieces depended on design and shape of ware.

The preparation of plaster mould is critical to the success of a slip casting operation. Suppliers of plaster for the ceramic industry are well informed in this area. The amount of setting water used in mixing the plaster determines the strength and porosity of the resulting mould. Since the strength of plaster decreases and the porosity increases with an increase in the amount of setting water, the mixing ratio of plaster to water is always a compromise. The part weight of water and 100 parts of plaster is called consistency example consistency 70 is mean in plaster 100 have water 70 by weight. From 68 to 85 parts by weight of water to 100 parts plaster are used in the ceramic industry.

Ceramic products are cast in moulds made up of several close-fitting parts. The mould is disassembled after casting to remove the cast. The mould parts must be tightly held together during casting, as a significant hydrostatic pressure builds up in the mould due to the weight of the slip. If not held tightly closed, the slip will run out between the joints of the mould then cause of edge on the green product which must remove before dry because the edge must still until firing.



Fig. 2.22 Working mould for sanitary ware

The rheology of clay slip is important for casting process. The casting behavior of clay slip depended strongly on slip specific gravity, viscosity and thixotropy. The specific gravity is simply a measure of the amount of solids suspended in a volume of slip. In general, the specific gravity of slip is kept as high as possible, consistent with proper viscosity parameters. The viscosity of the slip is somewhat a function of the particle size distribution of the solids present. The rheology of clay slips are generally controlled by means of small amounts of dispersion agent (deflocculant). Common deflocculants used with slips containing clays are sodium silicate, sodium carbonate, sodiumhexametaphosphate, and a number of organic substances such as the polyacrylates (43).

If the particle size distribution of a slip is too coarse, the slip will be difficult to disperse and will settle out rapidly, giving uneven casts. If the size distribution is too fine, the slip will cast too slowly. Aging of freshly prepared clay slips often improves their casting behavior, but the proper aging time, specific gravity, temperature, and viscosity for proper casting must usually be determined by experiment.

Pressure casting

Slip casting with pressure applied to the slip in the mould was of limited use until the recent invention of strong nonplaster synthetic polymer mould such as resin. This process has particularly improved the productivity of sanitary ware and white ware products for growth market. The pressure casting process has developed dispersants and casting aids that dramatically increase productivity by reduce casting time from 3-4 hours to about 15 minutes. A conventional casting slip must be adjusted to make it suitable for pressure casting operations, with particle size distribution and slip specific gravity being key parameters to control. Better processing efficiencies can often be achieved by reformulation of conventional casting slips, replacing some of the plastic clay with nonplastic materials (44).



Fig 2.23 High pressure casting machine

2.12.3 Pressing

Ceramic ware can be formed under high pressure from powders with relatively low moisture content or often with no moisture at all. Dry forming of ceramics implies that the material contains 4-6% or less water. Spray-dried powders are particularly suitable for dry forming process because a granule of spray dryer is round shape and have small hole like a donut therefore granule can fill in the cavity mould even a shape of cavity mould is more complicate.

Dry pressing is accomplished by compacting powders under very high pressing pressures in steel dies or steel with rubber coating. In a typical dry pressing operation, the pressure for control dimension and %shrinkage is call specific pressing pressure. The calculation is force per area, force is come from hydraulic pressure in cylinder (sometime call plunger) which is related to area of cylinder. For area for calculated specific pressing pressure is cavity size of dies and amount of cavities in case of more than one.

Charging process is stage to fill powder from hopper into cavities mould. The granules are typical agglomerates which break down during pressing. The powder is compressed in the cavity by hydraulic plunger and upper punch and is then eject by upward movement of the lower plunger and lower punch after the upper punch is removed. That is a pressing cycle.

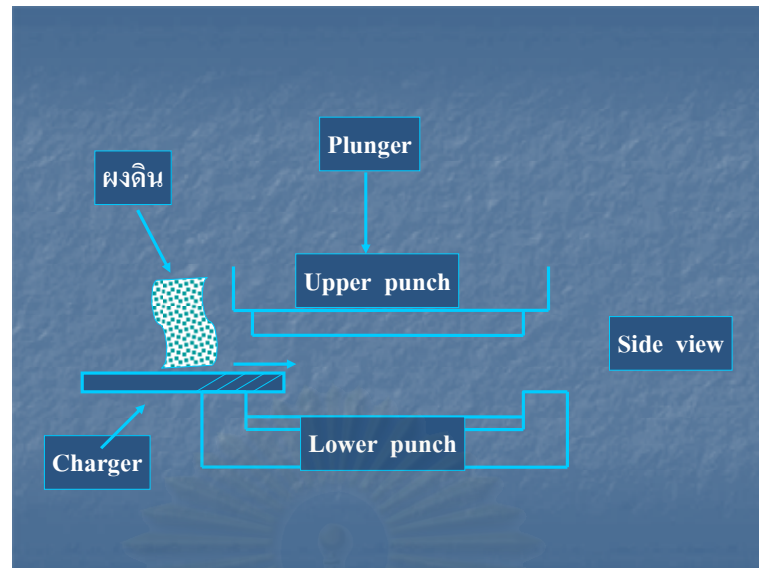


Fig 2.24 Cycle of pressing process



Fig 2.25 Upper and lower punch of pressing machine for cordierite kiln furniture

Important considerations for good quality dry pressing product include

1. The grain size distribution of the ceramic powder should be concern according to the nature of raw materials in body formula and the parts being pressed. Blending of variously sized particles to accomplish efficient packing is important to green strength, green bulk density, %drying shrinkage and firing shrinkage and also %water absorption of finished product.
2. The moisture of powder should be suitable range according to pressing pressure, the nature of raw materials in body formula and speed of the charger
3. The aging time of powder should be enough time in order to homogenize the moisture in powder
4. Parameter of pressing machine such as first die drop, second die drop, speed of charger, cycle of stroke, temperature of mould and punch
5. Design of mould and liner include a grid inside the charger



Fig 2.26 Grid inside the charger for sharing powder into the cavity mould

6. Specific pressing pressure should be design for suitable %shrinkage, %water absorption and firing strength

CHAPTER III

EXPERIMENTAL PROCEDURE

The ceramic bodies from ceramic factories used in this research are from sanitaryware, electrical insulator, terra cotta and ceramic tile. The body was prepared for pressing, slip casting and extruding processes.

The specimens were dried at 150 °C in an electric dryer and fired at the range of product requirement with 20 minutes soaking in an electric furnace. The fired samples were tested for drying, firing shrinkage, water absorption, and strength by 3-point bending method; Bulk densities of specimens were measured according to Archimedes' method. Phases of fired specimens were analyzed by XRD.

Microstructure of body that fired at 1250 °C was inspected by scanning electron microscope SEM. Thermal expansion coefficients of fired specimens were measured by a dilatometer.



สถาบันวิทยบริการ
จุฬาลงกรณ์มหาวิทยาลัย

3.1 Raw Materials and Characterization

3.1.1 Raw materials

Starting materials used in this research were different types of body from ceramic industry. Bodies used for the experiment were selected from sanitaryware, electrical insulator, terra cotta, and ceramic tile as shown in Table 3.1. All bodies were ground, mixed and went through the body preparation process from each factory.

Table 3.1 Type of bodies

Type of body	Type of product
Vitreous china	Sanitaryware
Porcelain	Electrical insulator
Stoneware	Floor tile
Earthenware	Wall tile
Terra cotta	Garden ware

3.1.2 Raw materials characterization

Determination of particle size distribution

Particle size distribution of starting materials was analyzed using a particle size analyzer (MALVERN Mastersizer 2000 particle size analyzer)

Sample preparation was started from weighing dry sample for 1 g. Put into a beaker with 20 cc distill water and then magnetic stirrer was used in order to deagglomerate the particles. Calgon was added as the dispersant to a small amount of the sample in a beaker and the result was usually noted. The sample was dispersed in water for 10 minutes, then put into a container for analyze.

The result was shown show as a histogram, each bar in the histogram represents a size band of particle and the height of the bar represents the percentage of the sample that is within that band. D(0.5), D(0.1) and D(0.9) were standard percentage reading from the analysis.

D(0.5) is the size in microns at which 50% of the sample is smaller and 50% is larger.

This value is also known as the Mass Median Diameter (MMD).

D(0.1) is the size of particle below which 10% of sample lies.

D(0.9) gives a size of particle below which 90% of the sample lies.

Span is the measurement of the width of the distribution. The narrower the distribution, the smaller the span becomes. The span is calculated as :

$$\text{Span} = [d(0.9) - d(0.1)]/d(0.5)$$

Concentration is calculated from the Beer-Lambert law and is expressed as a percentage.

Uniformity is a measure of the absolute deviation from the median.

SSA (Specific Surface Area) is defined as the total area of the particles divided by the total weight. Note that SSA figure is a mathematical calculation based on the assumption that the particle are both spherical and non-porous.

Characteristics of raw materials (Body composition)

Chemical composition of the bodies was analyzed by X-ray fluorescence (XRF) in order to check %oxide of every kind of bodies. The sample was prepared by fusion method. The sample was ground and passed through 200 mesh, mixed with flux ($\text{Li}_2\text{B}_4\text{O}_7$) in the ratio of powder: flux 0.7g : 7g and fused in a Pt crucible at 1100 °C for 10-15 minutes and quench in air. Fused sample was put into a sample holder to analyze by qualitative analysis.

3.1.3 Raw materials preparation and parameter for forming

Bodies from Table 3.1 were prepared in different ways for 3 forming processes as dry pressing, extruding, and slip casting processes.

- Preparation for dry process

All clay bodies from Table 3.1 except stoneware body and earthenware body from tile factory that already made granule were dried in an oven at 150 °C for 24 hours. The agglomerated grains were crushed and passed through a sieve 100 mesh and then weighed on an electric balance in order to control %moisture of about 5%. After the moisture content was calculated, the proportion between dry powder and water were mixed in a dry pan mill as shown in Fig3.1. The water was sprayed while the pan mill was rotated till the granules were formed and left for 24 hours aging prior to pressing process.



Fig.3.1 Dry pan mill

- Preparation for extruding process

All clay bodies from Table 3.1 were dried in an oven at 150 °C for 24 hours , crushed the agglomerated grain and passed through a sieve no. 100 mesh and then weighed on an electric balance in order to control %moisture of about 18 %. The

powder and water were mixed and kneaded by hand with the proportion that calculated for specific %moisture until homogeneous and left for 24 hours aging.

- Preparation for slip casting

Clay bodies were dried in an oven at 150 °C, the agglomerated grains were crushed and passed through a sieve no. 100 mesh and then weighed on an electric balance about 400 g in order to calculate %water content in clay slip for 40%, 50% and 60% water respectively. Specific amount of water was added to a 1000 cc bigger and dry powder was also added into a bigger while mixing by a high speed stirrer. The speed of stirrer used was 350 rpm and Na_2SiO_3 was added as a deflocculant to adjust viscosity and thixotropy of body slip. The viscosity and thixotropy were measured by using a Brook field viscometer with a spindle number 4 and then aged body slip for 24 hours before casting.

3.2 Forming Process

The forming processes used in this research were dry pressing, extruding, and Slip casting.

3.2.1 Dry pressing

The body powder was charged into a cavity mould by manual and then made a smooth surface in order to control thickness of green tile, The rectangular mould with 100x50x5 mm dimension was used by a hydraulic pressing machine as shown in Fig 3.2 at various pressures; 50, 100 and 150 bar in all clay bodies for 10 pieces of each forming pressing and each kind of clay bodies.

After ejected from the cavity mould, size and weight of green tiles were measured.



Fig.3.2 Hydraulic pressing machine

3.2.2 Extruding

The clay body that prepared for extruding process was prepared from dry powder of all clay bodies and water that calculated from 18% moisture. After clay body was kneaded by hand until homogeneous, aged in a closed plastic bag for 24 hours. The mixed clay was put into a vacuum extruder as shown in Fig 3.3 until vacuum gauge was stable and almost vacuum. A round shape die with 2 cm diameter was used in this experiment.

When the clay body was passed through a metal die then cut to a cylindrical shape of 12 cm length. The green specimen was marked as a 10 cm length for shrinkage measurement and weighed. The amounts of specimens were 10 pieces in each formula.



Fig.3.3 Extrusion machine

3.2.3 Slip casting

Preparation of the plaster mould

α -plaster mixed with water for a consistency of 60 using a plaster mixing machine to make homogeneous slurry of plaster then poured in the block to make a case mould. The size of the cavity mould was 80x10x10 mm as shown in Fig. 3.4. When case mould was finished. β -plaster with water was mixed for a consistency of 70 by plaster mixing machine and a box for the slurry was poured top up a case mould to produce a working mould. After finish up to get rid of bubbles and pinholes, the working mould was dried in an oven at 40 °C for 5 hours.



Fig.3.4 Mould for slip casting

Clay slip was poured into the mould and tapped gradually in order to prevent bubbles inside the green specimens. When the level of clay slip was reduced, more slip was added into a plaster mould until clay slip level was stable.

The forming parameters are shown in Table 3.2.

Table 3.2 Parameter for each forming process

Forming process	Parameter			
Pressing	Pressing pressure (bar)	50	100	150
Casting	%Water content	40	50	60
Extruding	Not vary in forming parameter			

Table 3.3 Dimension of specimens

Forming process	Dimension
Pressing	100x50x5 mm
Casting	80x10x10 mm
Extruding	110x20 mm (Cylinder)

The moisture content of powder for pressing were 5-6% and clay body for extruding was about 18 %.

3.3 Drying and Firing Process

The green specimens were formed and dried in air for 24 hours in order to prevent dry cracking and put into an oven at temperature of 150 ° C for 5 hours.

Firing temperatures in all kind of bodies were shown in Table 3.4 by using an electric furnace with a heating rate of 5 °C/min and soaked at the maximum temperature for 15 min. The temperature was varied for each kind of body to study the effects of firing temperatures on properties of fired products.

Table 3.4 Firing temperature for all kinds of product

Type of body	Firing temperature (°C)		
Vitreous china	1150	1200	1250
Porcelain	1150	1200	1250
Stoneware	1100	1150	1200
Earthenware	1050	1100	1150
Terra cotta	950	1000	1050

Range of firing temperature of all kind of bodies were selected from working temperature of each product.

3.4 Characterization of Fired Specimens

Shrinkage

The size of specimens was measured by a vernier caliper. Shrinkage of dried and fired specimens was calculated by equation (3.1).

$$\% \text{ Shrinkage} = \frac{(\text{length of green specimen} - \text{length of fired specimens})}{(\text{length of green specimen})} \times 100 \quad (3.1)$$

3.4.2 Water absorption

Water absorption of specimens was measured according to a method in ASTM C 373-88 and calculated using equation (3.2).

$$\% \text{ Water absorption} = \left[\frac{w_2 - w_1}{w_1} \right] \times 100 \quad (3.2)$$

w_1 =dry weight

w_2 =saturated weight

3.4.3 Bulk density

Bulk density of specimens was measured according to the Archimedes' method (ASTM C373-88). The air in opened pores of specimen was removed by applying 30 min vacuum and then the distilled water was poured over the specimens and the specimens were under vacuum for another 30 min. During this period, the vacuum equipment was shaken to get rid of the bubbles on the surface of specimens. Each specimen was then weighed in water. The suspended weight was taken as W_2 . The same specimen, after removing the water adhering on the surface with a piece of damp cloth was weighed again and the weight was taken as W_3 (saturated weight). Then the specimen was dried in an oven at 110 °C for 2 hours and weighed again. This weight was W_1 (or dry weight).

The bulk density was calculated according to equation (3.3),

$$\text{Bulk density} = \left[\frac{W_1}{W_3 - W_2} \right] \rho_{\text{water}} \quad (3.3)$$

Where ρ is density of water at the measurement temperature

Relative density was calculated from bulk density and theoretical density using equation (3.4)

$$\text{Relative density} = \frac{\text{bulk density}}{\text{Theoretical density}} \quad (3.4)$$

Theoretical densities of fired ceramic products were calculated from the specific gravity of each component using equation (3.5)

$$\text{Theoretical density} = \frac{1}{f_1 / \rho_1 + f_2 / \rho_2 + \dots} \quad (3.5)$$

Where f is fraction of each component

ρ is specific gravity of component

1, 2 ... is number of component

3.4.4 Bending strength

Bending strength of the fired specimen were measured using a three-point bending (Lloyd instrument model LRX plus) with crosshead speed of 0.30 mm/min. The modulus of rupture of the specimens was calculated using equation (3.6) for the modulus of rupture of extruded specimens, equation (3.7) was used.

$$\text{MOR} = 3WL/2bd^2 \quad (3.6)$$

W= Load of pressure

L= Span length

b= Width of specimen

d= Thickness

For cylindrical shape

$$\text{MOR} = 8WL/\pi D^3 \quad (3.7)$$

D= Diameter of cylinder specimen

3.4.5 Phase analysis

The phases of fired specimens were analyzed by X-ray diffractometer (BRUKER D8 ADVANCE (Ni-filtered Cu $K\alpha$ radiation; $\lambda = 1.5406 \text{ \AA}$)) using 2 theta in the range of 15° to 80°, scanning speed of 0.1° /1 second, and power voltage of 40 kV and 30 mA with Cu anode. The firing specimens were crushed in a mortar, and sieved through a no. 100 mesh screen prior to XRD determination in order to get a good compact for specimen preparation.

3.4.6 Microstructure examination

Microstructure of fired specimens was inspected by a scanning electron microscope (JEOL JSM-6480 LV) equipped with energy dispersive spectroscopy (EDS). The surfaces of fired specimens were ground with SiC paper #140, #240, and #400, respectively, and polished with diamond particles of 6, 3, and 1 μm in sizes⁴⁵. The specimens were cleaned by ethanol in an ultrasonic bath after polishing. The specimens were etched by 10 % HF acid for 15-20 second (46) and cleaning with water on order to get rid of residual of HF on the surface of specimens. Then dried in an oven at 110 °C for 2 hour. After that the specimen was sputtered by gold for 5 minutes before put in a scanning electron microscope chamber.

3.4.7 Thermal expansion coefficient

Thermal expansion coefficient of fired specimens was inspected by a dilalometer (NETZSCH DIL 402 C) up to 1000°C with a heating rate of 10°C/min and using an alumina rod for calibration. The size of fired specimens was 5x5x20 mm and the temperature range of the examination were 20-500 °C and 500-600 °C with a heating rate of 10 °C/min.



Fig.3.5 Dilatometer



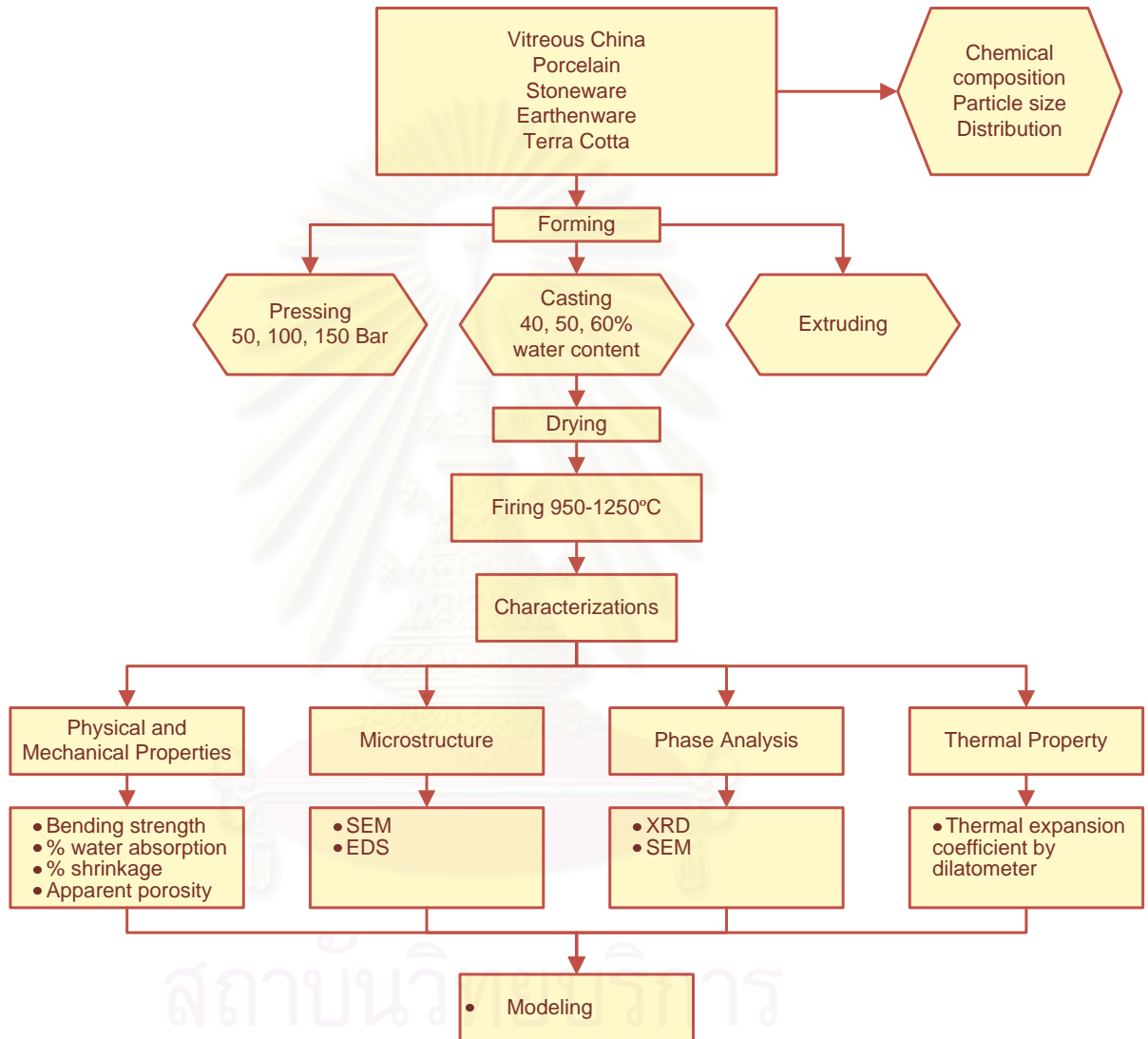
Fig.3.6 Sample and thermal couple



สถาบันวิทยบริการ
จุฬาลงกรณ์มหาวิทยาลัย

The experimental procedure are summarized and shown in fig 3.7

Fig.3.7 Flow chart of the preparing of body in different forming process



CHAPTER IV

EXPERIMENTAL RESULT AND DISCUSSION

4.1 Raw Material Characterization

4.1.1 Particle size determination

Particle size distribution was measured by a laser scattering particle size analyzer. Table 4.1 shows the average particle size at d (0.9) and surface area of each raw material used for the experiment.

Table 4.1 Average particle size and deviation of raw materials

Types of body	D 0.9 (μm)	Surface area (m^2/g)
Porcelain	61.65	1.021
Vitreous china	72.37	0.939
Stoneware	93.83	0.724
Earthenware	58.66	0.999
Terra cotta	88.83	0.436

From particle size distribution data show that porcelain body has smaller particle size than vitreous china body and also has higher surface area. Particle size and surface area are parameter relating to degree of sintering, the smaller particle size and the higher surface area resulting in higher sinterability.

In addition, particle size distribution and surface area are depended on raw materials, grinding parameter, sieving process and body preparation process of each factory. In this research the effects of forming processes on properties of each kind of body have been studied. Average particle size shown on Table 4.1 could not be compared because each body has been prepared from different conditions. The particle size characterized and shown in Table 4.1 are just for reference and can not be related to other physical properties.

4.1.2 Chemical composition of starting materials analyzed by X-Ray Fluorescence

Raw materials for this experiment were bodies from ceramic industry. They were analyzed by XRF in order to examine main oxide content in each body and also %impurities such as Fe_2O_3 and TiO_2 . The analyzed oxide contents of bodies are shown in Table 4.2

Table 4.2 Oxide content of ceramic bodies analyze by X-RAY fluorescence

Body	%SiO ₂	%Al ₂ O ₃	%Fe ₂ O ₃	%TiO ₂	%CaO	%MgO	%Na ₂ O	%K ₂ O	%LOI
Vitreous china	71.09	23.51	0.84	0.28	0.53	0.54	0.24	2.03	6.65
Porcelain	71.20	23.36	1.62	0.40	0.36	0.22	0.58	2.24	4.88
Terra cotta	74.88	18.29	3.65	0.81	0.38	0.47	0.07	1.40	5.75
Earthenware (wall tile)	71.30	16.03	2.03	0.41	7.61	0.56	0.25	1.66	10.56
Stoneware (floor tile)	71.58	17.94	4.24	0.36	0.42	0.28	2.64	2.46	5.12

4.1.3 Calculation of thermal expansion coefficient by percentage of oxide in the body formula

The analyzed oxide contents of bodies are shown in Table 4.2 were used for calculation of the theoretical thermal expansion coefficient of the body. Thermal expansion coefficient of each oxide are shown in Table 4.3

Table 4.3 Thermal expansion coefficient of oxide in ceramic body (47), (48), (49)

Oxide	SiO ₂	Al ₂ O ₃	Fe ₂ O ₃	TiO ₂	CaO	MgO	Na ₂ O	K ₂ O
COE(x10 ⁻⁶)	8	8	5	3	13	5	39.5	46.5

The formulation for calculation of thermal expansion coefficient by using thermal expansion coefficient of each oxide is

$$\text{COE}_{\text{body}} = (\text{Fraction of oxide}_1 \times \alpha_1) + (\text{Fraction of oxide}_2 \times \alpha_2) + \dots$$

Table 4.4 The calculation value of thermal expansion coefficient of every body formula

Body formula	COE ($\times 10^{-6}$)
Porcelain	8.99
Sanitary ware	8.79
Terra cotta	8.40
Floor tile (Stone ware)	8.98
Wall tile (Earthen ware)	9.63

4.1.4 Rheology of body slip

Viscosity of body slips were checked by using a Brook field viscometer with a spindle number 4. Na_2SiO_3 was added as a deflocculant of body slip to adjust viscosity and thixotropy of body slip.

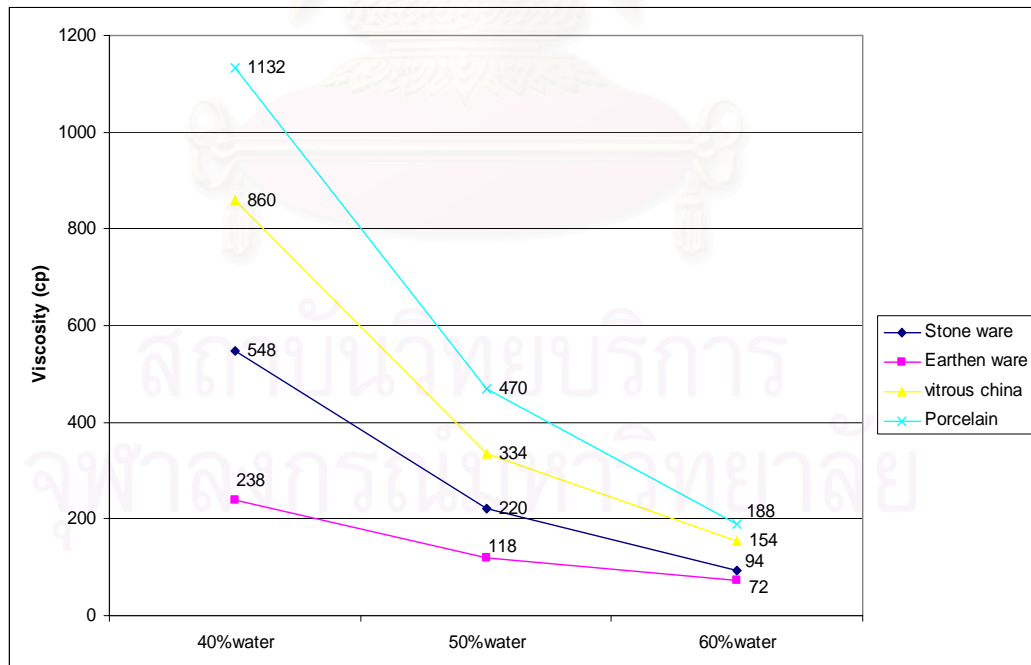


Fig 4.1 Relationship between viscosity of body slip and %solid content in various body formula (using spindle no.4)

From Fig 4.1 viscosity of porcelain slip is higher than others in all ranges of water content especially 40 %water content because the porcelain body contains high proportion of ball clay then the body slip is more viscous than other bodies.

For terra cotta body, its rheology is not suitable for casting because of its high content of red clay which is monmorillonite then body slip is very easy to swollen and very high thixotropy. The rheology of terra cotta body could not be adjusted properly by adding of deflocculant.

4.2 Characterization of Fired Specimens

4.2.1 Porcelain body

4.2.1.1 Shrinkage

As show in Fig.4.2, at low firing temperature (1150 and 1200 °C), shrinkage of fired specimens are not significantly differ but at 1250 °C, when pressing pressure for forming the specimen increases, shrinkage decreases and difference in shrinkage value between the specimen pressed with pressure of 50 bar and 150 bar was about 3% at maximum firing temperature. For slip casting, shrinkage of specimen was increased when %water content of clay slip increased.

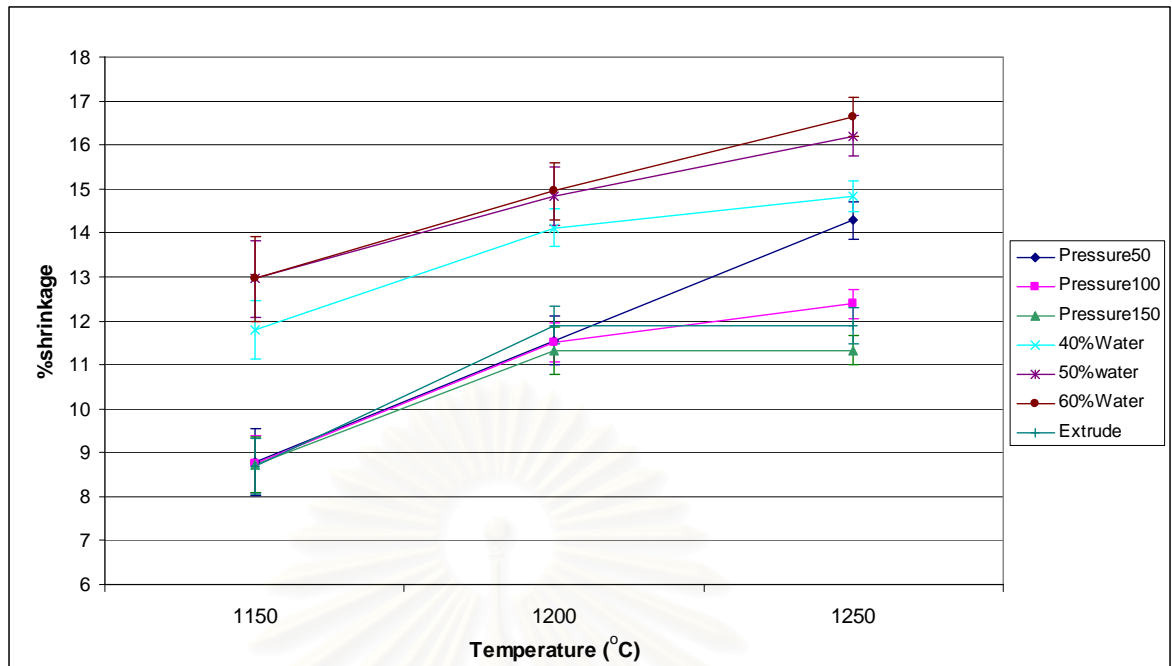


Fig 4.2 Relationship between %shrinkage and forming process in various firing temperature of porcelain body

Fig 4.2 shows %shrinkage of specimens from various forming process, the %total shrinkage of porcelain bodies from three different forming processes are clearly different. Pressed specimens show lower shrinkage than the cast ones due to higher solid content and the shrinkage decreases from 14.29% to 11.33% when increasing pressure from 50 to 150 bars due to better compaction. The high shrinkage of the cast specimens is obviously dependent on the solid content. However it is found that there is not much difference in the %total shrinkage of the 3 types of forming at low firing temperatures(1150-1200 °C) but as the temperature increases to 1250 °C, the difference becomes large. The %total shrinkage of the extruded specimen can be regarded in the same order as the pressed specimens due to the similar solid content. Moreover it seems that the shrinkage of pressed specimens at 100, 150 bars, and the extruded ones have attained their maxima at ~1200 °C.

4.2.1.2 %Water absorption

Fig 4.3 shows that the water absorption of porcelain body formed by pressing has not changed much at 1150 °C but dramatically decreases at 1200 °C and is almost zero at 1250 °C especially specimens with 150 bar pressure. Water absorption of slip casting specimens as a function of water content. All of specimens have the same tendency when temperature is increased and closely obtained zero water absorption at 1250 °C. The water content of clay slip is affected to %water absorption of fired specimen. The fired specimen of porcelain body which formed by slip casting at 40 %water content shows the lowest value of %water absorption compares to others specimens at 1250 °C.

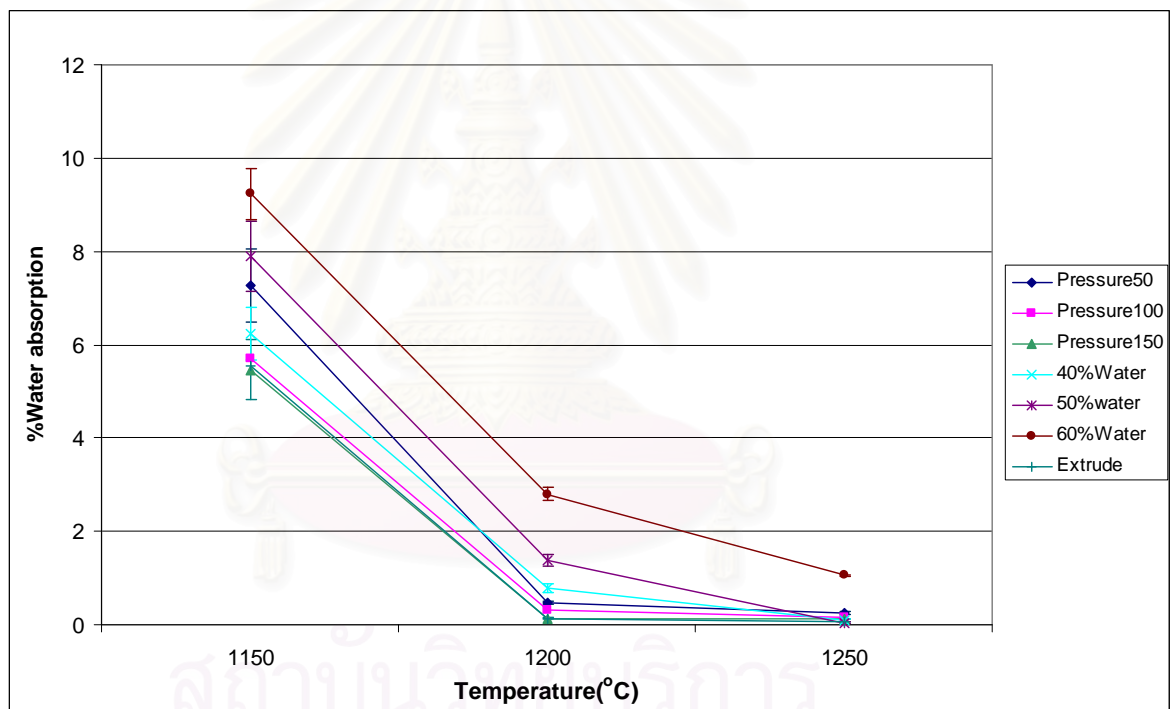


Fig 4.3 Relationship between %water absorption and forming process in various firing temperature of porcelain body

Fig 4.3 shows %water absorption of specimens from most forming processes are nearly zero except the cast body with 60%water content is 1.05%. At this temperature, porcelain body completely vitrified especially the specimens that formed by extrusion. It means that the apparent porosity of extruded body is lower than others.

However, water absorption data is not the only key to conclude the sinterability of the body but it must be compared with bulk density of the fired specimens (50).

4.2.1.3 Bulk density

Densities of sintered specimens were measured by Archimedes' method. The relationship between bulk density and firing temperature of porcelain body at various forming process is shown in Fig.4.4

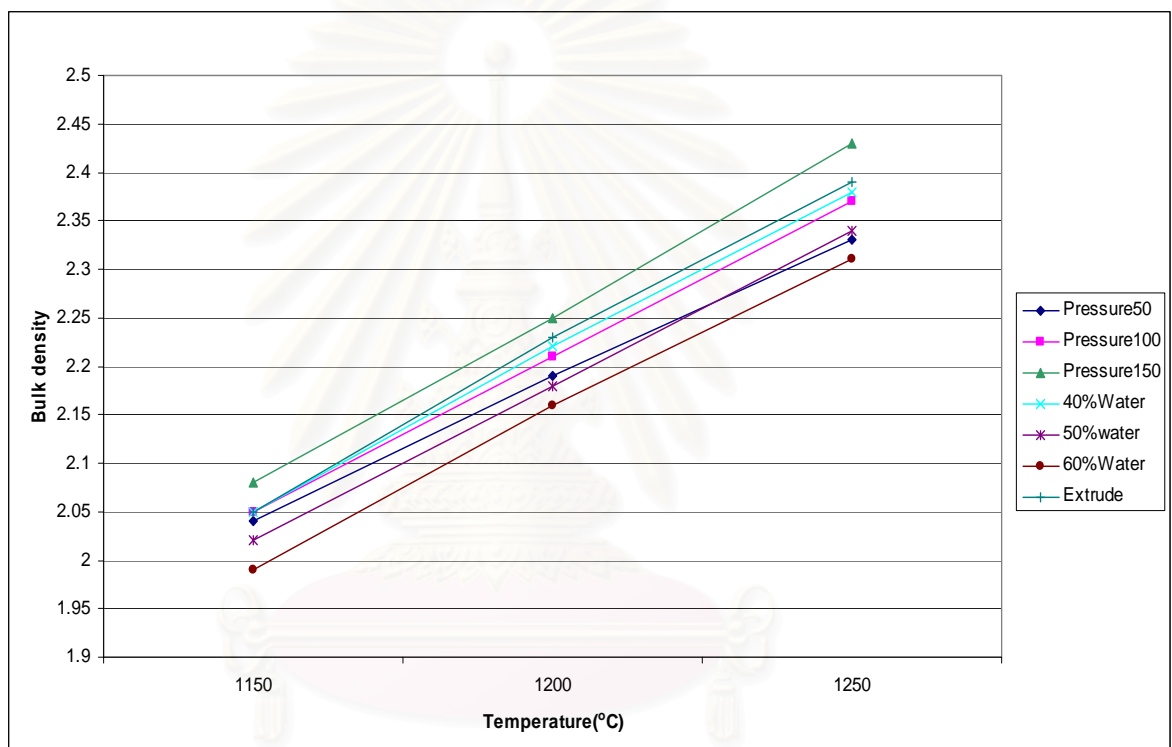


Fig 4.4 Relationship between Bulk density and various forming process in various firing temperature of porcelain body

From Fig 4.4, the bulk density of fired specimens formed by pressing at 150 bars is the highest followed by the extruding and the pressing at 100 bars, and the lowest one is the cast specimen with 60% water content, the value are 2.43, 2.39, 2.37 and 2.31 respectively. The bulk density shows the densification of specimen from different forming processes that the specimen pressed with high pressing pressure is the most densified one.

The high pressing pressure may affect the closed pores. The final bulk density is still improved by a high green density (51). Thus, the benefits of high pressing pressure are a higher sintered density and more compact rigidity. It is surprising to find that extrusion process effectively reduces porosity both in term of close and open pores due to the homogeneity of the body. The reason is a vacuum system of extrusion reduced air bubbles in extrudes clay therefore green density of specimen is as high as the pressed specimen with 150 bar pressure (52).

4.2.1.4 Bending strength

The bending strength of porcelain body increased with an increase of firing temperatures and attained maximum values of about 750 kg/cm² at 1200 °C until 1250 °C which is formed by extrusion. The strength of sintered bodies of high pressing pressure were almost the same while casted body with 60%water content obtained the lowest bending strength at maximum firing temperature.

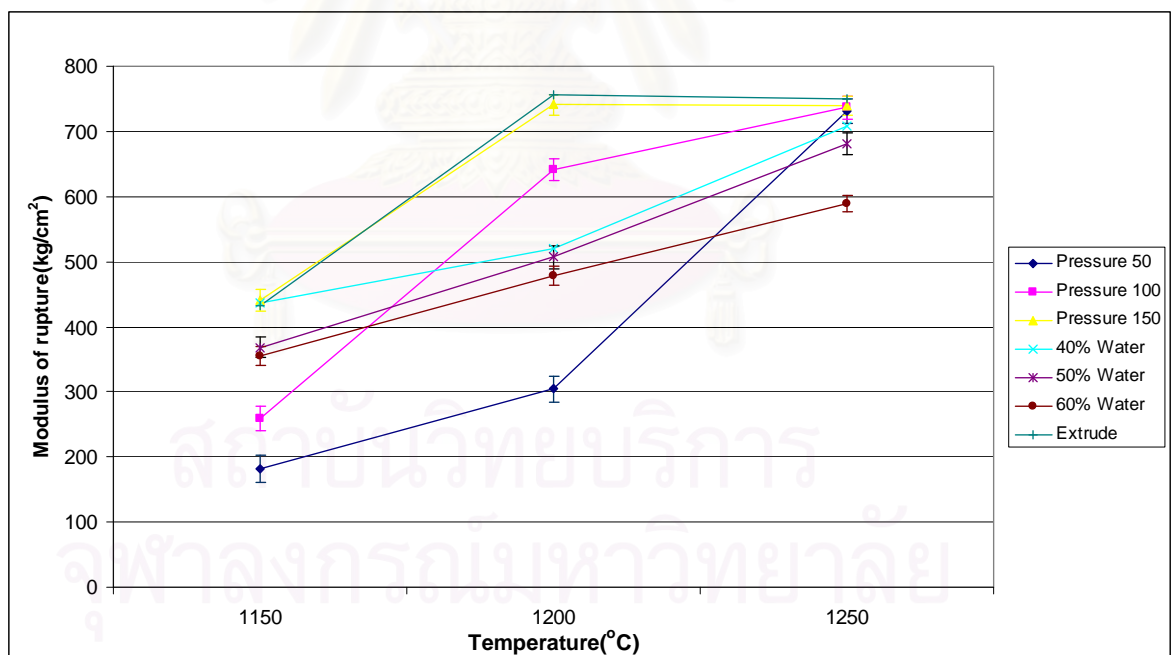


Fig 4.5 Relationship between bending strength and various forming process in various firing temperature of porcelain body

The fired specimens which were pressed at 150 bar and extruded reached the maximum strength at lower firing temperature whereas bending strength of the

other specimens of low pressing pressure obtained nearly the maximum values at higher firing temperature. Theoretically, a maximum bending strength developed when the apparent porosity decreased to zero that is fully vitrification (53).

4.2.1.5 Phase analysis by X-Ray diffraction (XRD)

Crystal phases of fired specimens of porcelain body were analyzed by X-Ray diffractometer in order to know the reaction at different firing temperatures. The effect of sintering temperature on phase transformation of mullite is shown in Fig 4.6. At temperature 1150 °C mullite phase was not occurred until 1200 °C. XRD pattern shows the small peak of mullite at 1200 °C and quartz peak is decreased when temperature is increased (54).

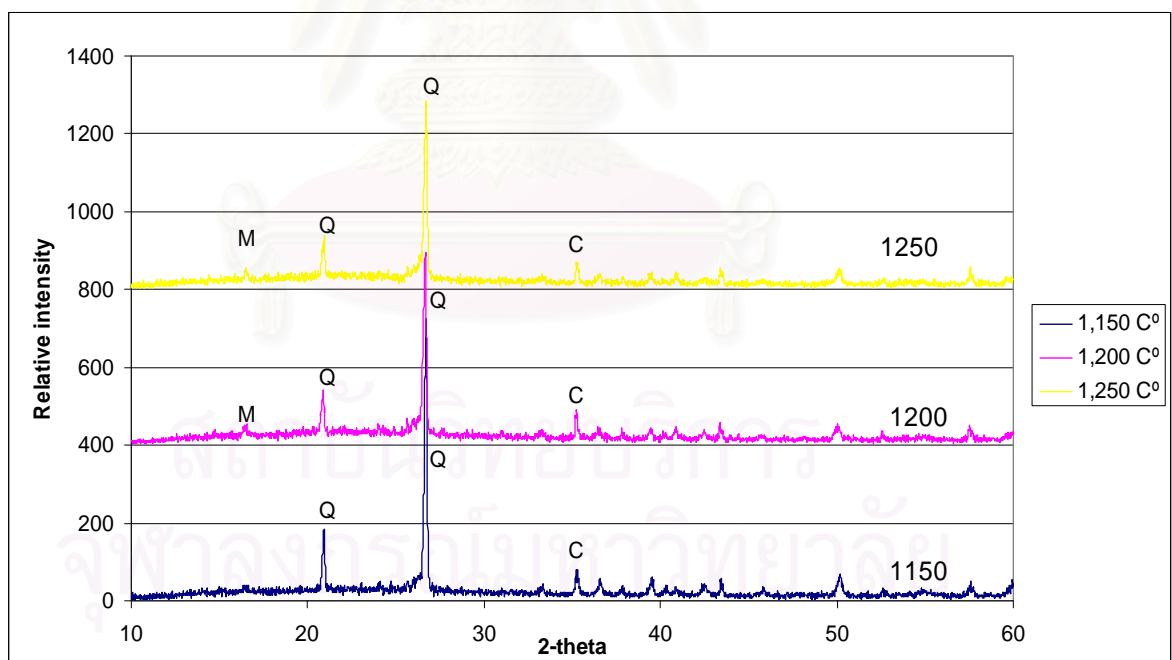


Fig 4.6 XRD pattern of porcelain forming by pressing at 150 psi and firing in various temperature

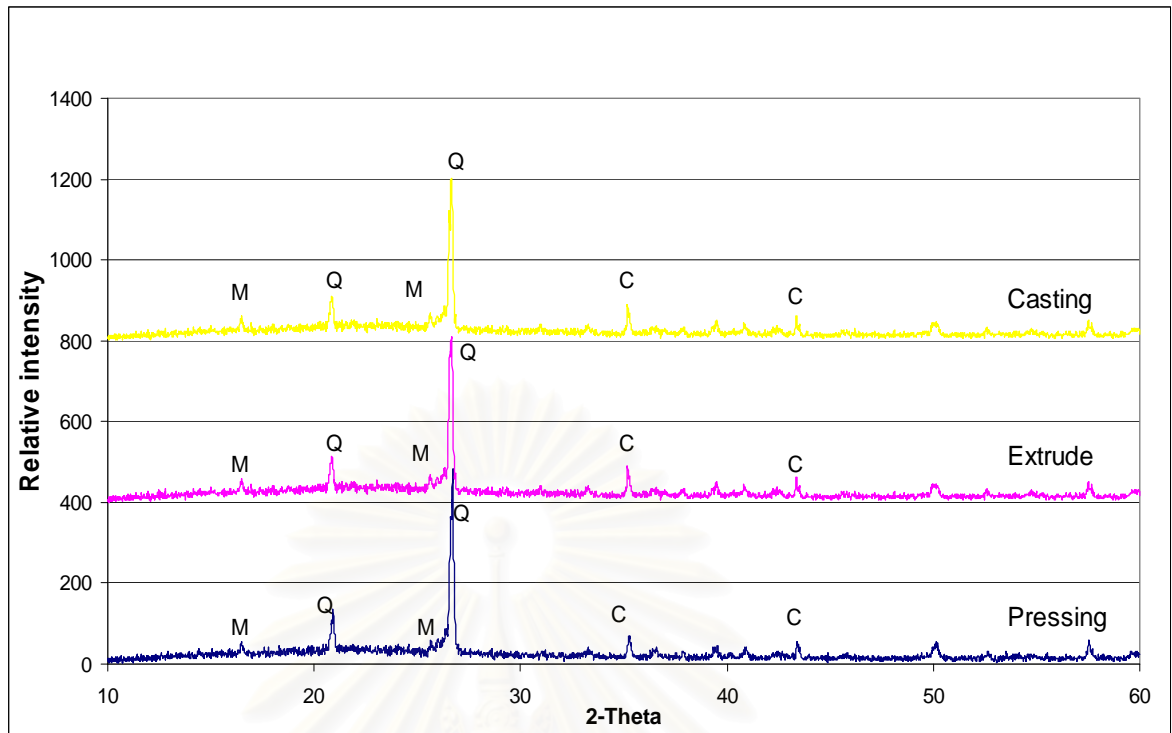


Fig 4.7 XRD pattern of porcelain body firing at 1250 °C in various forming process

Fig 4.7 shows XRD pattern of pressed specimens at pressure 150 bar, extruded specimens and cast specimens at 40 % water content fired at 1250 °C. XRD pattern shows that the intensity of quartz peak at 26.5° (55) of pressed specimen is higher than cast specimen therefore that glassy phase and free quartz of pressed specimens are higher than cast specimens (56), (57), (58).

สถาบันวิทยบริการ
จุฬาลงกรณ์มหาวิทยาลัย

4.2.1.6 Microstructure examination by Scanning electron microscope (SEM)

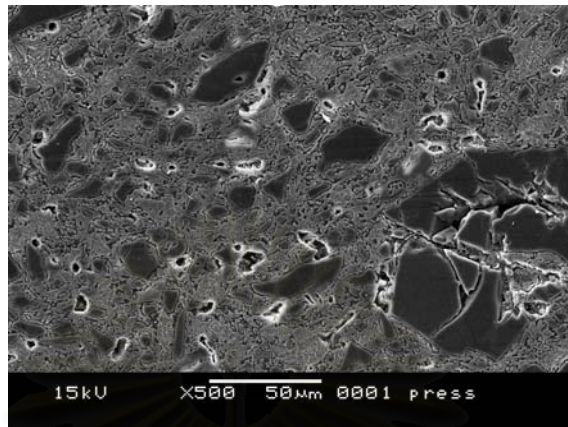


Fig 4.8 SEM images of sintered porcelain body forming by pressing at 150 psi (Firing at 1250 °C) at 500X

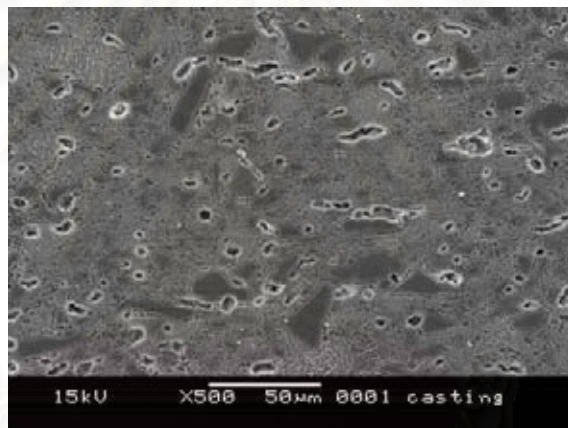


Fig 4.9 SEM images of sintered porcelain body forming by casting at 40% water content (Firing at 1250 °C) at 500X

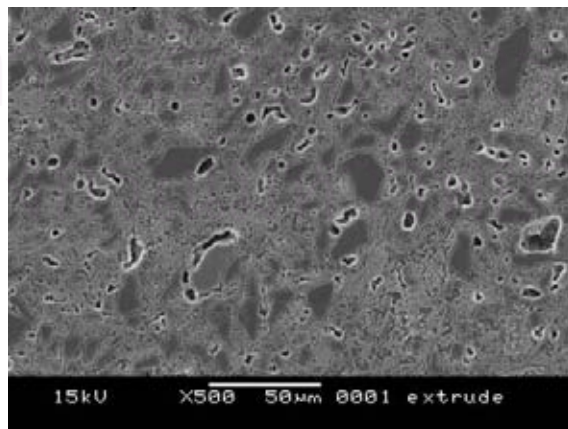


Fig 4.10 SEM images of sintered porcelain body forming by extruding (Firing at 1250 °C) at 500X

In order to examine the effect of forming force on crystal orientation and thermal expansion, the morphologies of fired specimen were examined by cutting the specimen in the direction perpendicular to the forming force. Low magnification SEM micrographs in Fig 4.8, 4.9, 4.10 shows the variation of shape and amount of porosities in the specimens from pressing, casting and extruding processes fired at 1250 °C. SEM examination revealed that the closed porosity developments are due to the glassy phase and trapped gases in pores (59). The pore shapes of the specimens from casting process are cylindrical pores and the amount of pores are more than other specimens. The specimens which formed by extrusion has less tendency to obtain cylindrical pores than casting specimens while pressed specimen has round shape pores and less amount of pores than extruded and cast specimens (60).

Pores are an inherent part of liquid phase sintering. Pores are presented in the compaction of green specimens as interparticle voids and also can resulted from viscosity of the glassy phase while firing temperatures are increased. Shapes of pores are depends on the surface tension of the glassy phase. The particle shape, size of particle and pores, contact angle between particles, amount of glassy phase is affected to surface tension of the glassy phase (61).

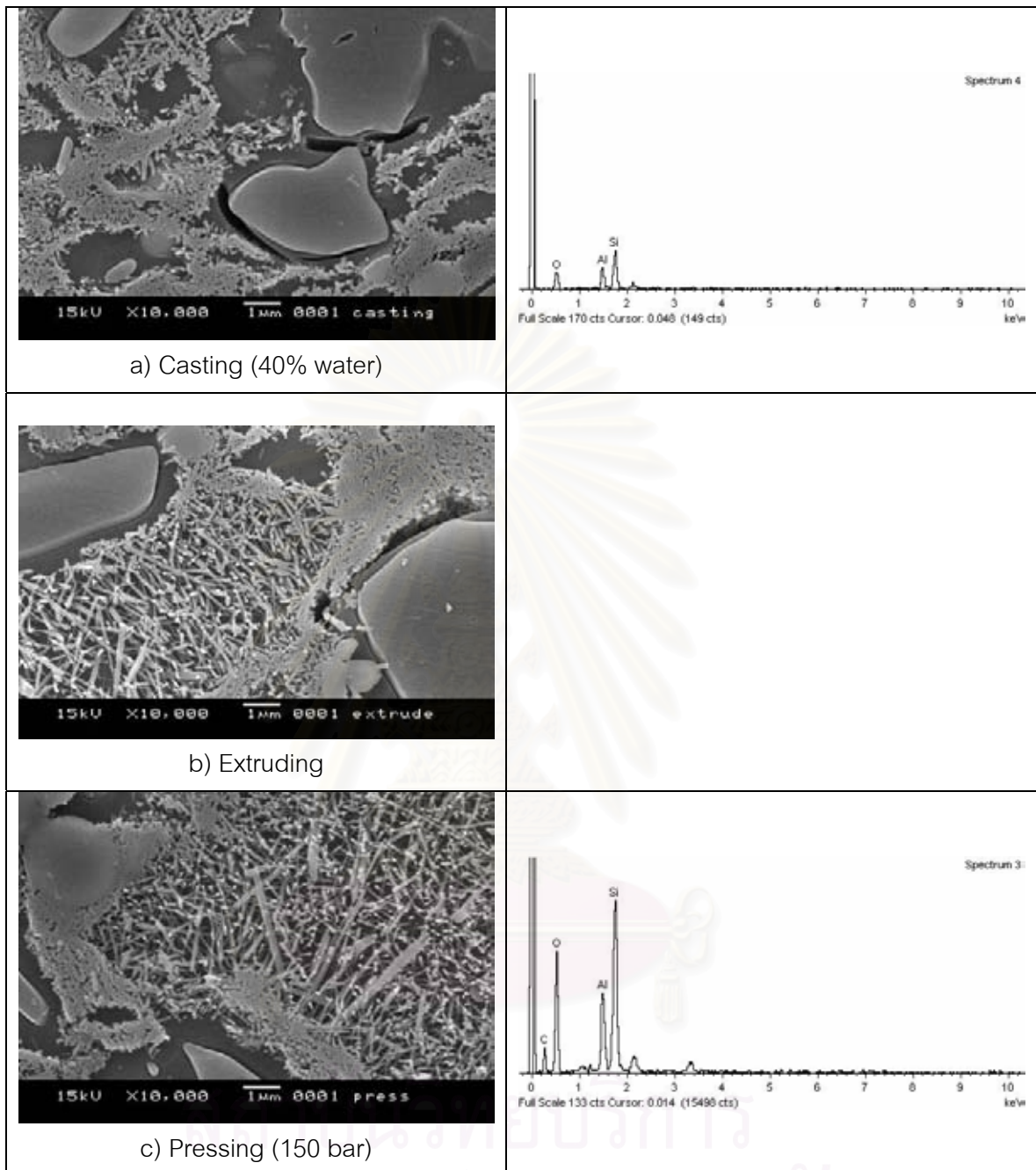


Fig.4.11 SEM image and EDS graphs of sintered porcelain body at 1250 °C formed by different forming process at 10,000X

Fig 4.11 shows the acicular mullite crystals and quartz grains in fired porcelain body. From XRD result there was no evidence in the different phase formation. However, there is clearly difference in morphology of mullite crystals formed in the specimens from different processes. As can be seen in Fig 4.11 (a) the morphology of crystallized mullite

is interlocked short needle (62) which can be distinguished from mullite crystals in Fig 4.11 (b) and (c). Morphology of mullite crystals in the specimens from extruding and pressing are interlocked mullite crystals with higher aspect ratio compares to the morphology of mullite in the cast specimen. From EDS analysis the short needle mullite of cast specimens are primary mullite (63) while long needle mullite of press specimens is secondary mullite (64). In general primary mullite trends to change to secondary mullite with increasing of firing temperature, soaking time or change in composition (65) but this research shows the densification of specimen has an effect on morphology of mullite crystal.



สถาบันวิทยบริการ
จุฬาลงกรณ์มหาวิทยาลัย

4.2.1.7 Thermal expansion coefficient

As shown in Fig.4.12, the thermal expansion coefficient of the porcelain body prepared by different was pressing pressure. When pressing pressure was increased, thermal expansion coefficient increased as firing temperature increased.

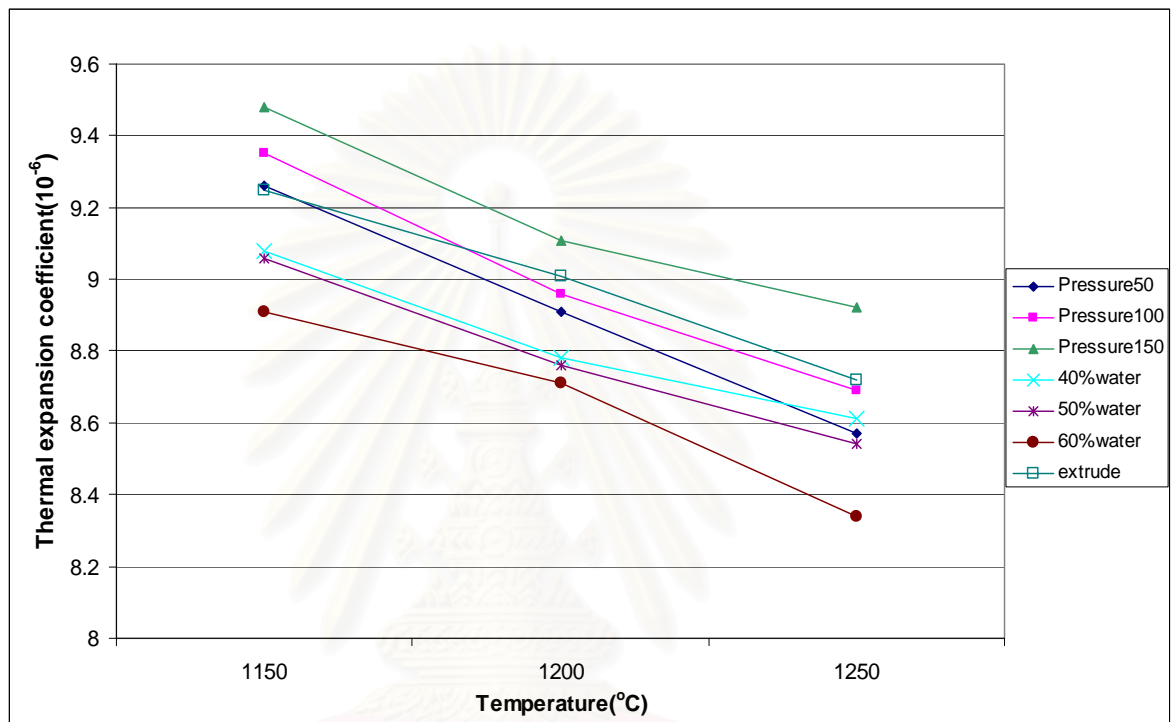


Fig 4.12 Relationship between thermal expansion coefficient and various forming process in various firing temperature of porcelain body (range of temperature 20-500 °C)

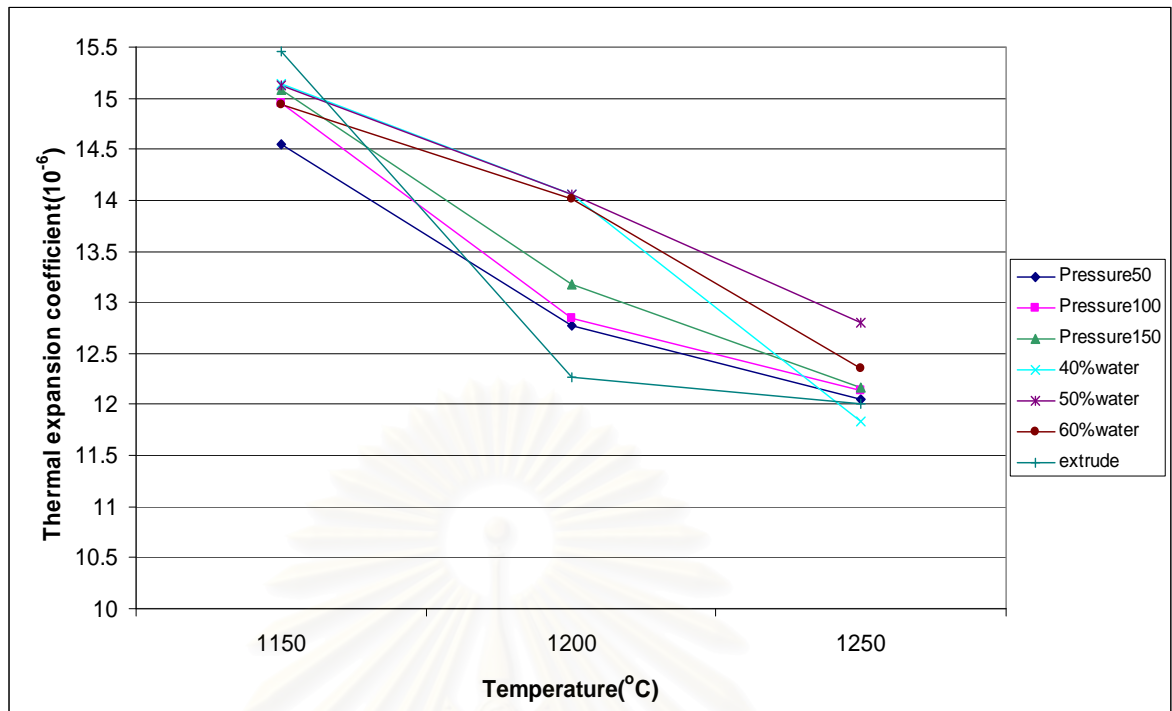


Fig 4.13 Relationship between thermal expansion coefficient and various forming process in various firing temperature of porcelain body (range of temperature 500-600 °C)

As shown in Fig.4.12, the thermal expansion coefficient of the porcelain body prepared by different %solid content. When %solid content was increased, thermal expansion coefficient increased as firing temperature increased.

Fig 4.12 shows pressed with 150 bar pressure are higher than that of the specimens pressed with 50 bar about 4 %. The cast specimens with high solid content has higher thermal expansion coefficient than the specimen with low solid content because of the higher bulk density.

The dilatometric data show that the thermal expansion coefficient of pressed specimens of 150 bar is about $8.93 \times 10^{-6} \text{ } ^\circ\text{C}^{-1}$ which is higher than the extruded and cast specimens fired at all firing temperatures. The reason is related to bulk density. The body which has the same chemical composition and firing temperatures but different in forming process exhibits different thermal expansion. The specimen formed by high bulk density process (high pressure pressing) obtained higher thermal expansion than low bulk density process after firing. The theoretical value of thermal expansion coefficient calculated from proportion of oxides in porcelain body from

Table 4.4 is $8.99 \times 10^{-6} \text{ } ^\circ\text{C}^{-1}$. The measured thermal expansion of the specimen with low bulk density has lower thermal expansion than the calculated value. On the other hand the measured and calculated thermal expansion of the specimen with high bulk density did not show any significant difference. Therefore, thermal expansion coefficient can be estimated from bulk density of fired specimens. Forming process has strong effect on densification of the specimen and related to the difference of thermal expansion as well.

Fig 4.13 show thermal expansion coefficient of the specimens at 500-600 $^\circ\text{C}$ which is a range of quartz inversion (66). From the graph there is no significant different to explain the relation between thermal expansion coefficient at 500-600 $^\circ\text{C}$ and 20-500 $^\circ\text{C}$.



สถาบันวิทยบริการ
จุฬาลงกรณ์มหาวิทยาลัย

4.2.2 Vitreous China

4.2.2.1 Shrinkage

As shown in Fig.4.14, at low firing temperature (1150 °C), shrinkage of fired specimens are not significantly differ but at 1200 °C, when pressing pressure for forming the specimen increases, shrinkage decreases and difference in shrinkage value between the specimen pressed with pressure of 50 bar and 150 bar was about 2.5% at maximum firing temperature. Moreover it seems that the shrinkage of pressed specimens at 50, 100, 150 bars have attained their maxima at ~1200 °C. For slip casting, shrinkage of specimens is increased when %water content of clay slip increases.

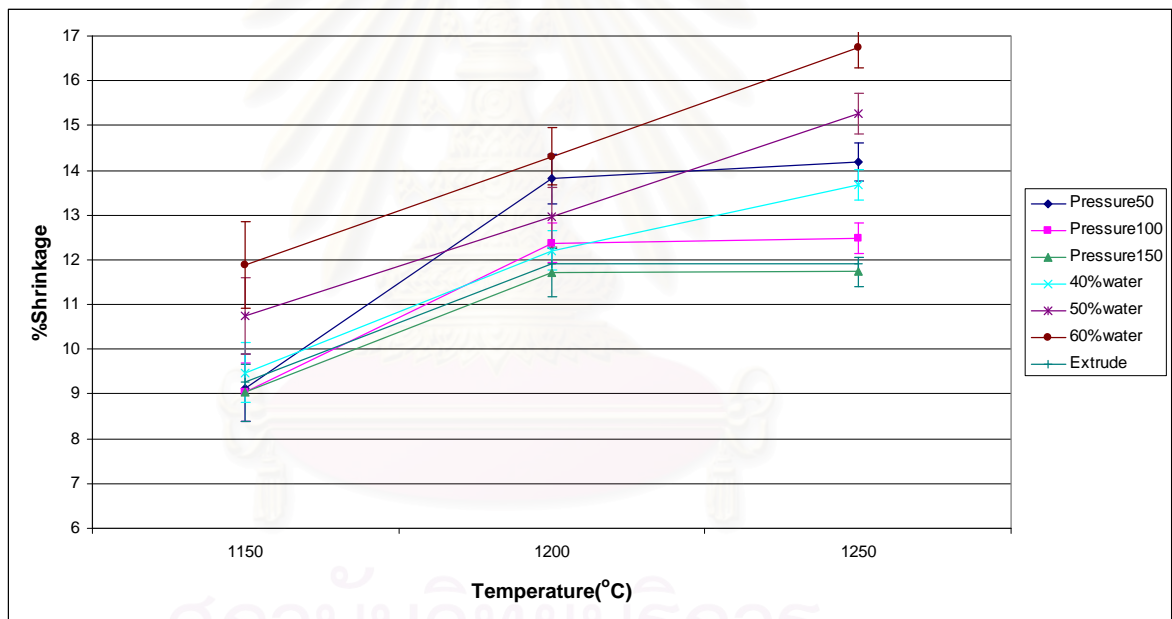


Fig 4.14 Relationship between %shrinkage and forming process in various firing temperature of vitreous china body

Fig 4.14 shows %shrinkage of specimens from various forming processes. %shrinkage of the pressed specimen with 150 bar pressure is the lowest one while the cast specimen with 60% water content is the highest value and the different of the lowest and highest value is about 5%. Even this body formula is designed for casting process but cast specimen is higher shrunk than pressed and

extruded specimens because they have more moisture content between drying process.

4.2.2.2 Water absorption

Fig 4.15 shows that the water absorption of vitreous china body formed by pressing has not changed much at 1150 °C but dramatically decreases at 1200 °C and is almost zero at 1250 °C especially specimens with 150 bar pressure. Fig 4.15 shows water absorption of slip casting specimens as a function of water content. All of specimens have the same tendency with pressing process but at 1200 °C %water absorption of casted specimen is higher than pressed specimen. When temperature is increased to 1250 °C, water absorption of casted specimen is closely obtained zero. The water content of clay slip is affected to %water absorption of fired specimen. The fired specimen of vitreous china body which formed by slip casting at 40 %water content show the lowest value of %water absorption when compares to other specimens at 1250 °C.

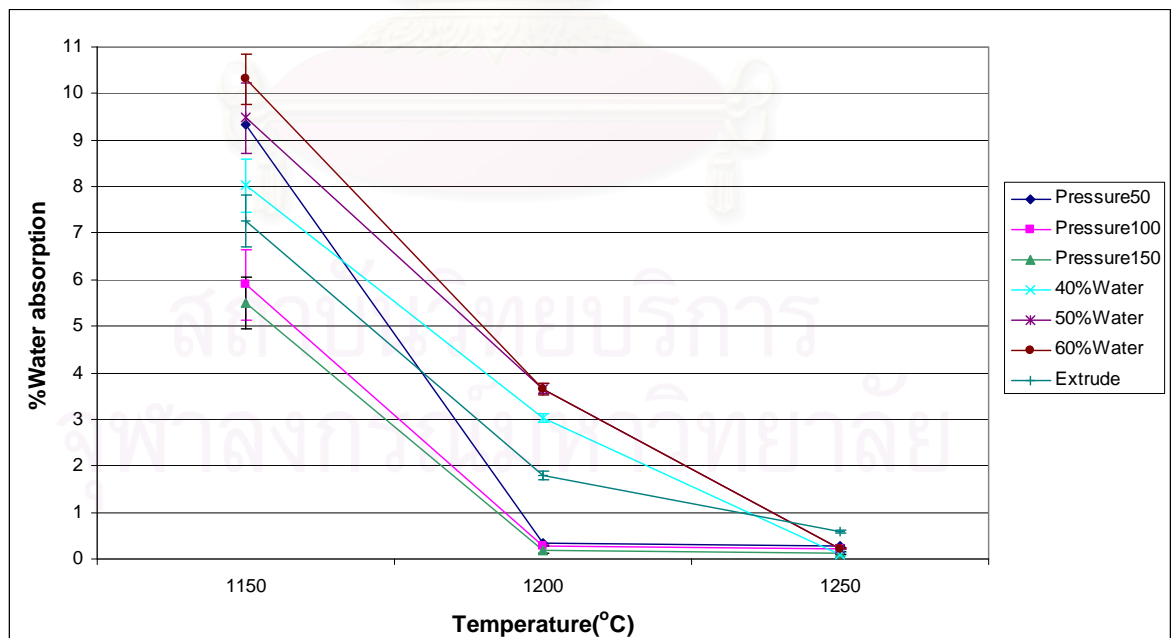


Fig 4.15 Relationship between %water absorption and forming process in various firing temperature of vitreous china body

4.2.2.3 Bulk density

From Fig 4.16, the bulk density of specimens casted at 40% water content is the highest followed by the pressed at 150 bars and the extruded, and the lowest one is the pressed specimen with 50 bar pressure, which is in agreement with the results shown in Fig.4.15. The high solid content in body may affect the closed pores. This vitreous china body is designed for slip casting processes which have good clay for rheology then cast specimens have higher bulk density than pressed specimens.

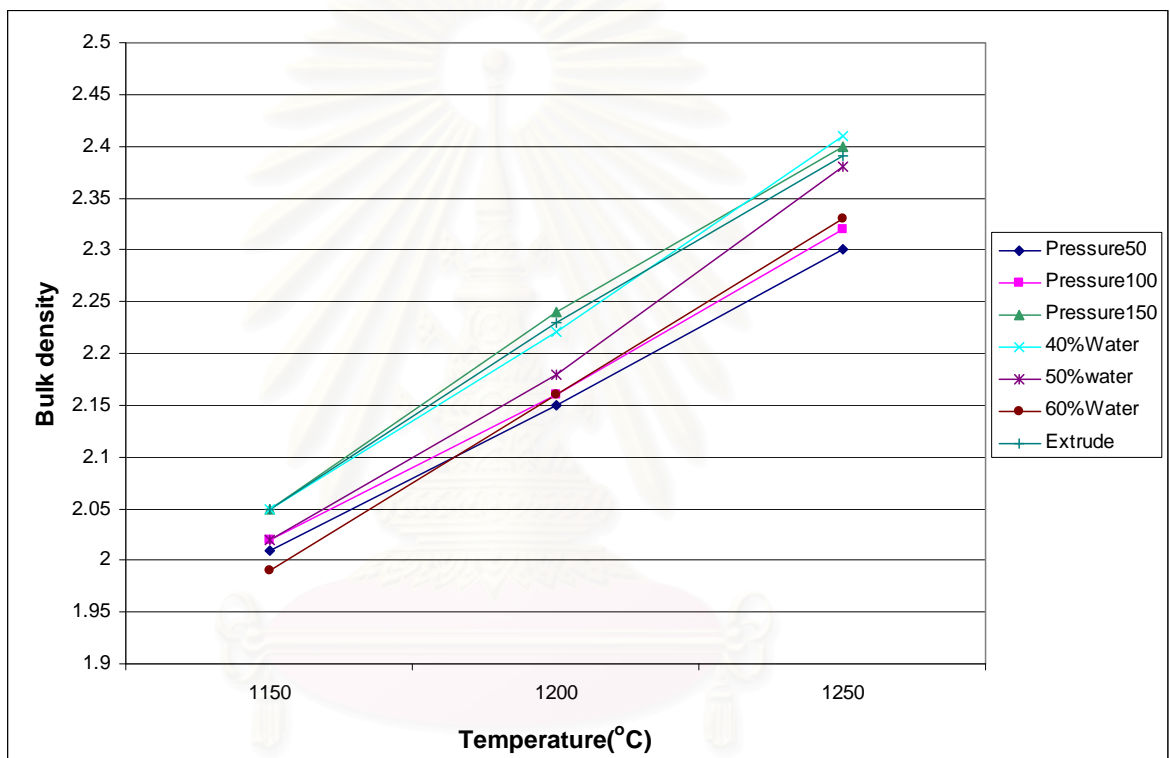


Fig 4.16 Relationship between Bulk density and various forming process in various firing temperature of vitreous china body

4.2.2.4 Bending strength

Fig.4.17 shows the bending strength of vitreous china body increased with an increase of firing temperatures and attained maximum values of about 573 kg/cm² at 1250 °C. The strength of sintered bodies of high pressing pressure are almost the same value at 1200 °C to 1250 °C and at 1200 °C, pressed specimens have higher bending strength than other process. It is mean that pressed specimen is fully sintered at lower temperature while cast specimens and extruded specimens obtained lower bending strength at 1200 °C.

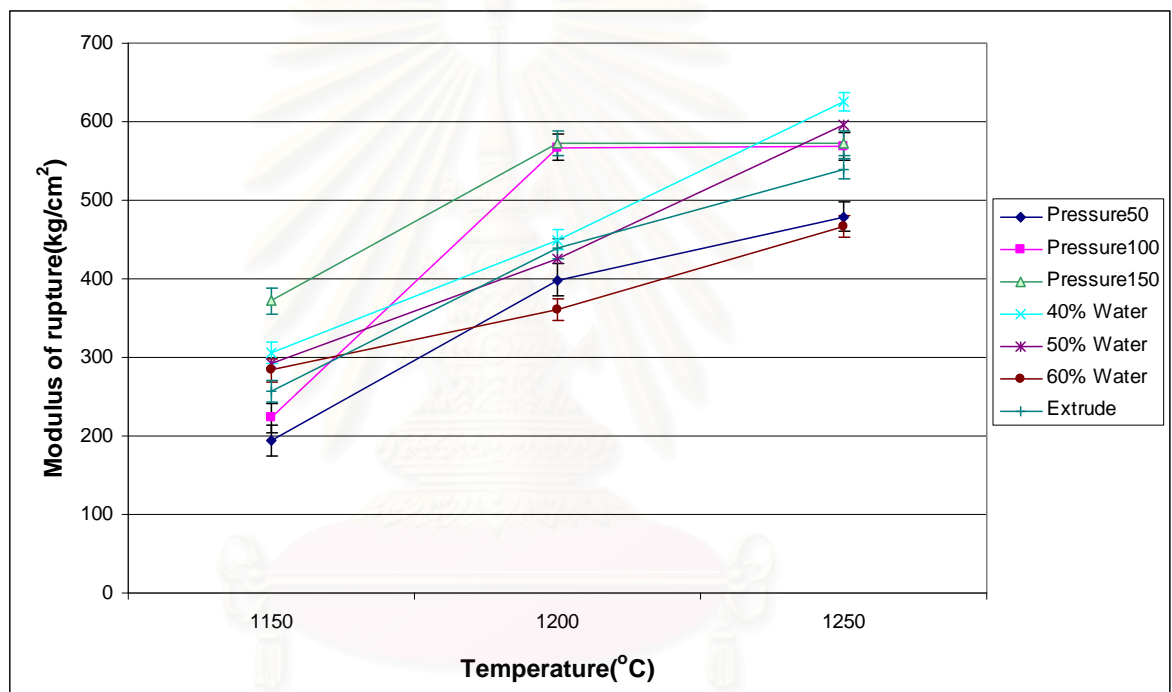


Fig 4.17 Relationship between bending strength and forming process in various firing temperature of vitreous china body

The fired specimens which are cast with 40% and 50% water content reached the maximum strength at max firing temperature whereas bending strength of the specimens at low pressing pressure obtained the lowest values. The difference of the strength from the highest value was about 175 kg/cm² at max firing temperature. From the result is presented that even if the same body formula but different in forming process is generated wide range of bending strength. Theoretically, a maximum

bending strength developed when the apparent porosity decreased to zero which achieved fully vitrification.



สถาบันวิทยบริการ
จุฬาลงกรณ์มหาวิทยาลัย

4.2.2.5 Phase analysis by X-Ray diffraction (XRD)

Crystal phases of fired specimens of vitreous china body are analyzed by X-Ray diffractometer in order to know the reaction at different firing temperatures. The effect of sintering temperature on phase transformation of mullite is shown in Fig 4.19. At temperature 1150 °C mullite phase was not occurred until 1200 °C the mullite phase was shown. XRD patterns show the small peak of mullite at 1200 °C and 1250 °C, the intensity of quartz peak is decreased when temperature is rise.

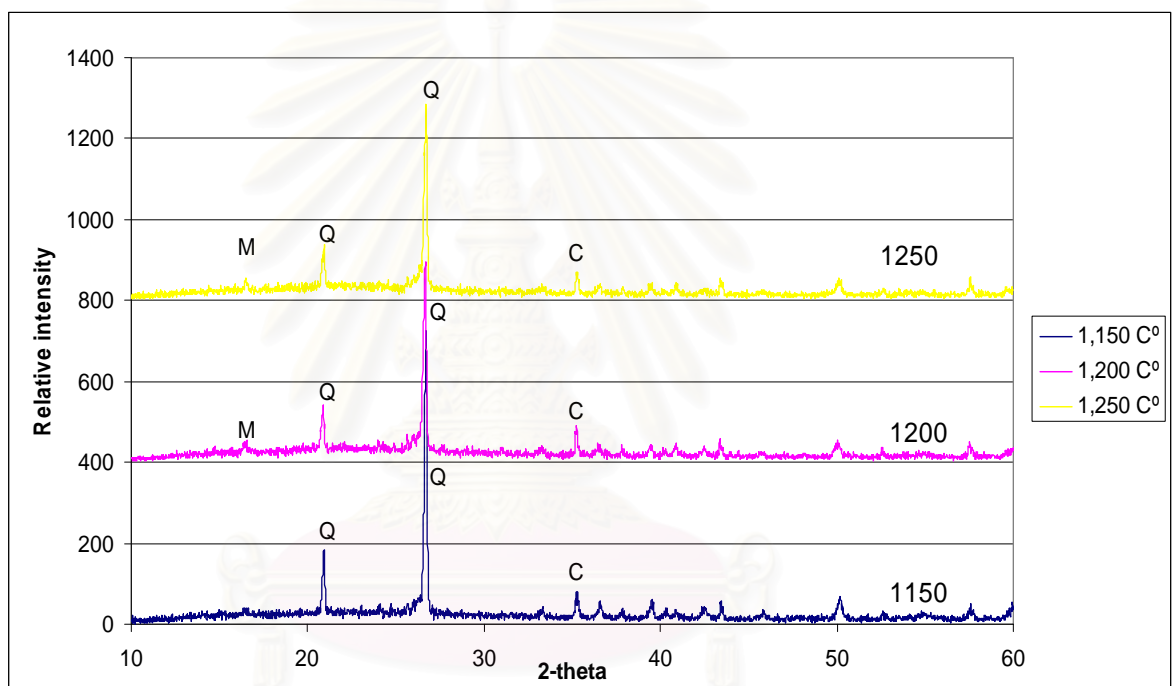


Fig 4.18 XRD pattern of vitreous china forming by pressing at 150 psi and firing in various temperature

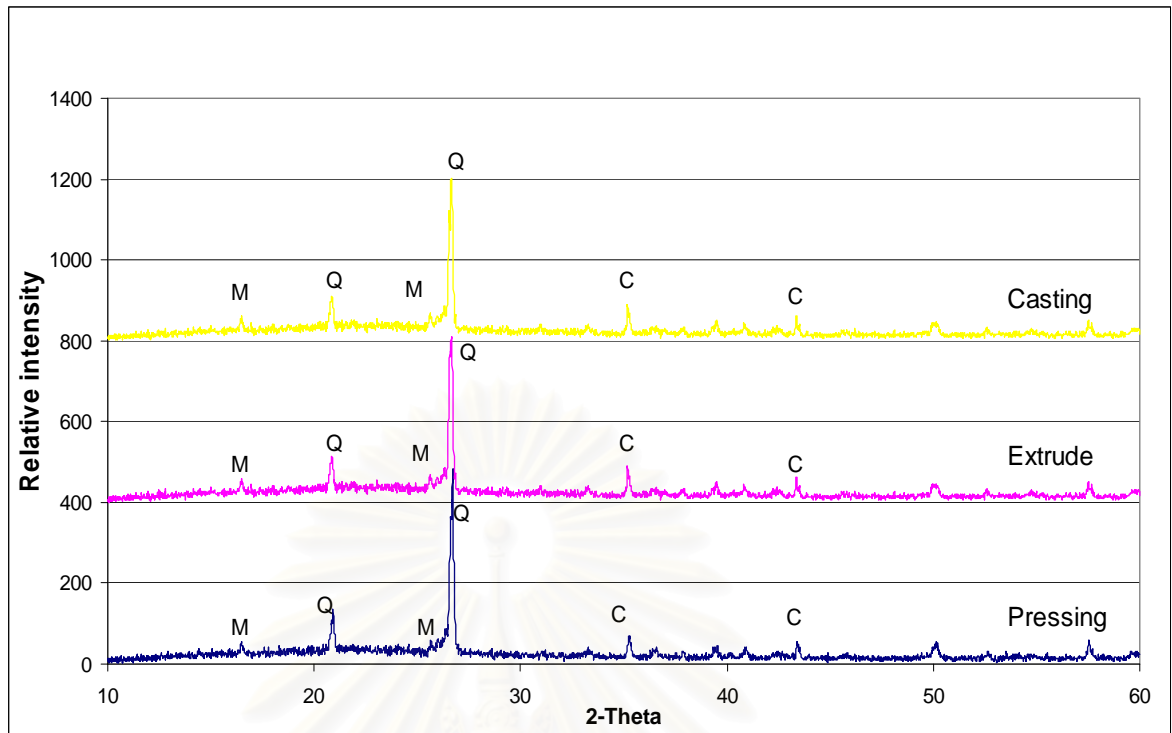


Fig 4.19 XRD pattern of vitreous china body firing at 1250 °C in various forming process

Fig 4.19 shows XRD patterns of pressed specimens at pressure 150 bar, extruded specimens and cast specimens at 40 % water content fired at 1250 °C. XRD patterns show that the intensity of quartz peak of pressed specimen is higher than cast specimen therefore; glassy phase and free quartz of pressed specimens are higher than the cast specimens.

4.2.2.6 Microstructure examination by Scanning electron microscope (SEM)

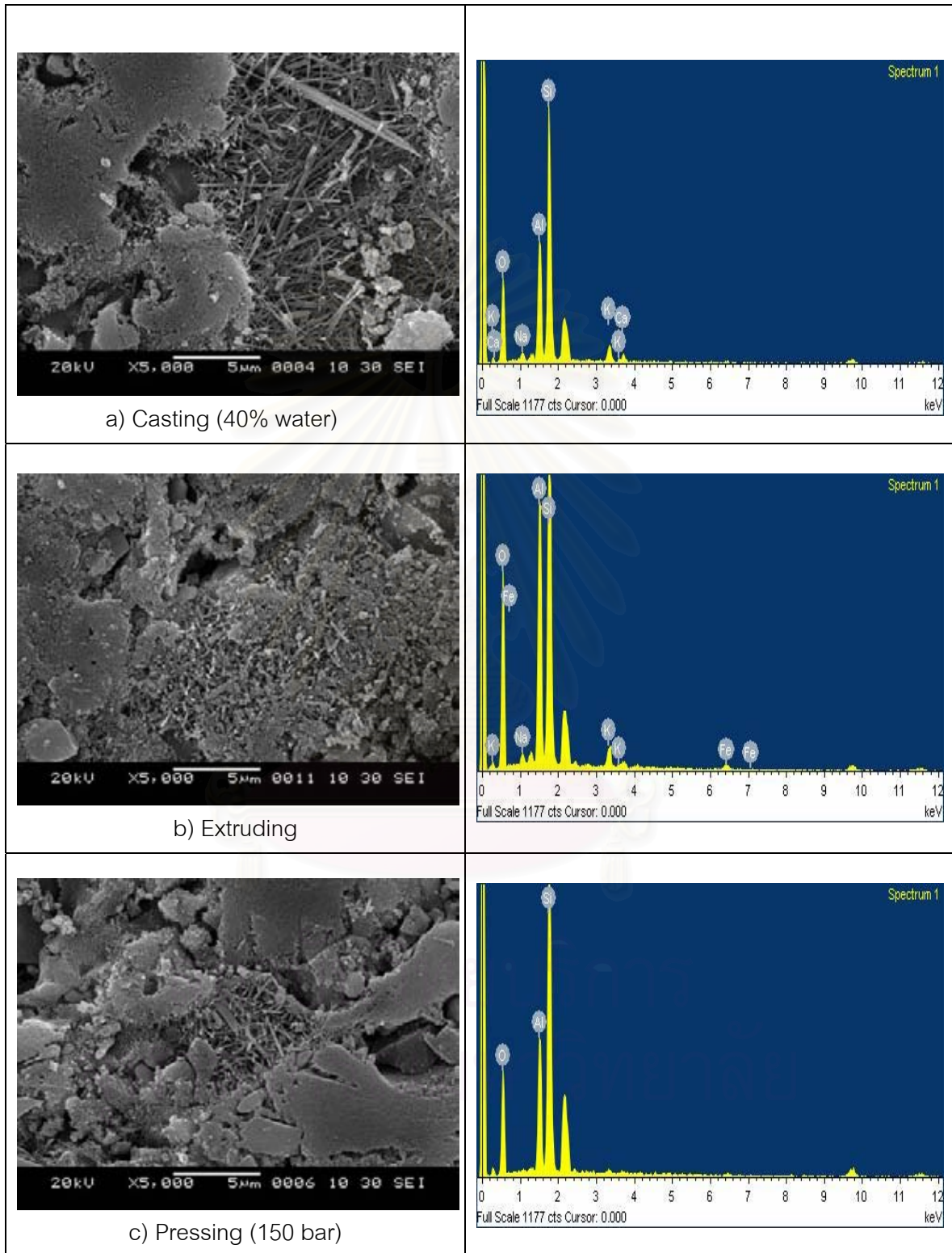


Fig.4.20 SEM image and EDS graphs of sintered vitreous china body at 1250 °C by various forming process at 5000X

Fig 4.20 shows the acicular mullite crystals and quartz grains in fired vitreous china body. From XRD result there was no evidence of the different phase formation. However, there is clearly difference in morphology of mullite crystals formed in the specimens by different forming processes. As can be seen in Fig 4.20 (a) and (c) the morphology of crystallized mullite is long needle which can be distinguished from mullite crystals in Fig 4.20 (b). Morphology of mullite crystals in the cast and pressed specimens are long needle mullite crystals with higher aspect ratio compares to the morphology of mullite in the extruded specimen. From EDS analysis the short needle mullite of extruded specimens are primary mullite while long needle mullite of cast and pressed specimens are secondary mullite. In general primary mullite trends to transform to secondary mullite with an increasing of firing temperature, soaking time or change in composition but this research shows the densification of specimen has an effect on morphology of mullite crystal.



4.2.2.7 Thermal expansion coefficient

As shown in Fig.4.21, the thermal expansion coefficient of the vitreous china body pressed by different pressing pressures. When pressing pressure was increased, thermal expansion coefficient increased at as firing temperature.

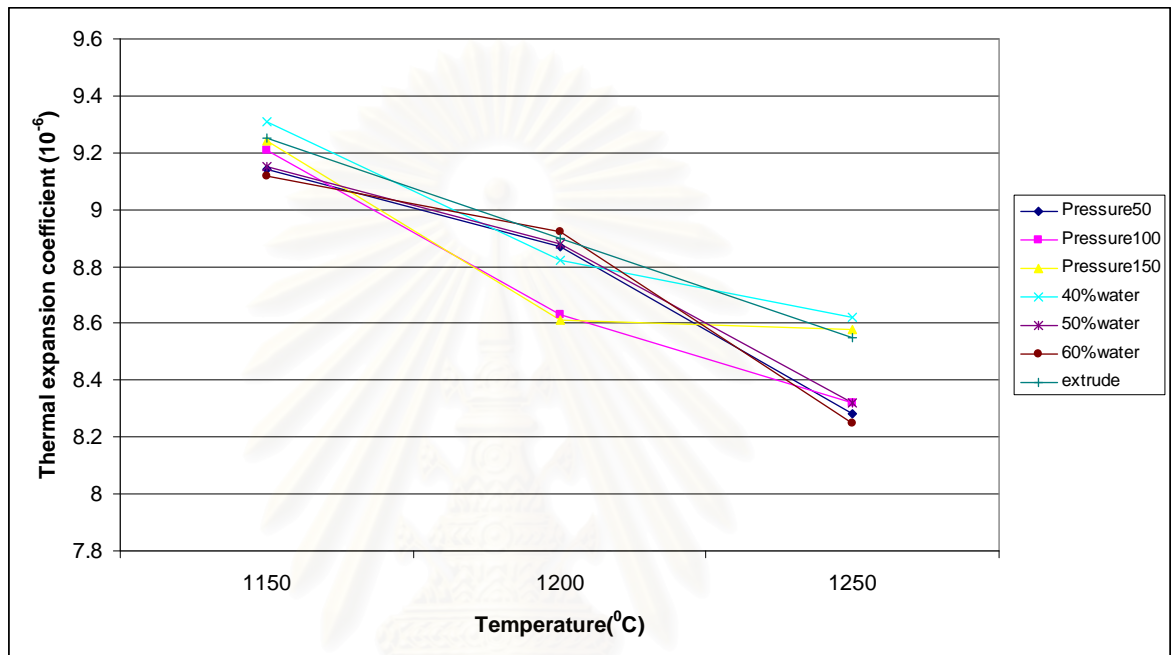


Fig 4.21 Relationship between thermal expansion coefficient and forming process in various firing temperature of vitreous china body (range of temperature 20-500 °C)

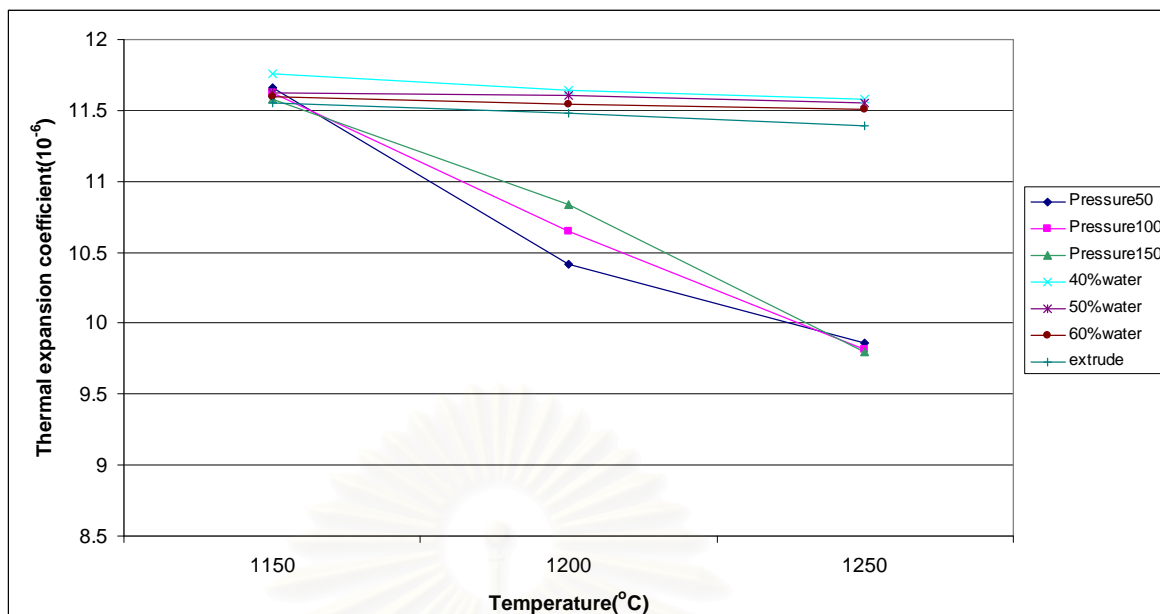


Fig 4.22 Relationship between thermal expansion coefficient and forming process in various firing temperature of vitreous china body (range of temperature 500-600 °C)

As shown in Fig.4.21, the thermal expansion coefficient of the vitreous china body prepared by different %solid content. When %solid content was increased, thermal expansion coefficient increased at max firing temperature

The cast specimens with high solid content has higher thermal expansion coefficient than the specimen with low solid content because of the higher bulk density.

The dilatometric data show that the thermal expansion coefficient of cast specimens of 40% water content is about $8.62 \times 10^{-6} \text{ } ^\circ\text{C}^{-1}$ which is higher than the extruded and pressed specimens at all firing temperatures. The reason is related to bulk density. The body which has the same chemical composition and firing temperatures but different in forming process exhibits different thermal expansion. The specimen formed by high bulk density process (high %solid content) obtained higher thermal expansion than low bulk density process after firing. The theoretical value of thermal expansion coefficient calculated from proportion of oxides in vitreous china body from Table4.4 is $8.79 \times 10^{-6} \text{ } ^\circ\text{C}^{-1}$. The measured thermal expansion of the specimen with low bulk density has lower thermal expansion than the calculated value. On the other hand the measured and calculated thermal expansion of the specimen with high bulk density did not show any significant difference. Therefore, thermal expansion

coefficient can be estimated from bulk density of fired specimens which is in the same tendency as porcelain body. Forming process has strong effect on densification of the specimen and related to the difference of thermal expansion as well.

Fig 4.22 shows thermal expansion coefficient of the specimens at 500-600 °C which is in a range of quartz inversion. The graph shows very significant about thermal expansion coefficient of the pressed specimens and cast specimens at 1250 °C but thermal expansion coefficient at 500-600 °C and 20-500 °C are not related.



สถาบันวิทยบริการ
จุฬาลงกรณ์มหาวิทยาลัย

4.2.3 Stoneware Body

4.2.3.1 Shrinkage

As show in Fig.4.23, at low firing temperature (1100 and 1150 °C), shrinkage of fired specimens are not significantly differ but dramatically decreases at 1200 °C. Shrinkage value between the pressed specimens with pressure of 50 bar is higher than that of 150 bar about 1.5% at 1150 °C firing. For slip casting, shrinkage of specimen was increased when %water content of clay slip increase. When the temperature was rise to 1200 °C the decrease of shrinkage is due to the stoneware body contains high percentage of Na_2O and K_2O and Fe_2O_3 which are fluxing agent then this type of body is considered low melting point. The stoneware body bloated or overfiring at maximum firing temperature therefore size of specimens is expanded then seems to be shrinkage is decreased.

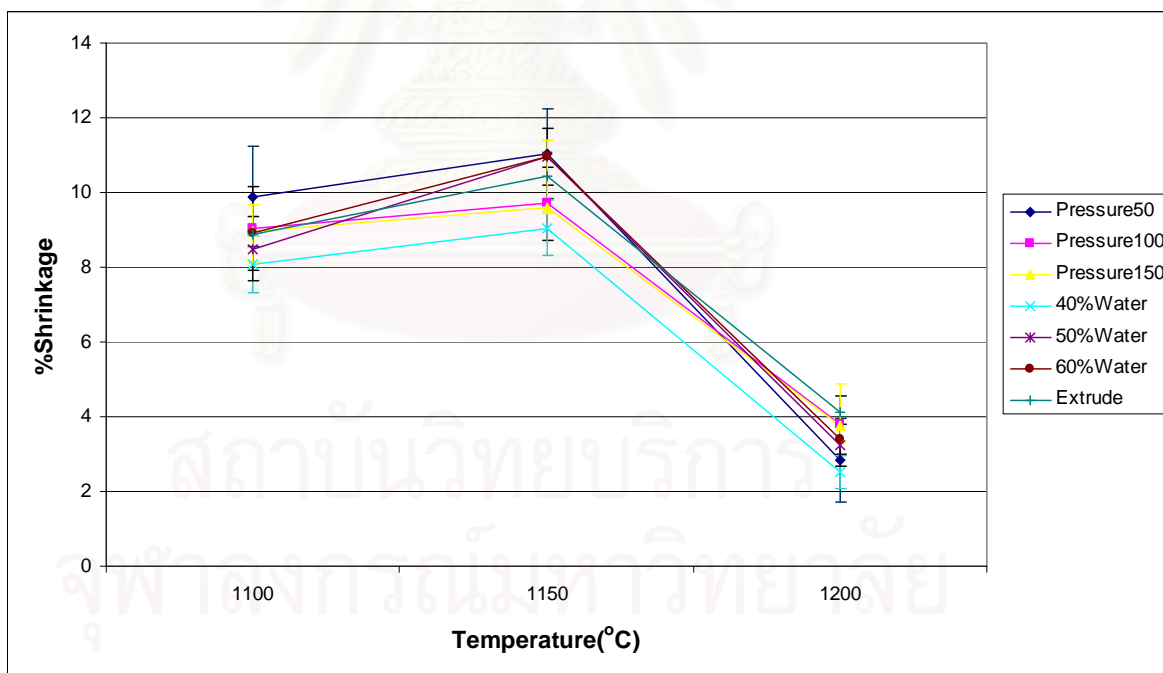


Fig 4.23 Relationship between %shrinkage and forming process in various firing temperature of stoneware body

4.2.3.2 Water absorption

Fig 4.24 shows that the water absorption of stoneware body formed by pressing has significant different between high pressure and low pressure at 1100 °C but almost the same value in each pressing pressure at 1150 °C. At 1200 °C, water absorption of specimens is increased because of the bloating effect (as shown in Fig.4.25). Fig 4.24 shows water absorption of slip cast specimens as a function of water content. All of specimens have the same tendency with pressing process but at 1200 °C %water absorption of cast specimen at 40%water content is higher than pressed specimen.

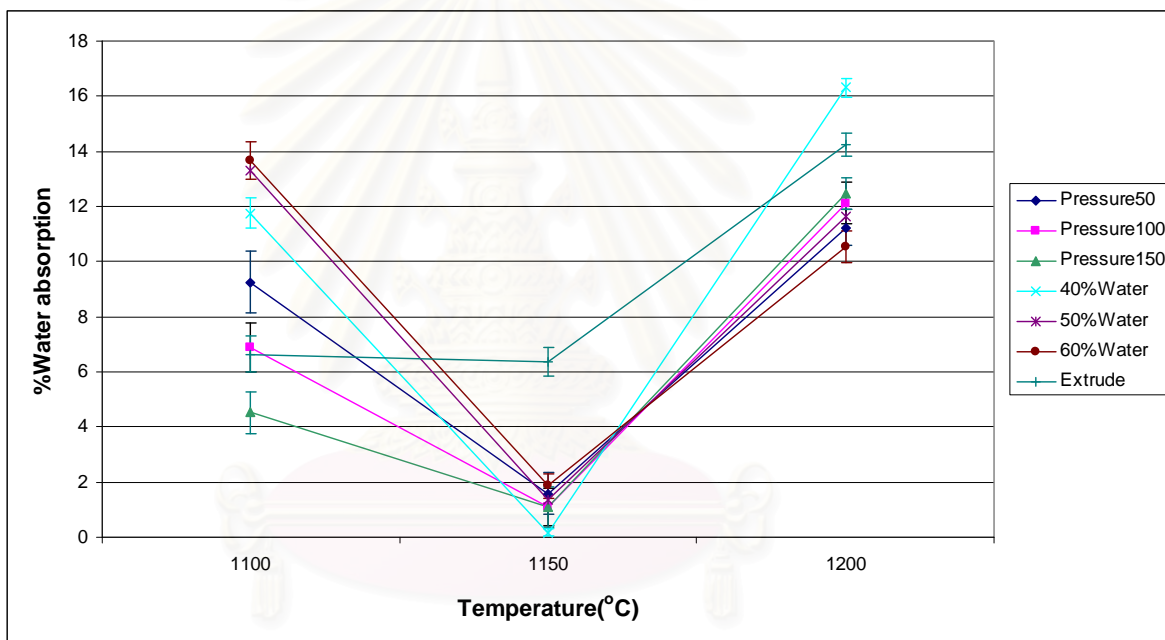


Fig 4.24 Relationship between %water absorption and forming process in various firing temperature of stoneware body

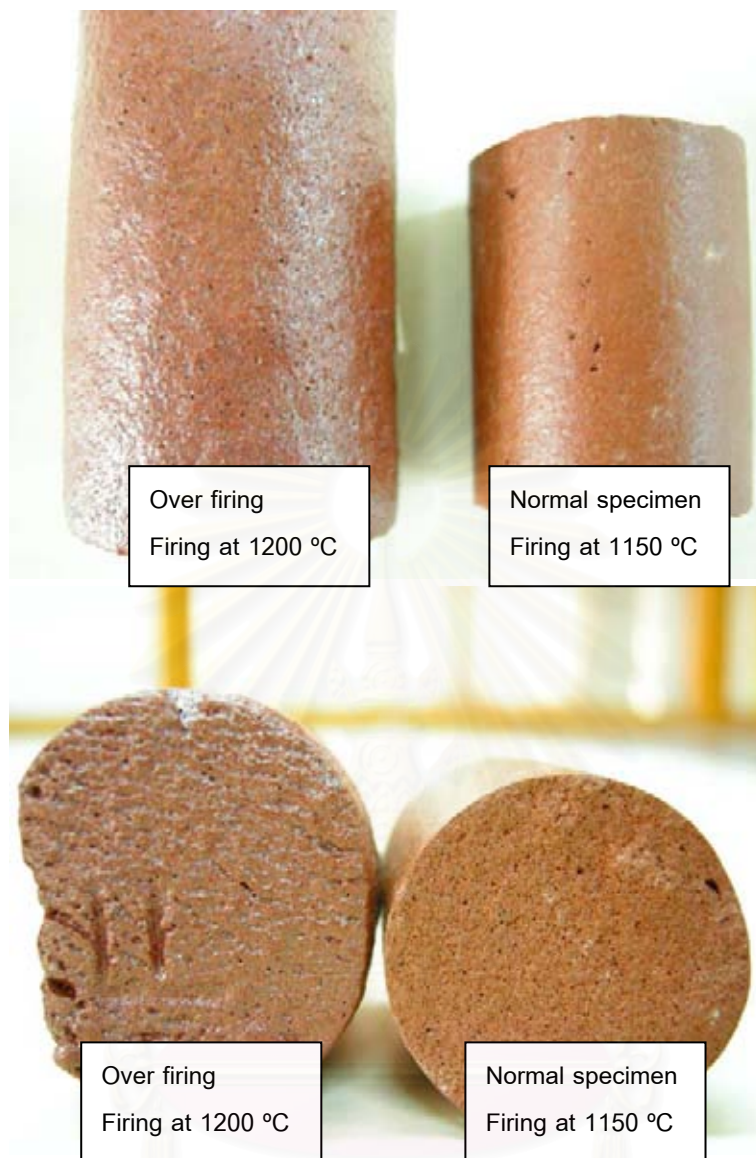


Fig4.25 show over firing of stoneware body

สถาบันวิทยบริการ
จุฬาลงกรณ์มหาวิทยาลัย

4.2.3.3 Bulk density

As shown in Fig 4.26, at 1150 °C the bulk density of specimens pressed at 150 bar is the highest followed by the cast of 40% water content and the extruded, and the lowest one is the pressed specimen at pressure 50 bar. The high pressing pressure in body may affect the pores inside green specimens and also fired specimens. This stoneware body is designed for pressing process which has good particle packing for pressing then pressed specimens have higher bulk density than cast specimens. At 1200 °C, the bulk density is decreased significantly because the specimen fired at this temperature is over fired.

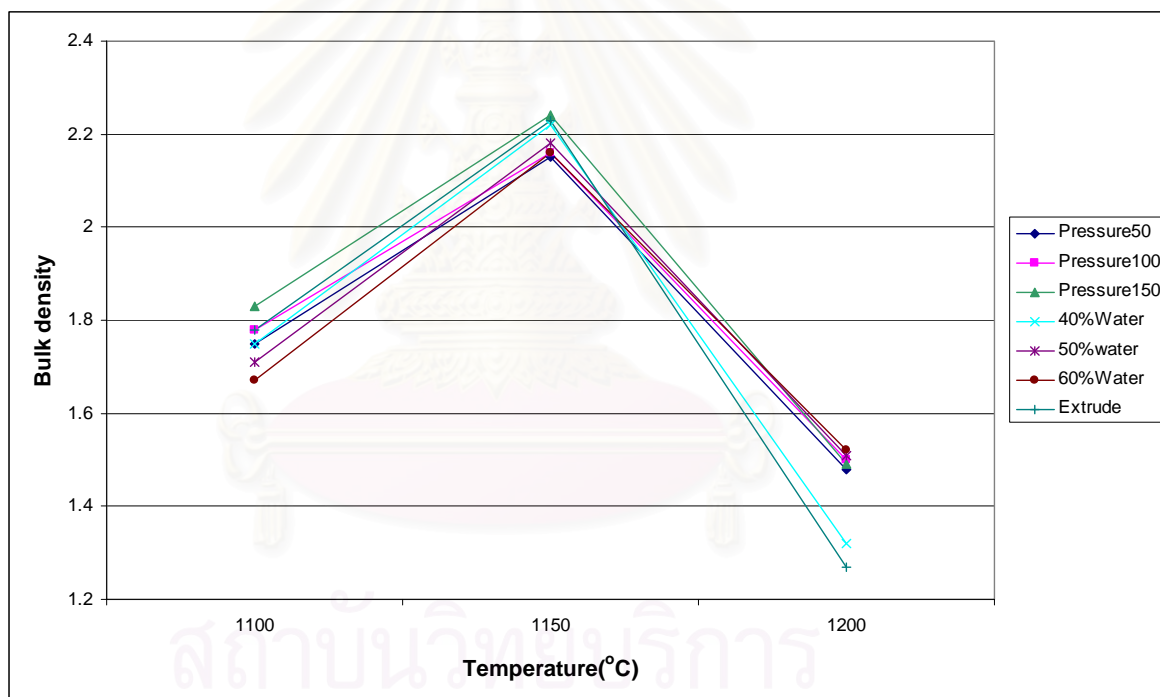


Fig 4.26 Relationship between Bulk density and various forming process in various firing temperature of stoneware body

4.2.3.4 Bending strength

Fig.4.27 shows the bending strength of stoneware body increased with an increase of pressing pressure and firing temperatures and attained maximum values of about 423 kg/cm² at 1150 °C. The strength of sintered bodies of high pressing pressure are almost the same value as the low pressing pressure at 1100 °C to 1150 °C. At 1200 °C, pressed specimens have lower bending strength because over firing. It is mean that press specimen is fully sintered at 1150 °C. Fig.4.26 shows the bending strength of cast specimens increased with its %solid content and at 1150 °C, the bending strength of cast specimens of 40% water content is 478 kg/cm². From the result even the same body formula was used but different in forming process it is generated wide gap of bending strength. Theoretically, a maximum bending strength developed when the apparent porosity decreased.

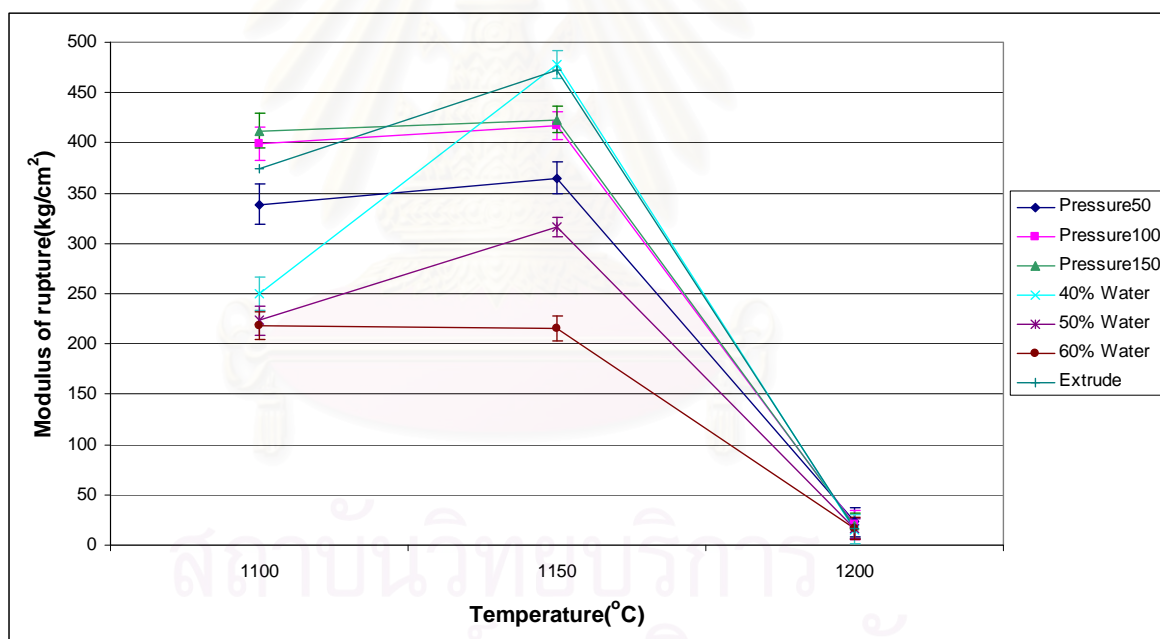


Fig 4.27 Relationship between bending strength and forming process in various firing temperature of stoneware body

4.2.3.5 Microstructure examination by Scanning electron microscope (SEM)

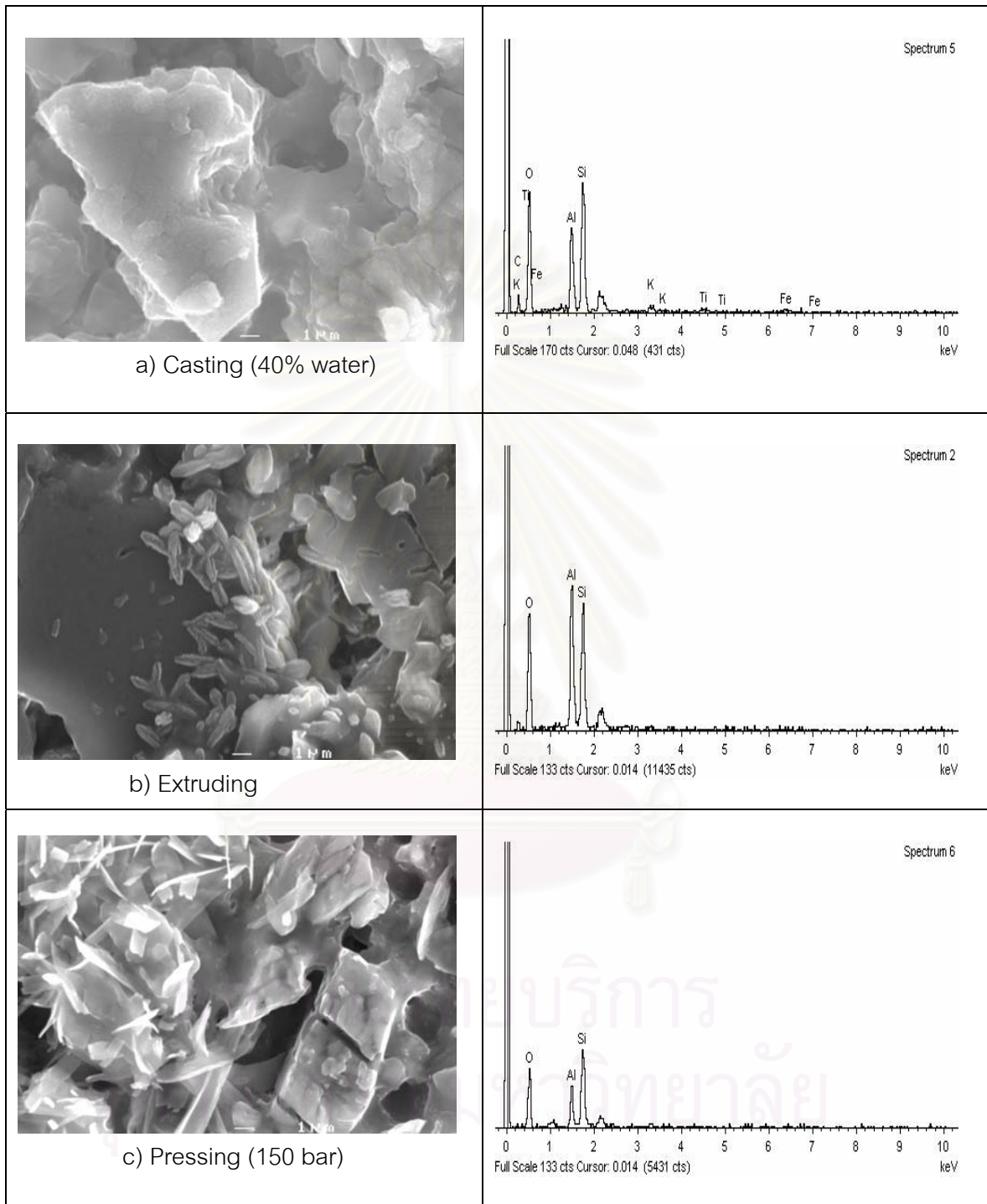


Fig.4.28 SEM image and EDS graphs of sintered stoneware body at 1150 °C by various forming process at 5000X

Fig 4.28 shows the small needle mullite crystals and quartz grains in fired stoneware body forming by extruding and pressing. There is clearly difference in morphology of mullite crystals formed in the specimens from different processes. As can be seen in Fig 4.28 (a) the morphology of crystallized is grain which can be distinguished from mullite crystals in Fig 4.28 (b) and (c). Morphology of mullite crystals in the specimens from extruding and pressing are needle mullite crystals with higher aspect ratio compares to the morphology of crystallized in the cast specimen. From EDS analysis the crystal grain of cast specimens are microcline while needle mullite of extrude specimens is primary mullite and needle mullite of press specimens is secondary mullite. In general primary mullite trends to change to secondary mullite with increasing of firing temperature, soaking time or change in composition but this research shows the forming process of specimen has an effect on morphology of mullite crystal.



สถาบันวิทยบริการ
จุฬาลงกรณ์มหาวิทยาลัย

4.2.3.6 Thermal expansion coefficient

As shown in Fig.4.29, the thermal expansion coefficient of the stoneware body prepared by different pressing pressures. When pressing pressure was increased, thermal expansion coefficient increased. At 1200 °C, thermal expansion coefficient of pressed specimens is decreased because the body is increased porosities from bloating.

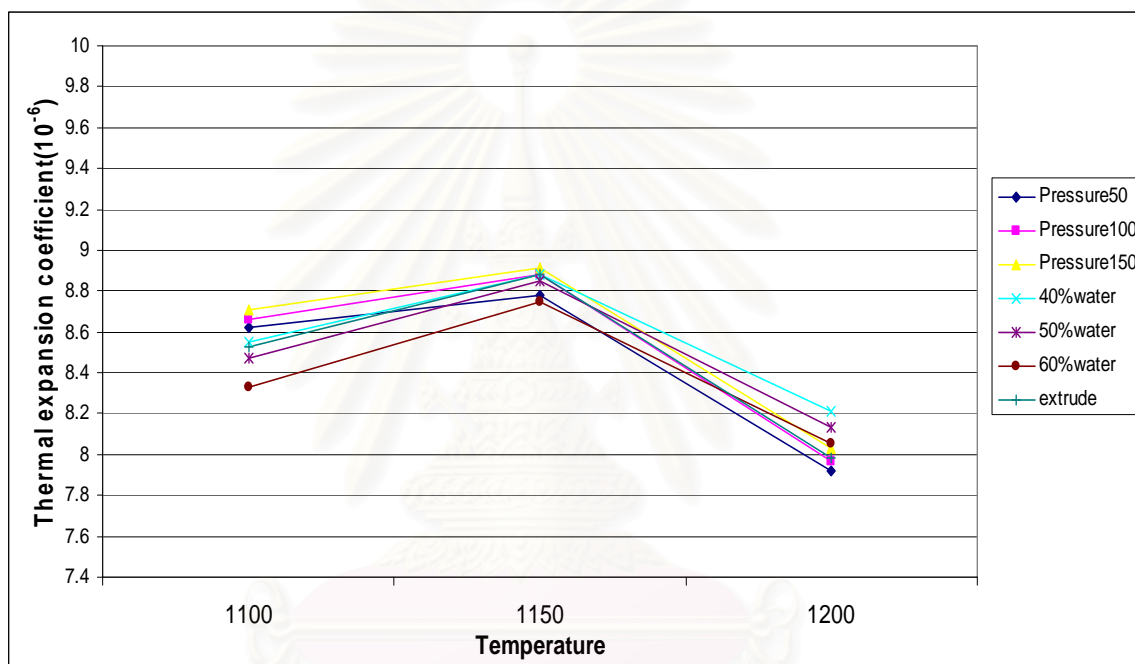


Fig 4.29 Relationship between thermal expansion coefficient and various forming process in various firing temperature of stoneware body (range of temperature 20-500 °C)

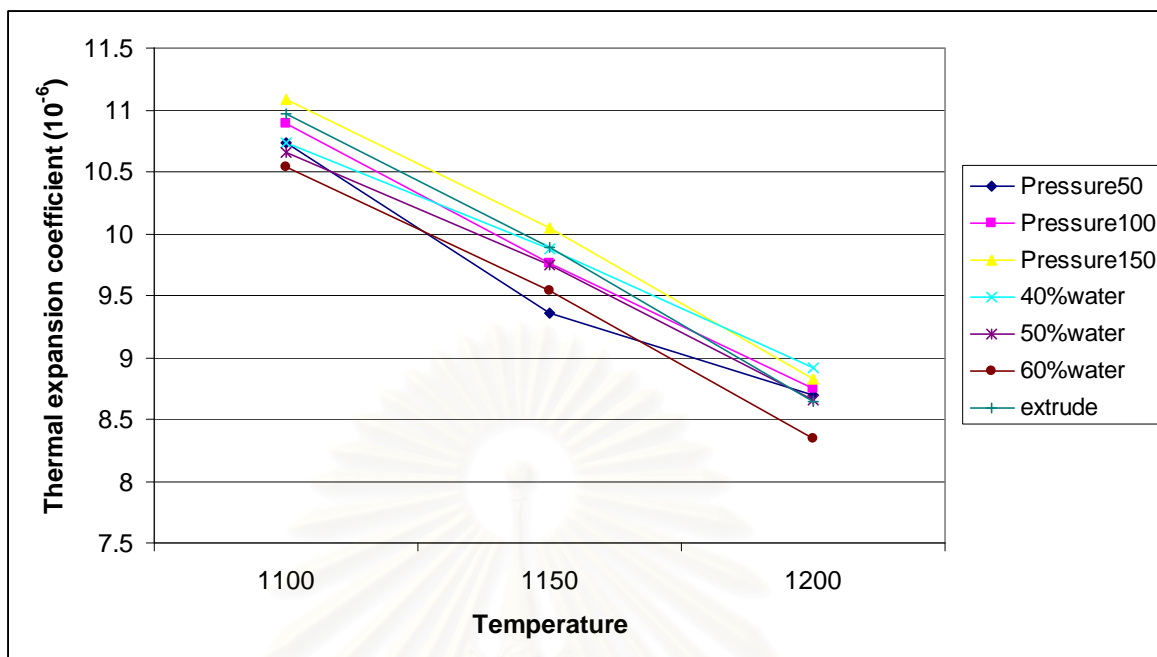


Fig 4.30 Relationship between thermal expansion coefficient and various forming process in various firing temperature of stoneware body (range of temperature 500-600 °C)

The dilatometric data show that the thermal expansion coefficient of pressed specimens at 150 bar is about $8.91 \times 10^{-6} \text{ } ^\circ\text{C}^{-1}$ which is higher than the extruded and cast specimens at 1150 °C. The specimen formed by high bulk density process (high pressing pressure) obtained higher thermal expansion than low bulk density process after firing. The theoretical value of thermal expansion coefficient calculated from proportion of oxides in stoneware body from Table 4.4 is $8.98 \times 10^{-6} \text{ } ^\circ\text{C}^{-1}$ compare with the highest one ($8.91 \times 10^{-6} \text{ } ^\circ\text{C}^{-1}$). The measured thermal expansion of the specimen with low bulk density has lower thermal expansion than the calculated value. Therefore, thermal expansion coefficient can be estimated from bulk density of fired specimens which is in the same tendency to porcelain and vitreous china bodies but range of different is narrower than porcelain and vitreous china bodies. Forming process has strong effect on densification of the specimen and related to the difference of thermal expansion as well.

Fig 4.30 shows thermal expansion coefficient of the specimens at 500-600 °C which is in the range of quartz inversion. From the graph it is shown no significant about

thermal expansion coefficient of the different forming process in the range of firing temperature.

4.2.4 Earthenware Body

4.2.4.1 Shrinkage

As shown in Fig.4.31, at low firing temperature (1050 °C), shrinkage of fired specimens are zero but at 1150 °C, when pressing pressure increased, shrinkage decreased and difference in shrinkage value among the specimens pressed with 50 and 150 bar pressure was about 2 % at maximum firing temperature. Moreover it seems that the shrinkage of pressed specimens at 50, 100, 150 bars have attained their maxima shrinkage at ~1150 °C. For slip casting, shrinkage of specimens are increased when %water content of clay slip increased.

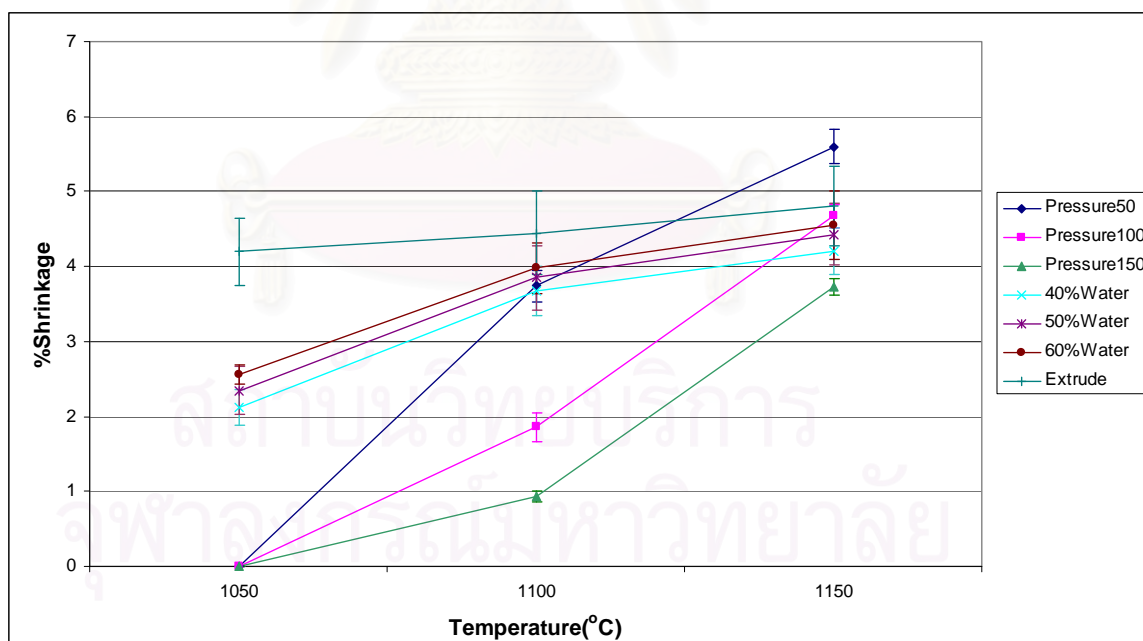


Fig 4.31 Relationship between %shrinkage and forming process in various firing temperature of earthenware body

4.2.4.2 Water absorption

Fig 4.32 shows water absorption of earthenware body formed by pressing has not changed much in this range of firing (1050-1150 °C) but shows more difference when pressing pressure changed. The lower pressing pressure specimen has higher water absorption than the high pressing pressure specimen. Water absorption of slip casting specimens as a function of water content. All of the specimens have the same tendency as pressed specimens when temperature is increased, water absorption is not changed much, however, at 1150 °C water absorption of casted specimens have tendency to decrease. The water content of clay slip is not affected much to water absorption of fired specimen. The fired specimen of earthenware body which formed by slip casting at 60 %water content shows the highest value of %water absorption compares to others specimens fired at 1150 °C.

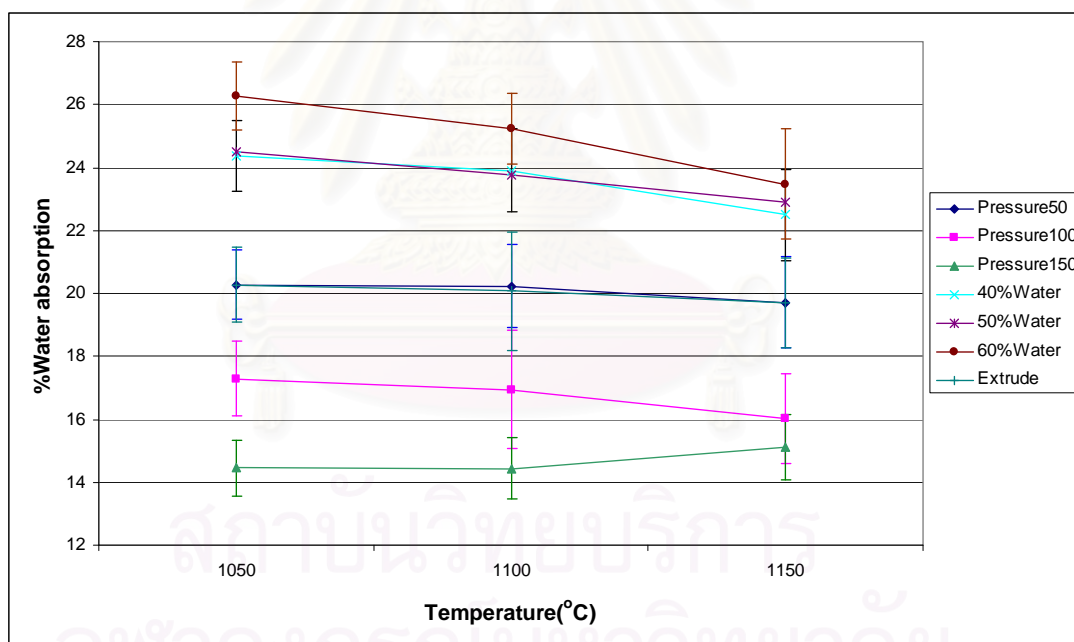


Fig 4.32 Relationship between water absorption and forming process in various firing temperature of earthenware body

4.2.4.3 Bulk density

Fig 4.33 shows the bulk density of earthenware body for different forming processes. The bulk density were not changed much in this range of firing (1050-1150 °C)

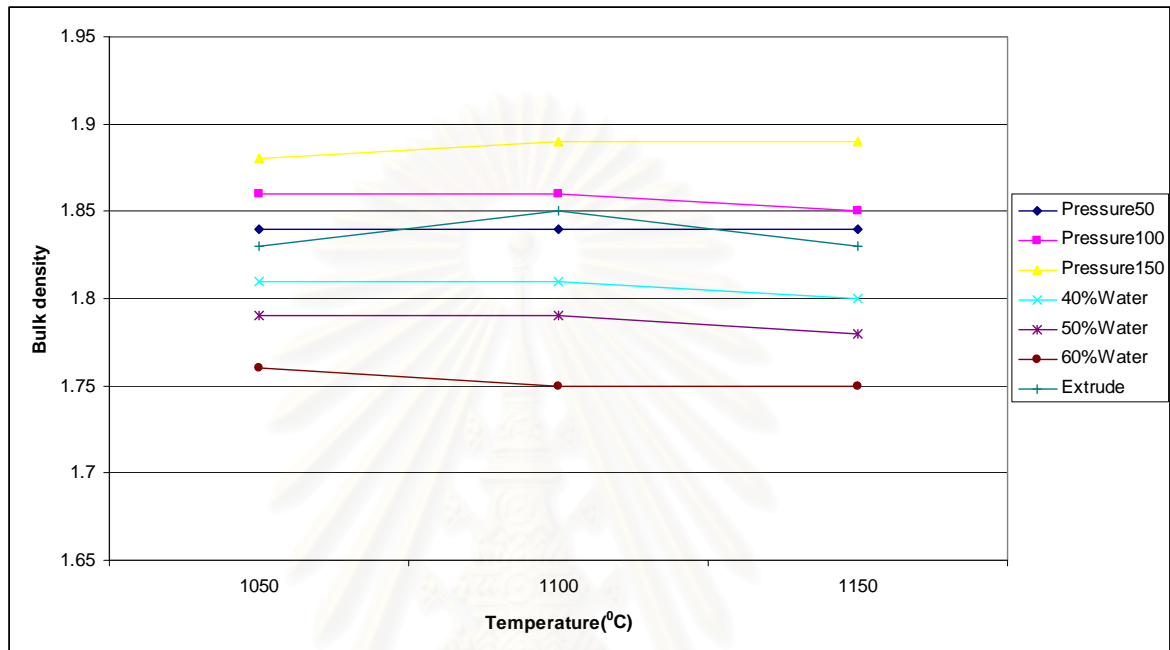


Fig 4.33 Relationship between bulk density and forming process in various firing temperature of earthenware body

This graph is of crucial importance to understanding of the effect of calcareous addition on the densification of wall tile bodies. It is clear that the densification depends substantially on forming processes; temperature is not highly affected in this range of firing temperatures.

Between 800 and 900 °C, the CaCO_3 decomposes to CaO accompanied by the evolution of CO_2 outside the structure of fired specimen. The series of reaction with the formation of small liquid phase volume result in the specimens having high open porosity. Also, water absorption and bulk density are practically constant within a wide firing temperature range (67).

4.2.4.4 Bending strength

Fig.4.34 shows the bending strength of earthenware body increased with an increase of pressing pressure and firing temperatures and attained maximum values of about 259 kg/cm² at 1100 °C. The strength of sintered bodies of high pressing pressure are almost the same value at 1050 °C to 1100 °C and at 1150 °C, pressed specimens have lower bending strength because over firing. It is mean that pressed specimen should not be fired over 1100 °C. The bending strength of cast specimens increased when %solid content increased. At 1150 °C, the bending strength of cast specimens of 40% water content is 218 kg/cm² which are higher than pressed specimen. It is also related to water absorption of cast specimen that is decreased at 1150 °C, seem to be cast specimen is start densified later than pressed specimen depended on bulk density. From the result is presented that even the same body formula but different in forming process is generated wide range of bending strength.

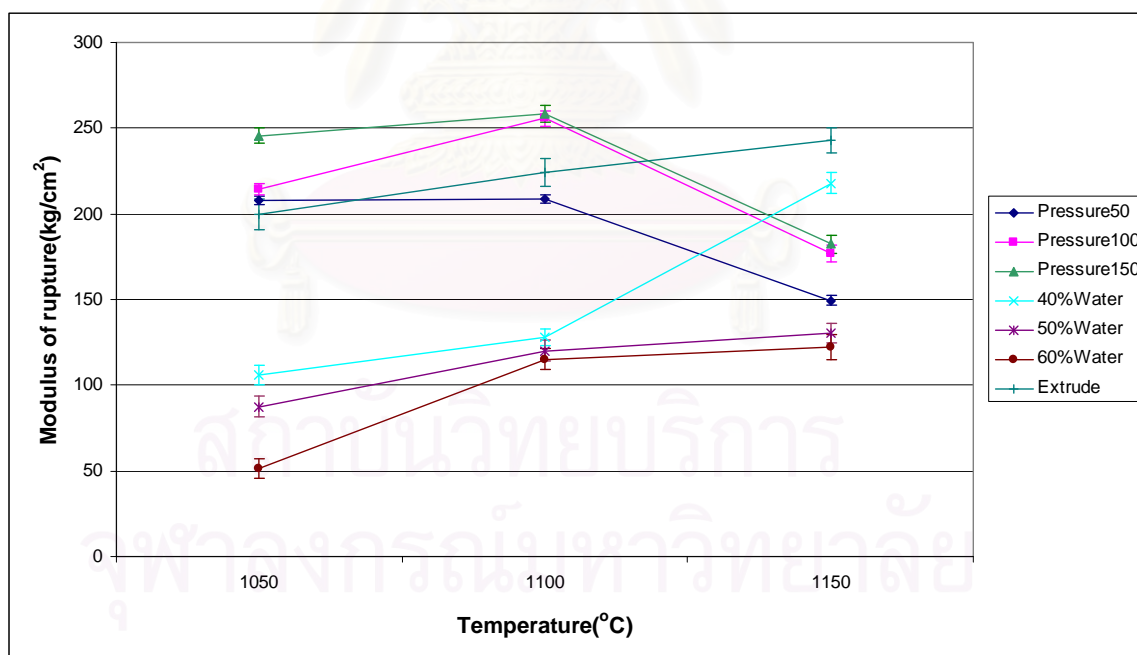


Fig 4.34 Relationship between bending strength and forming process in various firing temperature of earthenware body

4.2.4.5 Microstructure examination by Scanning electron microscope (SEM)

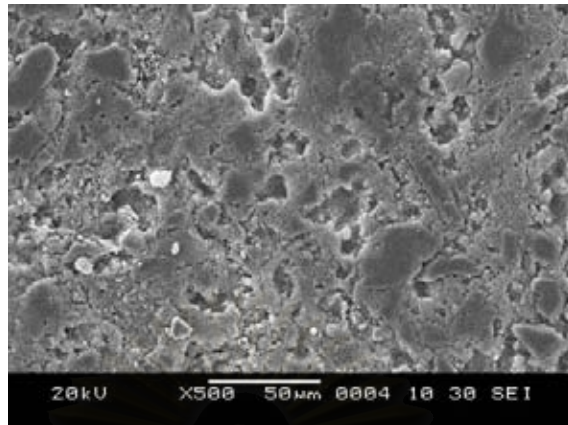


Fig 4.35 SEM images of sintered earthenware body forming by extruding (Firing at 1150 °C) at 500X

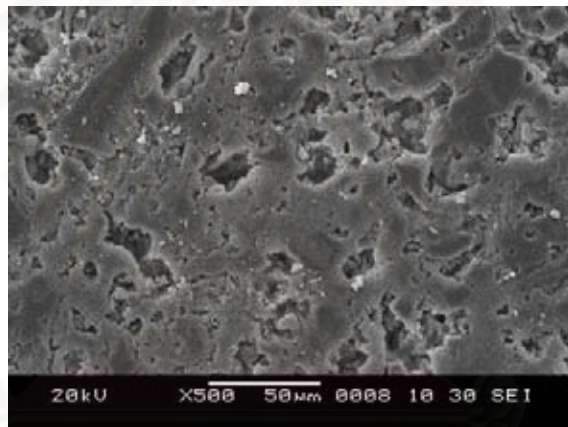


Fig 4.36 SEM images of sintered earthenware body forming by pressing at 150 psi (Firing at 1150 °C) at 500X

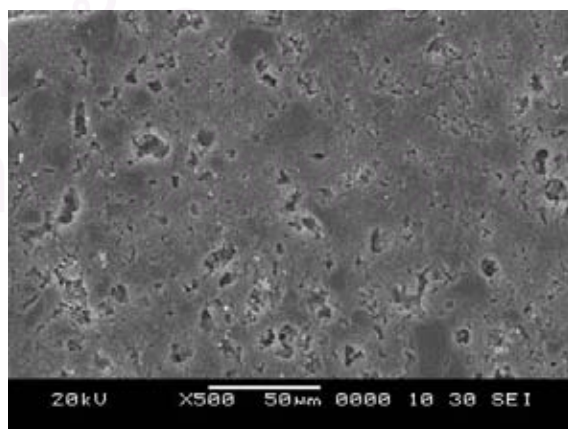


Fig 4.37 SEM images of sintered earthenware body forming by casting with 40%solid (Firing at 1150 °C) at 500X

Fig 4.35, 4.36, 4.37 shows SEM images of sintered earthenware body in different forming process firing at 1150 °C. The amount of porosity and shape is not significantly differenced because earthenware is designed for porous body therefore raw materials used in this body are not generated glassy phase after firing (low amount of alkali oxide) but it is generated pores. Even if the forming processes were changed but the amount of porosity inside the bodies were still high.

Fig 4.38 shows SEM images at 2500X and EDS graphs of sintered earthenware body at 1150 °C formed by pressing process. Fig 4.38 a shows EDS pattern of Quartz grain which is dispersed in whole body. Fig 4.38 b and c show EDS pattern of anorthite, gehlenite, metakaolinite and hematite.

The present phases are quartz (SiO_2), hematite (Fe_3O_4), gehlenite ($2\text{CaOAl}_2\text{O}_3\text{SiO}_2$), anorthite ($\text{CaOAl}_2\text{O}_32\text{SiO}_2$), and primary mullite. In the firing process, carbonates in earthenware body such as wall tile composition, the preferential sequence of the reactions is given metakaolinite-gehlenite-anorthite in ternary phase of SiO_2 -CaO- Al_2O_3 (67). The metakaolinite was formed from kaolinite by the removal of the hydroxyl groups of the silicate lattice at temperature above 500 °C. Firstly, the gehlenite is crystallized as a metastable intermediate phase from metakaolinite and CaO. Later, anorthite is formed from gehlenite, which is combined with silica and alumina rich phases due to the metakaolinite structure breaks and the remaining fine quartz. The hematite appear is due to the presence of a moderate iron level (From Table 4.2) in the starting raw materials in a formulation for red wall tile.

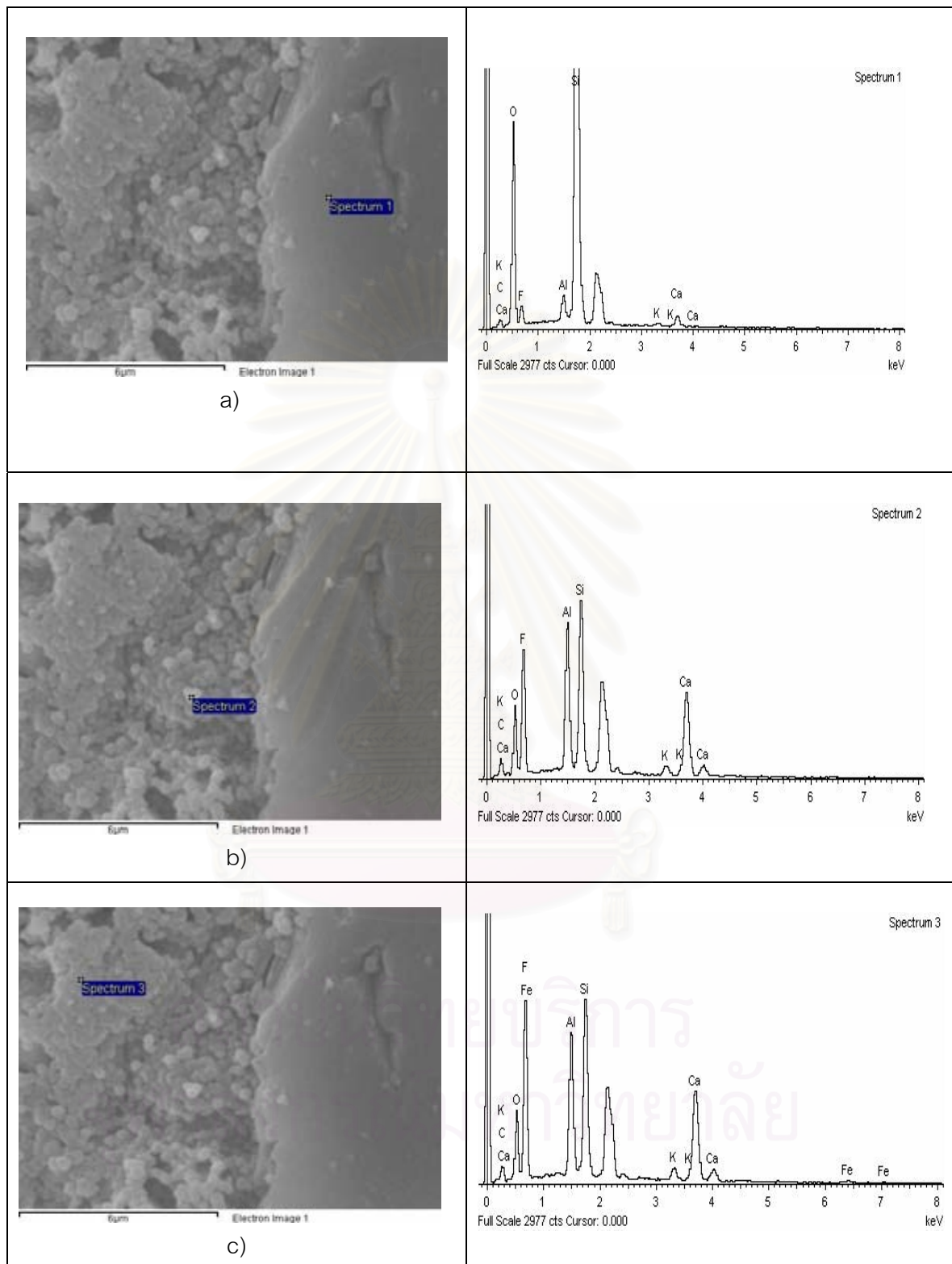


Fig.4.38 SEM image and EDS graphs of sintered earthenware body at 1150 °C formed by pressing process at 2500X

4.2.4.6 Thermal expansion coefficient

As shown in Fig.4.39, the thermal expansion coefficient of the earthenware body prepared by different pressing pressures. When pressing pressure was increased, thermal expansion coefficient increased as firing temperature increased.

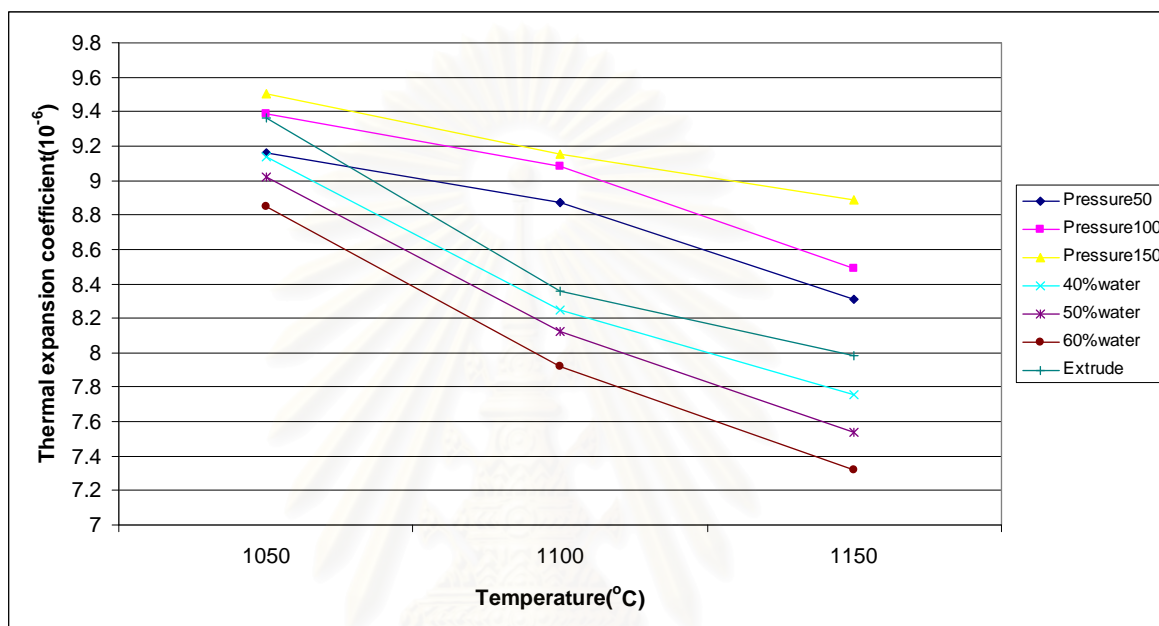


Fig 4.39 Relationship between thermal expansion coefficient and forming process in various firing temperature of earthenware body (range of temperature 20-500 °C)

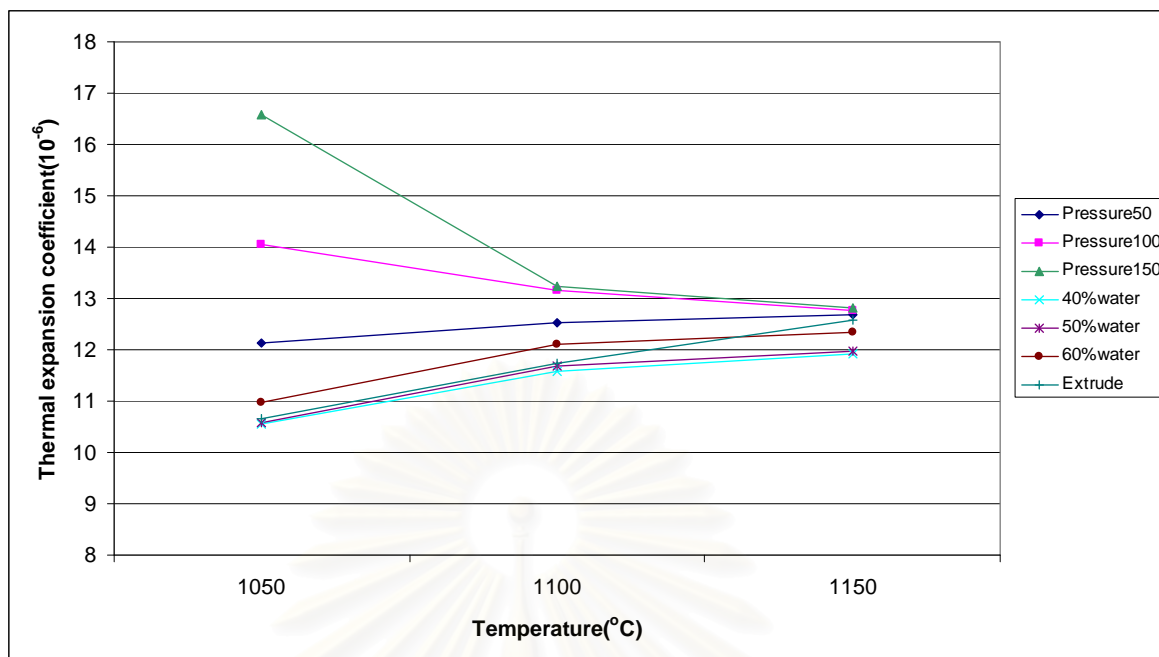


Fig 4.40 Relationship between thermal expansion coefficient and forming process in various firing temperature of earthenware body (range of temperature 500-600 °C)

Fig 4.39 shows thermal expansion coefficient of the specimens, at 1150 °C pressed with 150 bar pressure is higher than that of the specimens pressed with 50 bar of about 5 %. The cast specimens with high solid content has higher thermal expansion coefficient than the specimen with low solid content because of the higher bulk density.

As shown in Fig.4.39 the thermal expansion coefficient of the earthenware body prepared by casting at different %solid content. When %solid content was increased, thermal expansion coefficient increased firing temperature increased.

The dilatometric data show that the thermal expansion coefficient of pressed specimens of 150 bar is about $8.89 \times 10^{-6} \text{ } ^\circ\text{C}^{-1}$ which is higher than the extruded and cast specimens at all firing temperatures. The reason is related to bulk density. The body which has the same chemical composition and firing temperatures but different in forming process exhibits different thermal expansion. The specimen formed by high bulk density process (high pressure pressing) obtained higher thermal expansion than low bulk density process after firing. The theoretical value of thermal expansion coefficient calculated from proportion of oxides in earthenware body from Table4.4 is

$9.63 \times 10^{-6} \text{ } ^\circ\text{C}^{-1}$. The measured thermal expansion of the specimen with low bulk density has lower thermal expansion than the calculated value.

Fig 4.40 shows thermal expansion coefficient of the specimens at 500-600 °C which is a range of quartz inversion (68). From the graph there is no clearly to evidence explain the relation between thermal expansion coefficient at 500-600 °C and 20-500 °C.



สถาบันวิทยบริการ
จุฬาลงกรณ์มหาวิทยาลัย

4.2.5 Terracotta Body

4.2.5.1 %Shrinkage

As shown in Fig.4.41, at low firing temperature (950 °C), shrinkage of the extruded specimens is higher than pressed specimens of about 3%. At 1050 °C, the extruded specimens are shrunk about 9.4% while the shrinkage pressed specimens at 150 bar are 7.5 %. The difference shrinkage is come from the content of moisture in forming bodies.

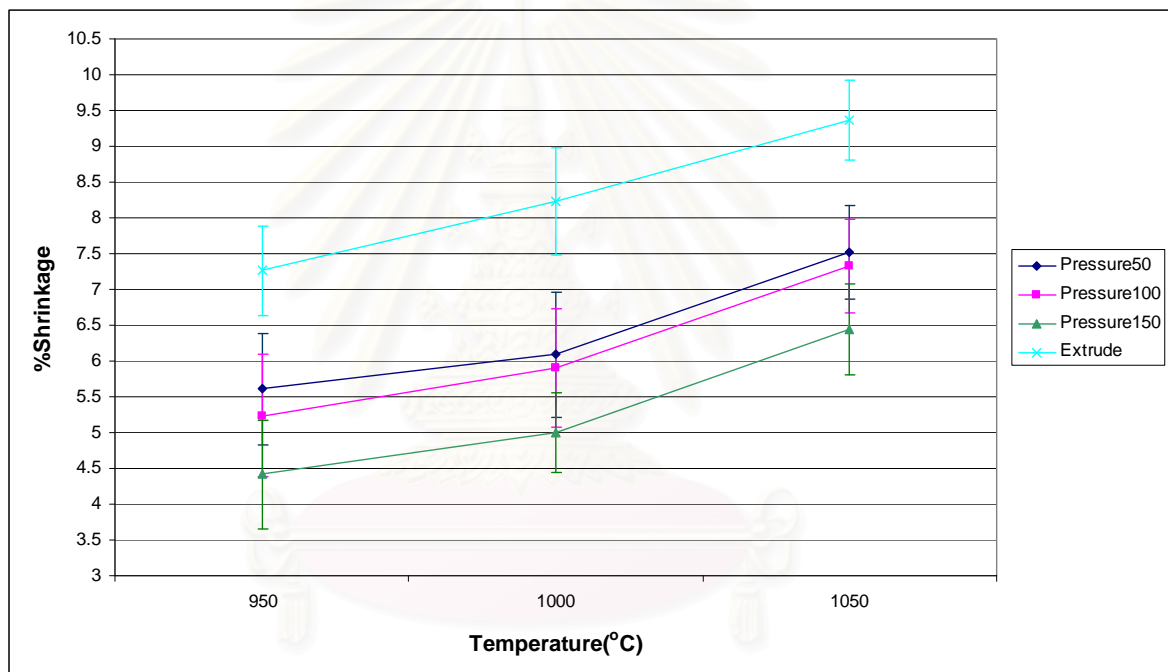


Fig 4.41 Relationship between %shrinkage and forming process in various firing temperature of terracotta body

4.2.5.2 Water absorption

Fig 4.42 shows that the water absorption of terracotta body formed by pressing is decreased when temperature is increased especially specimens with pressure 150 bar. At 1050 °C, the different of water absorption between pressed specimens at 150 bar and 50 bar is 4%

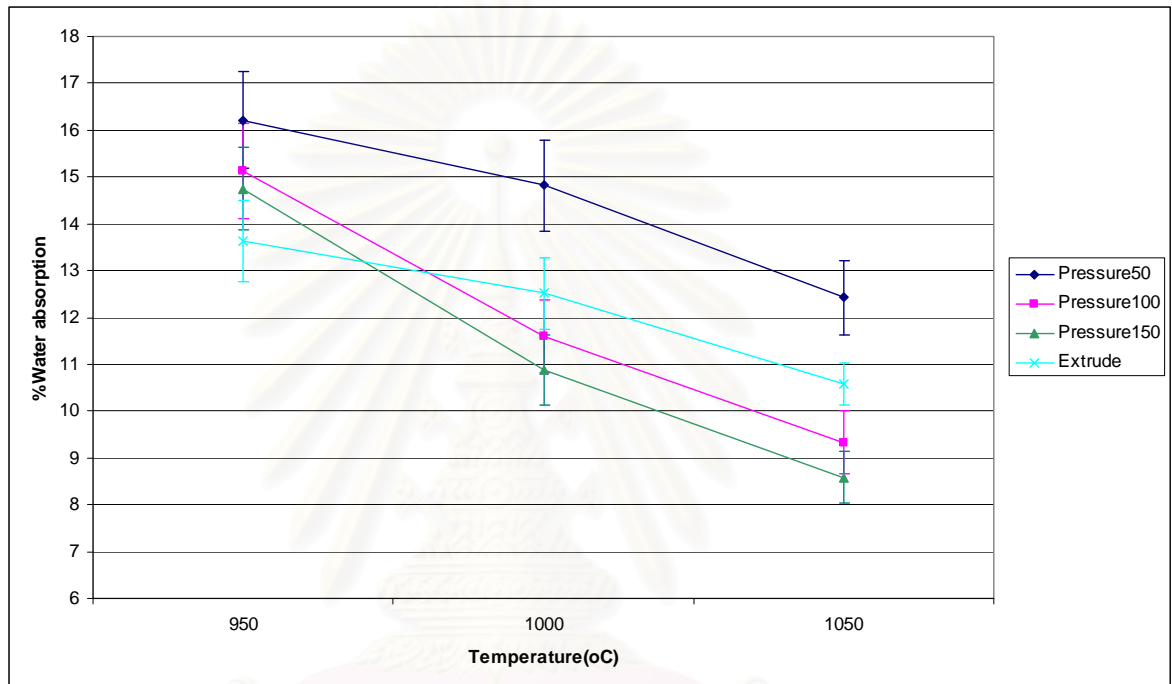


Fig 4.42 Relationship between water absorption and forming process in various firing temperature of terracotta body

4.2.5.3 Bulk density

Fig.4.43 shows the bulk density of terracotta body forming by pressing and extruding. The bulk density of extruded specimen is 1.94 g/cc and pressed specimen is 1.90 g/cc. The bulk density value is not related to water absorption which is shown in Fig.4.42. It is mean that extruded specimens have lower closed pore than pressed specimens. The difference bulk density between extruded specimen and pressed specimen of pressure 50 bar is about 8.2%.

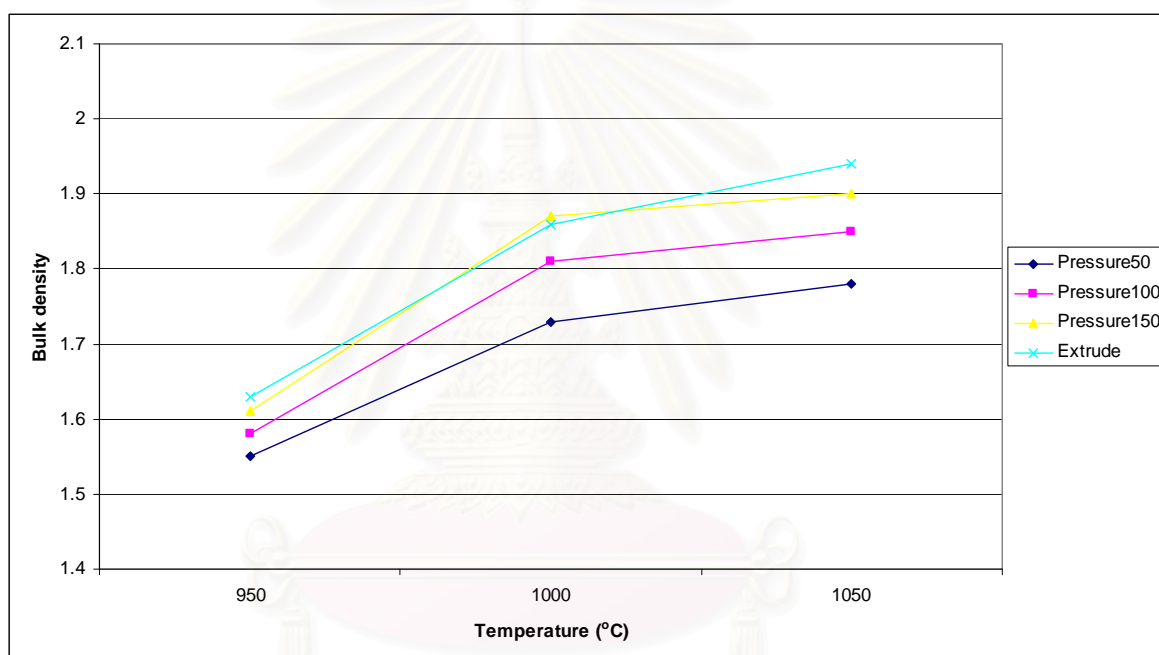


Fig 4.43 Relationship between bulk density and forming process in various firing temperature of terracotta body

4.2.5.4 Bending strength

The bending strength of terra cotta body is increased with an increase of firing temperatures and attained maximum values of about 176 kg/cm^2 at $1050 \text{ }^\circ\text{C}$ which is formed by extrusion. The strength of pressed specimens has lower bending strength than extruded specimens especially at lower temperature. The reason is might be this body formula is composed of red ball clay, coarse sand and chamotte when the raw material is mixed with water in order to form by extrusion, the red ball clay has a good plasticity than dry forming process like pressing then extruded specimen is packed better than pressed specimen. When temperature is increased, densified specimen has good sinterability than porous specimen.

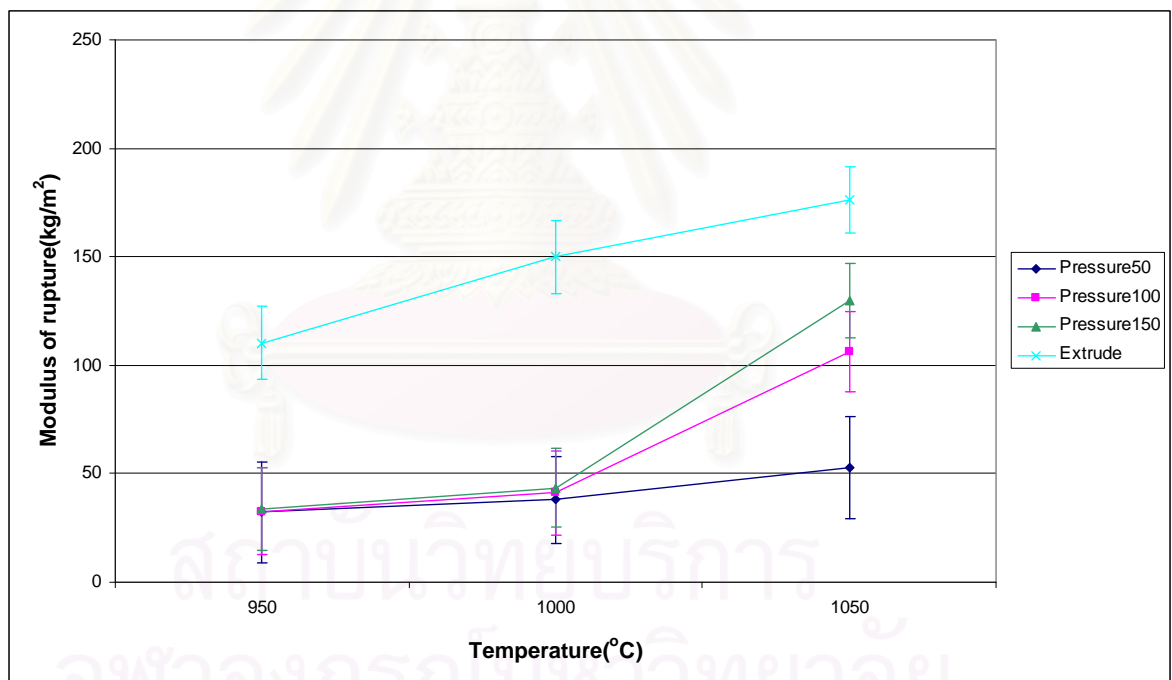


Fig 4.44 Relationship between bending strength and forming process in various firing temperature of terracotta body

4.2.5.5 Thermal expansion coefficient

As shown in Fig.4.45, the thermal expansion coefficient of the terracotta body prepared by different pressing pressures and extruding. At 1050 °C, when pressing pressure is increased, thermal expansion coefficient increased but the highest value is for extruded specimen.

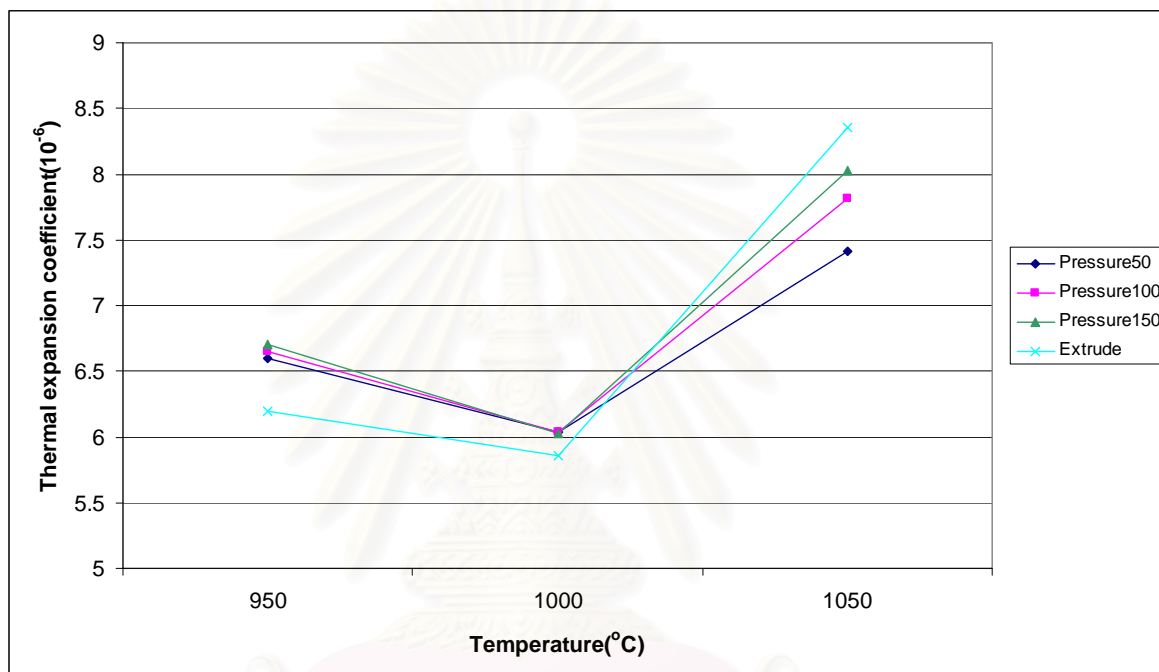


Fig 4.45 Relationship between thermal expansion coefficient and forming process in various firing temperature of terracotta body (range of temperature 20-500 °C)

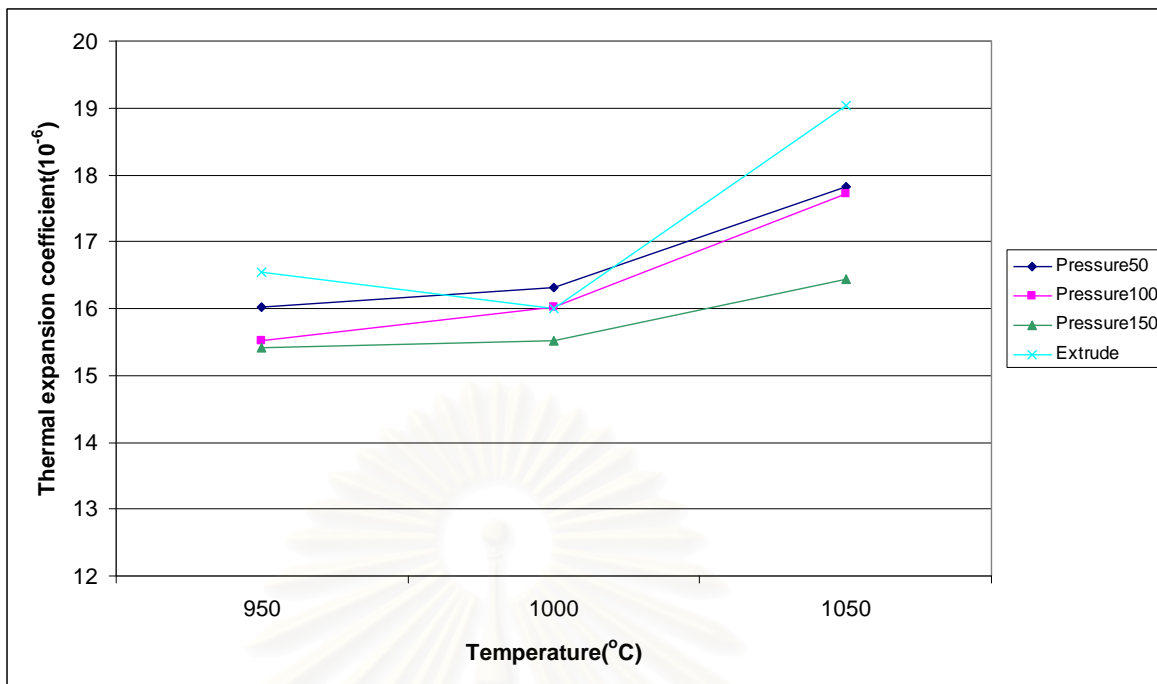


Fig 4.46 Relationship between thermal expansion coefficient and forming process in various firing temperature of terracotta body (range of temperature 500-600 °C)

Thermal expansion coefficient of the specimens fired at 1050 °C extruded specimen has higher COE than that of the specimens pressed with 50 bar about 8%. It is almost the same bulk density difference for two forming processes when is about 8%.

The dilatometric data show that the thermal expansion coefficient of extruded specimens is about $8.39 \times 10^{-6} \text{ } ^\circ\text{C}^{-1}$. The reason is related to bulk density. The body which has the same chemical composition and firing temperatures but different in forming process exhibits different thermal expansion. The specimen formed by high bulk density process (low closed porosity) obtained higher thermal expansion than low bulk density process after firing. The theoretical value of thermal expansion coefficient calculated from proportion of oxides in terracotta body from Table 4.4 is $8.40 \times 10^{-6} \text{ } ^\circ\text{C}^{-1}$. The measured thermal expansion of the specimen with low bulk density has lower thermal expansion than the calculated value.

Fig 4.46 shows thermal expansion coefficient of the specimens at 500-600 °C which is a range of quartz inversion. From the graph should the same trend and significant to explain the relation between thermal expansion coefficient at 500-600 °C

and 20-500 °C. However, the trend of thermal expansion coefficient of terracotta body is completely different with other ceramic bodies because in this terracotta body using coarse sand about 10% in body formula and also body preparation process is only mixing then it is not made homogeneously. Therefore coarse sand (is high SiO₂ content) is effect to thermal expansion coefficient of the fired specimen.



สถาบันวิทยบริการ
จุฬาลงกรณ์มหาวิทยาลัย

4.3 The Relationship between Bulk Density and Thermal Expansion Coefficient of Each Body Formula

4.3.1 Porcelain body

Fig 4.47 shows thermal expansion coefficient of the specimen relative with bulk density, at 1250 °C. The relation between bulk density and thermal expansion coefficient of porcelain body was a statistically significant relationship.

Scatter diagram of Bulk density& COE Porcelain body at 1250 C

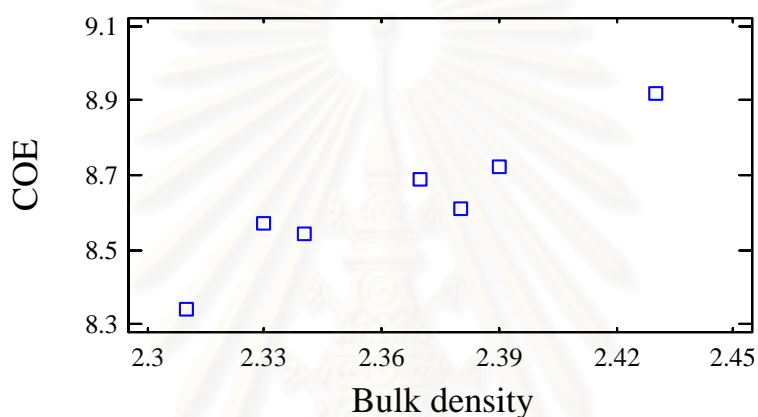
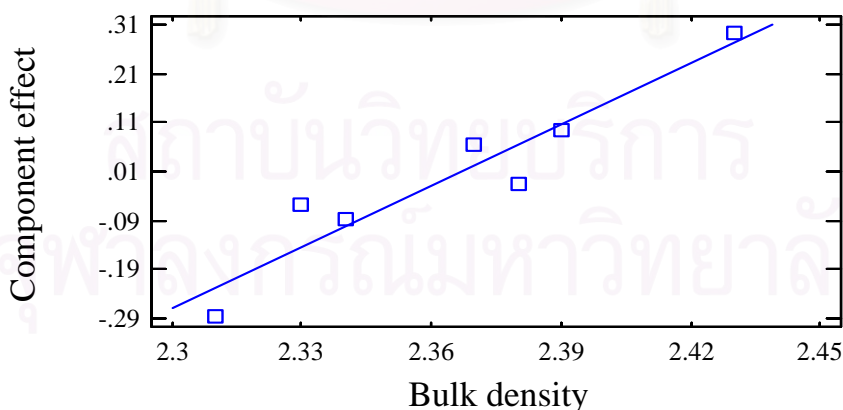


Fig 4.47 Scatter diagram for bulk density and thermal expansion coefficient of porcelain body fired at 1250 °C

Component+Residual Plot for Bulk density & COE of Porcelain body at 1250 C



$R^2=91.53$ $COE= -1.18566+ 4.15043 B.D$

Fig 4.48 Multiple regression analysis between bulk density and thermal expansion coefficient of porcelain body fired at 1250 °C

Scatter diagram of Bulk density & COE of porcelain at 1200 C

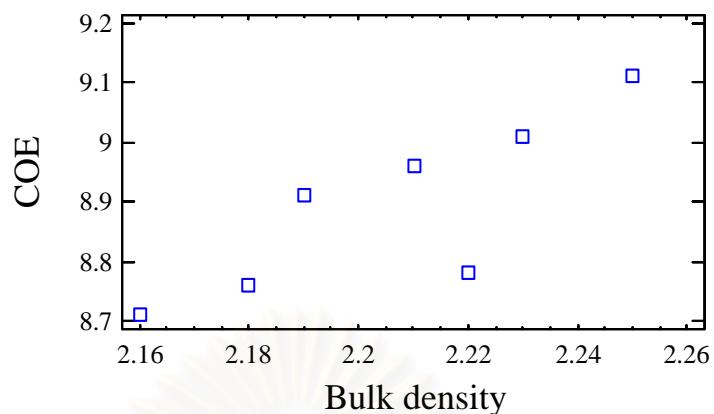
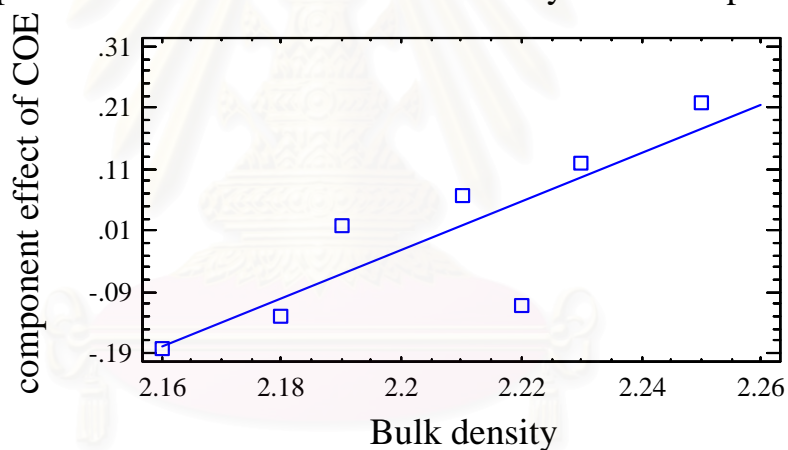


Fig 4.49 Scatter diagram for bulk density and thermal expansion coefficient of porcelain body fired at 1200 °C

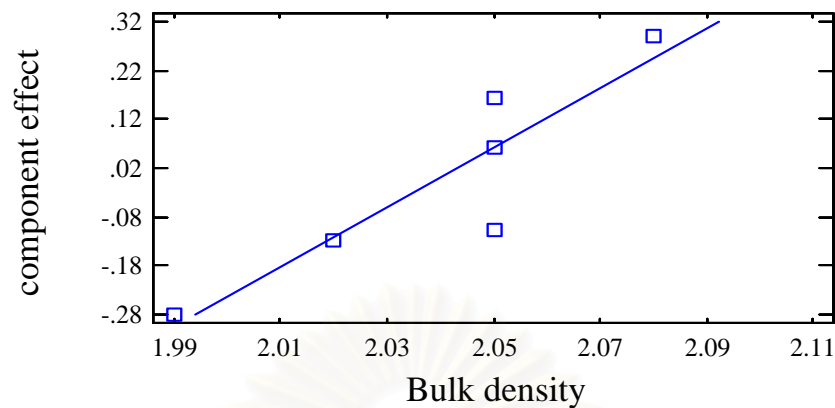
Component+Residual Plot for Bulk density & COE of porcelain at 1200 C



$$R^2=68.61 \quad \text{COE} = 0.237822 + 3.92327 \text{ B.D}$$

Fig 4.50 Multiple regression analysis between bulk density and thermal expansion coefficient of porcelain body fired at 1200 °C

Component+Residual Plot for Bulk density & COE of porcelain body at 1150 C



$$R^2=23.46$$

Fig 4.51 Multiple regression analysis between bulk density and thermal expansion coefficient of porcelain body fired at 1150 °C

Fig 4.48 shows the results of fitting a multiple linear regression model to describe the relationship between bulk density and thermal expansion coefficient. The equation of the fitted model is $COE = -1.18566 + 4.15043 \text{ B.D}$

The R-Squared statistic of firing specimen at 1250 °C was indicated that the model as fitted explains 91.53% of the variability in component effect. The value can be used to predict for the specimens will known value of bulk density.

However, when firing temperature of specimens were decreased to 1200 and 1150 °C. The R-Squared value was decreased to 68.61 and 23.46% respectively as show in Fig 4.50, 4.51. It is means that when specimens were not completely sintered, bulk density and thermal expansion coefficient were not related.

4.3.2 Vitreous china body

Fig 4.52 shows thermal expansion coefficient of the vitreous china specimen relative with bulk density, at 1250 °C. The relation between bulk density and thermal expansion coefficient of vitreous china body was a statistically significant relationship.

Scatter diagram of bulk density& COE of vitreous china at 1250 C

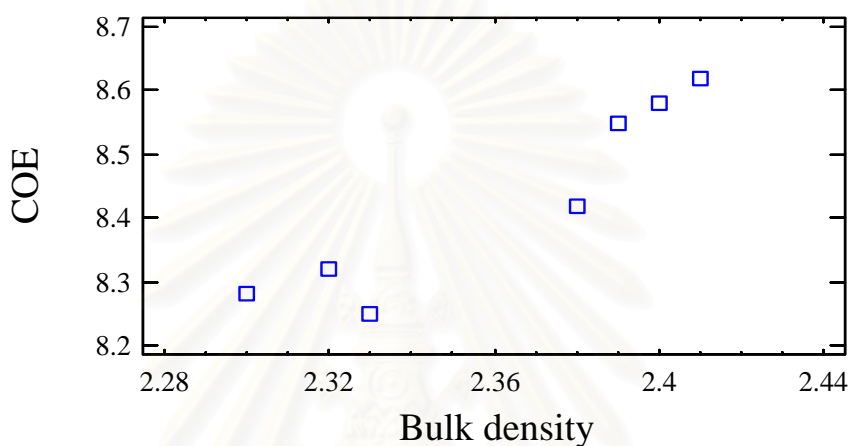
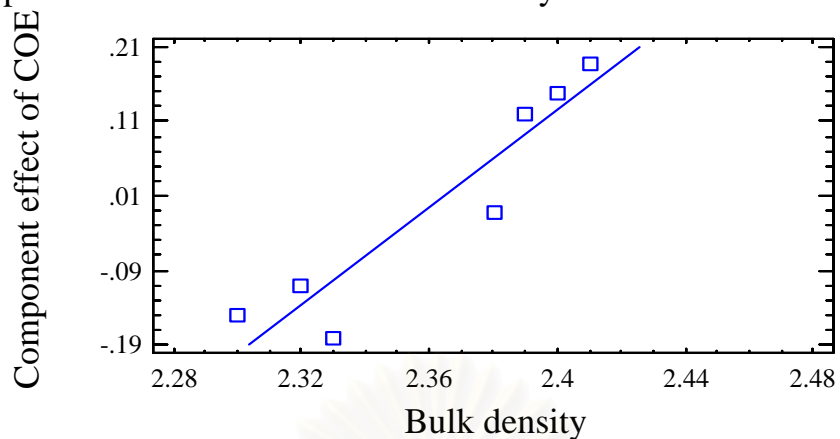


Fig 4.52 Scatter diagram of bulk density and thermal expansion coefficient of vitreous china body fired at 1250 °C

The R-Squared statistic of firing specimen at 1250 °C was indicated that the model as fitted explains 88.26% of the variability in component effect. The results of fitting a multiple linear regression model to describe the relationship between bulk density and thermal expansion coefficient. The equation of the fitted model is $COE = 0.683358 + 3.28109 \text{ B.D}$ as shown in Fig. 4.53.

Fig. 4.54 shows the R-Squared value of the specimens fired at 1200 °C is 5.78%. It means that when specimens were not reached sintering temperature, bulk density and thermal expansion coefficient were not related.

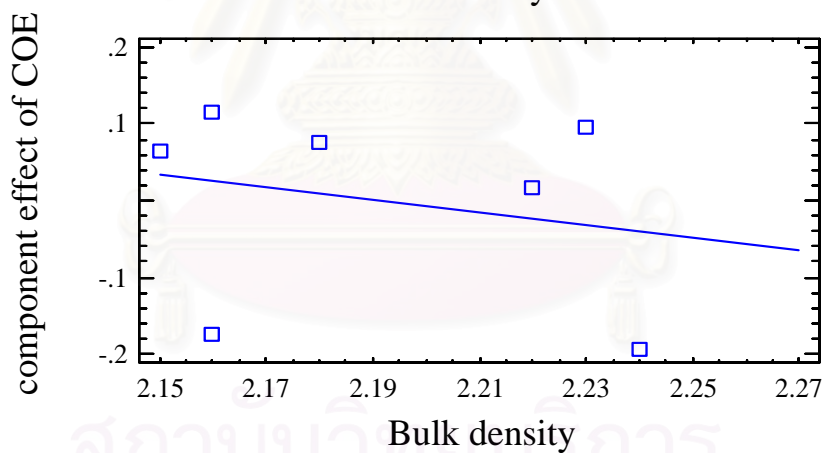
Component+Residual Plot for Bulk density & COE of Vitreous china at 1250 C



$$R^2=88.26 \quad \text{COE} = 0.683358 + 3.28109 \text{ B.D}$$

Fig 4.53 Multiple regression analysis between bulk density and thermal expansion coefficient of vitreous china body fired at 1250 °C

Component+Residual Plot for Bulk density & COE of vitreous china at 1200 C



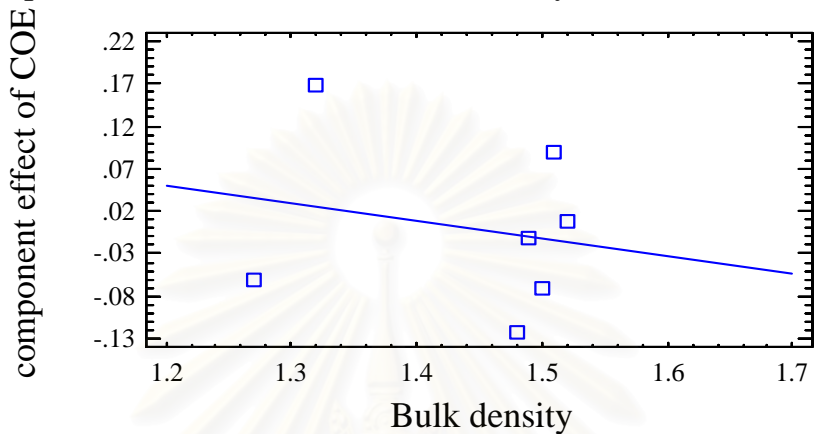
$$R^2=5.78$$

Fig 4.54 Multiple regression analysis between bulk density and thermal expansion coefficient of vitreous china body fired at 1200 °C

4.3.3 Stoneware body

Fig. 4.55 and 4.56 shows multiple regression analysis between bulk density and thermal expansion coefficient of stoneware body.

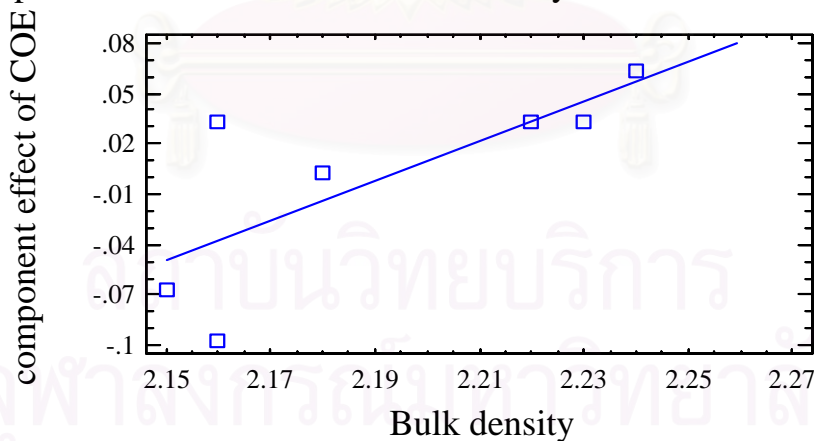
Component+Residual Plot for bulk density& COE of stoneware at 1200 C



$R^2=4.25$

Fig 4.55 Multiple regression analysis between bulk density and thermal expansion coefficient of stoneware body fired at 1200 °C

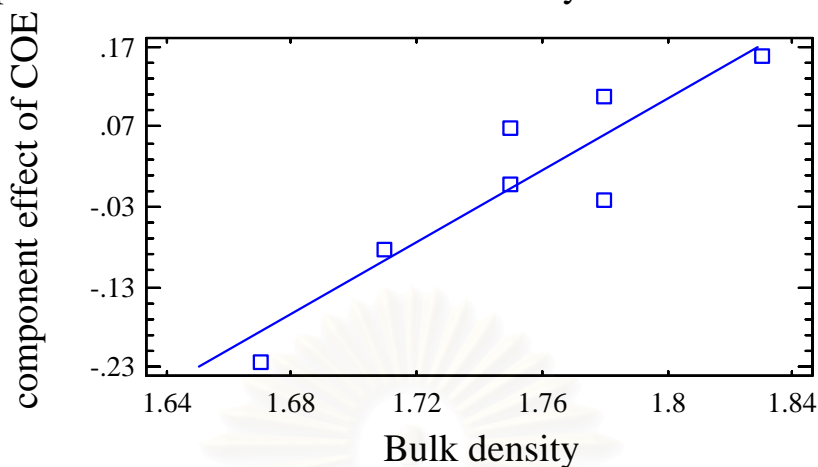
Component+Residual Plot for bulk density & COE of stoneware at 1150 C



$R^2=56.06$ COE= $-2.00499+0.47432$ B.D

Fig 4.56 Multiple regression analysis between bulk density and thermal expansion coefficient of stoneware body fired at 1150 °C

Component+Residual Plot for bulk density&COE of stoneware at 1100 C



$$R^2=83.25 \quad COE=4.61746+2.24513 \text{ B.D}$$

Fig 4.57 Multiple regression analysis between bulk density and thermal expansion coefficient of stoneware body fired at 1100 °C

At 1200 C°, stoneware body was overfired therefore bulk density and thermal expansion coefficient were not related as shown in Fig. 4.55.

Fig. 4.57 shows multiple regression analysis between bulk density and thermal expansion coefficient of stoneware body fired at 1100 °C. The R-Squared statistic of firing specimen at 1100 °C was indicated that the model as fitted explains 83.25% of the variability in component effect. The results of fitting a multiple linear regression model to describe the relationship between bulk density and thermal expansion coefficient. The equation of the fitted model is $COE = 4.61746 + 2.24513 \text{ B.D}$

The R-Squared value was not high enough to conclude that bulk density was related to thermal expansion coefficient because this body formula was designed for fast firing process then the sintering temperature range will be as narrow as than 50 °C.

4.3.4 Earthenware body

Fig 4.58 shows thermal expansion coefficient of the specimen relative with bulk density of earthenware body fired at 1150 °C. The relation between bulk density and thermal expansion coefficient of earthenware body was a statistically significant relationship.

Scatter diagram of Bulk density & COE of earthen ware at 1150 C

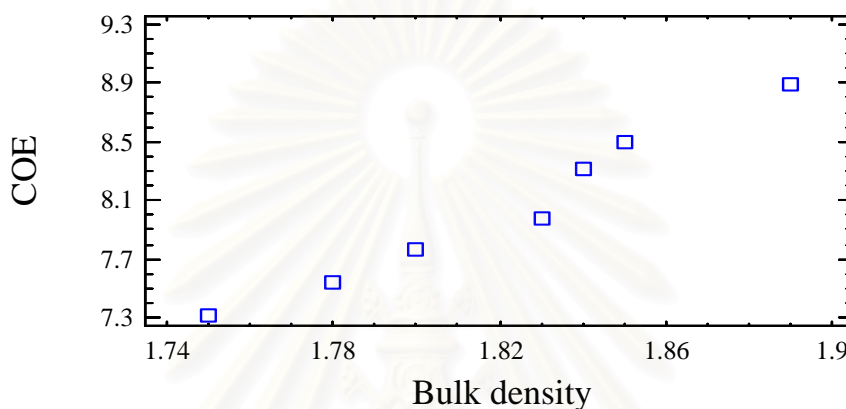
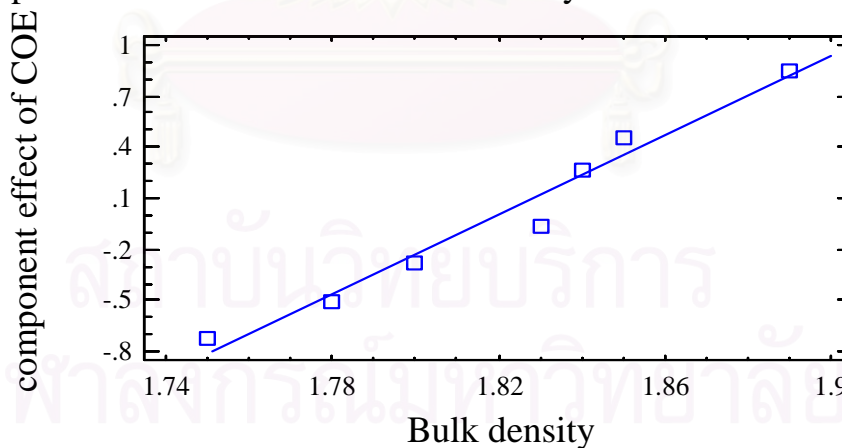


Fig 4.58 Scatter diagram for bulk density and thermal expansion coefficient of earthenware body fired at 1150 °C

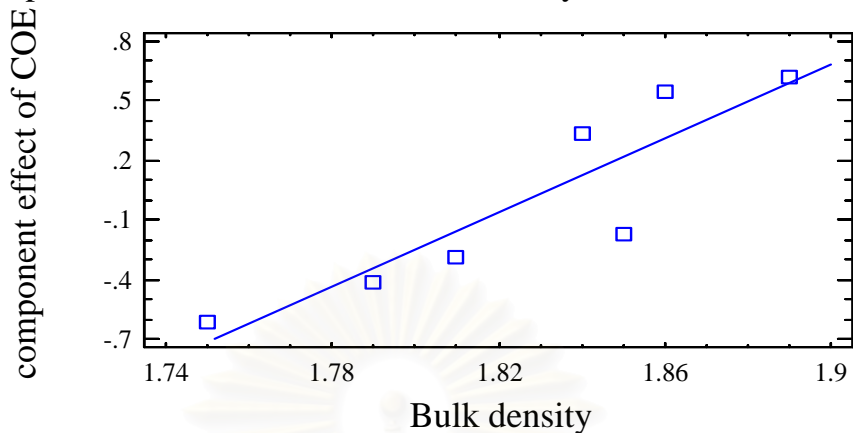
Component+Residual Plot for Bulk density & COE of earthenware at 1150 C



$R^2=96.95$ $COE= -13.1643+ 11.6515 B.D$

Fig 4.59 Multiple regression analysis between bulk density and thermal expansion coefficient of earthenware body fired at 1150 °C

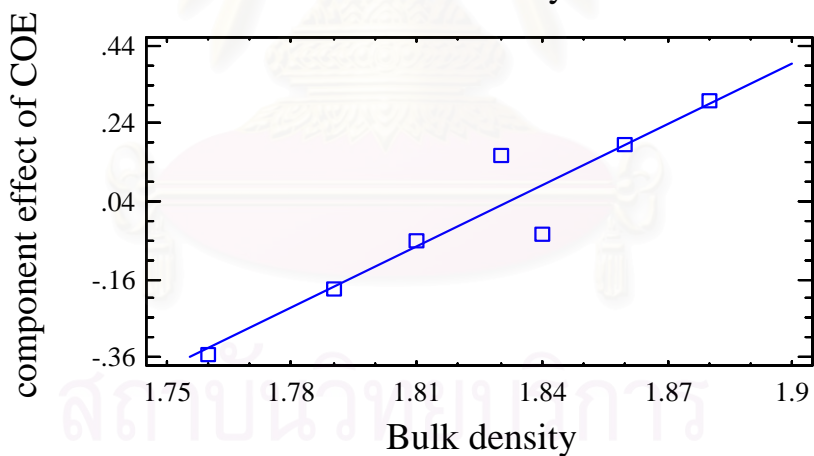
Component+Residual Plot for Bulk density& COE of earthenware at 1100 C



$R^2=80.28$ COE= $-8.5287+9.3394$ B.D

Fig 4.60 Multiple regression analysis between bulk density and thermal expansion coefficient of earthenware body fired at 1100 °C

Component+Residual Plot for Bulk density&COE of earthenware at 1050 C

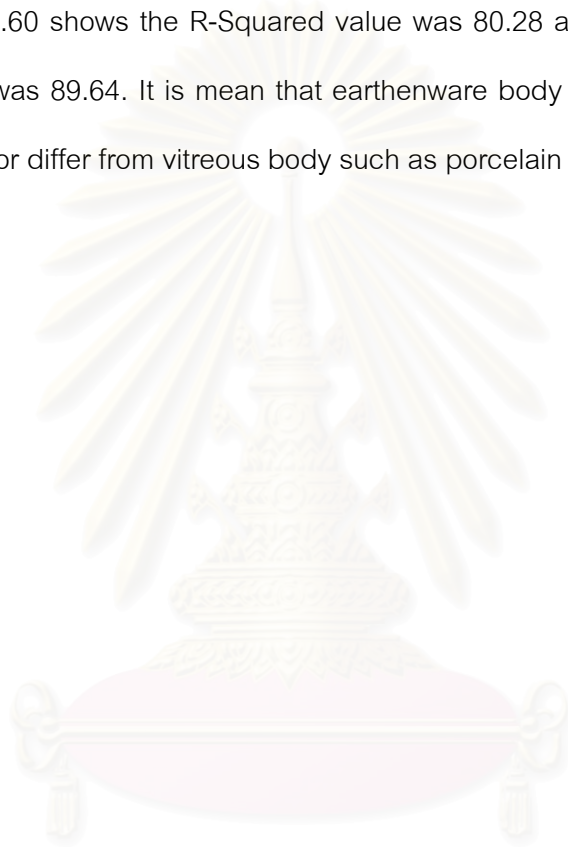


$R^2=89.64$ COE= $-0.35927+5.24157$ B.D

Fig 4.61 Multiple regression analysis between bulk density and thermal expansion coefficient of earthenware body fired at 1050 °C

Fig. 4.59 shows multiple regression analysis between bulk density and thermal expansion coefficient of earthenware body firing at 1150 °C. The R-Squared statistic of firing specimen at 1150 °C was indicated that the model as fitted explains 96.95% of the variability in component effect. The results of fitting a multiple linear regression model to describe the relationship between bulk density and thermal expansion coefficient. The equation of the fitted model is $COE = -13.1643 + 11.6515 B.D$

Fig. 4.60 shows the R-Squared value was 80.28 and Fig. 4.61 shows the R-Squared value was 89.64. It is mean that earthenware body which is porous body has sintering behavior differ from vitreous body such as porcelain and stoneware.



สถาบันวิทยบริการ
จุฬาลงกรณ์มหาวิทยาลัย

4.3.5 Terracotta body

Fig 4.62 shows thermal expansion coefficient of the specimen relative with bulk density of terracotta body fired at 1050 °C. The relation between bulk density and thermal expansion coefficient of terracotta body was a statistically significant relationship.

Scatter diagram of bulk density& COE of Terracotta at 1050 C

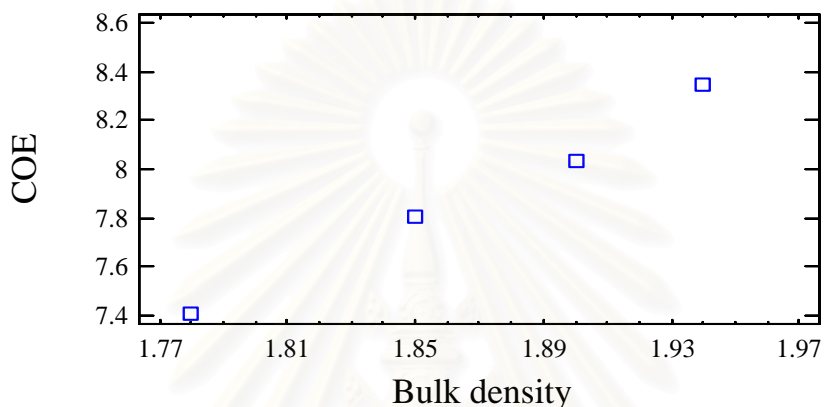
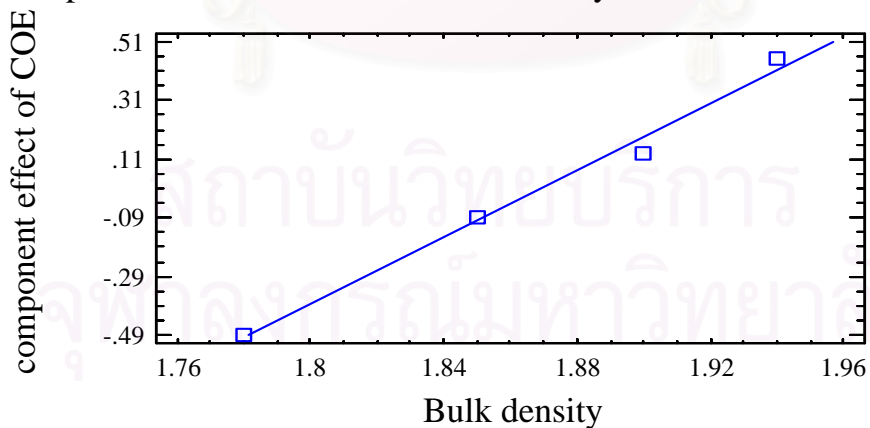


Fig 4.62 Scatter diagram of bulk density and thermal expansion coefficient of terracotta body fired at 1050 °C

Component+Residual Plot for Bulk density& COE of terracotta at 1050 C



$R^2=99.02$ $COE=-2.73592+5.69527 B.D$

Fig 4.63 Multiple regression analysis between bulk density and thermal expansion coefficient of terracotta body fired at 1050 °C

The R-Squared statistic of firing specimen at 1050 °C was indicates that the model as fitted explains 99.02% of the variability in component effect. The results of fitting a multiple linear regression model to describe the relationship between bulk density and thermal expansion coefficient. The equation of the fitted model is

$$\text{COE} = -2.73592 + 5.69527 \text{ B.D}$$

The R-Squared value was almost 100%. It is mean that relation between bulk density and thermal expansion coefficient is positive linear regression therefore when we have specimen with known bulk density we can predict thermal expansion value.

Thermal expansion coefficient is more difficult to measure because it needs a specific machine with high cost of measurement. Bulk density is more practical and can be measured in any laboratory. Moreover the measurement time of dilatometer can be reduced. However, when we change some process parameter which is effect to bulk density, we must concern with thermal expansion coefficient.

CHAPTER V

CONCLUSION

From the above discussion, it is clearly explanation that forming processes are affected to physical properties and also thermal properties of the ceramic body. In additional, the microstructure and crystal phases of the firing specimens are also differ when forming processes of the body were changed. The following conclusions were reached

Porcelain body

(1) The specimens from pressing process obtain higher bulk density and bending strength compared to the specimens from extrusion and casting process. While thermal expansion coefficient of pressed specimens was also higher than others process at the same firing temperature.

(2) Microstructure examined by SEM shown spherical shape of closed pores in pressed specimens, while the casted specimens shown elongated porosity and the amount of porosity was higher than pressed specimens therefore established lower thermal expansion coefficient than pressed specimens.

(3) Thermal expansion coefficient was changed when changing the bulk density and microstructure of the specimens.

(4) Thermal expansion coefficient was not affected only by raw materials used in the composition. Forming processes and their parameters should be taken into the account in order to understand mechanical and thermal properties of fired products for predicting better thermal mismatch problem and product life cycle.

(5) Thermal expansion coefficient was related with bulk density at fully sintering and the multiple regression analysis can be used to predict the relationship between bulk density and thermal expansion coefficient.

Vitreous china body

Trend of the result was the same as porcelain body except the highest value of thermal expansion coefficient was for casted specimen with 40% water content.

Stoneware body

The result at 1150 °C was almost the same porcelain body but at 1200 °C, the result was completely different because of the bloating effect.

Earthenware body

The earthenware body was a high porosity body thus water absorption, bulk density was not changed much when temperature was increased. However, the physical properties were depended on forming processes.

Thermal expansion coefficient was changed when changing the bulk density and microstructure of the specimens.

Multiple regression analysis was predicted relationship between bulk density and thermal expansion coefficient in wide range of firing temperatures because earthenware was porous body.

Terracotta body

Thermal expansion coefficient of terracotta body was changed when changing the bulk density. The specimen formed by high bulk density process (low closed porosity) obtained higher thermal expansion than low bulk density process after firing. However, at 1000 °C thermal expansion coefficient was not related to bulk density. For this terracotta body using Ratchaburi red clay, coarse sand and chamotte about 20% were used in body formula and also body preparation process is only mixing then it is not made homogeneously. Therefore, in this firing temperature coarse sand (is high SiO₂ content) and chamotte is affected to thermal expansion coefficient of the fired specimen.

CHAPTER VI FUTURE WORK

1. To study the effect of additive in body preparation on thermal expansion coefficient of firing specimens and its properties such as mechanical properties and microstructure.
2. To research the effect of green density on the thermal expansion coefficient.
3. For extrusion process, we should test the body in center of die and nearly the cover in order to study the relationship between the direction of clay and thermal expansion coefficient.
4. To study the differentiation of thermal expansion between normal slip casting and high pressure casting in sanitary ware industry.



สถาบันวิทยบริการ
จุฬาลงกรณ์มหาวิทยาลัย

REFERENCES

- (1) R. Newcomb, Jr., Ceramic Whitewares: New York Pitman Publishing Cooperation, 1947
- (2) L.H. Van Vlack, Physical Ceramics for Engineers: New York and London John Wiley & Sons, 1995
- (3) S.C.Carniglia and G.L.Barna, Handbook of industrial refractories technology: U.S.A, Noyes publication, 1992
- (4) J.S.Reed, Introduction to the Principles of Ceramic Processing: New York John Wiley & Sons, 1988
- (5) K.K.Kelly. High temperature heat-content, heat-capacity, and entropy data for the elements and inorganic compounds, J.Am.Ceram.Soc. 24 (12) (1960) : 864-880.
- (6) M.W.Barsoum, Fundamentals of ceramics: Boston, Mcgraw-hill international, 2000
- (7) R.W.Cahn, P.Haasen and E.J.Kramer, Materials science and technology: Newyork, VCH publishers Inc, 1996
- (8) R.W.G.Wyckoff, Crystal structure: Newyork, Wiley publishing Inc, 1971
- (9) L.H.Van Vlack, Element of materials science and engineering: Massachusetts, Addison-Wesley, 1985
- (10) I.J.Liebermann, About the important correlation between microstructure properties and product quality of strength-stressed high-voltage insulators, Interceram, 53 (2004) : 238-241.
- (11) J.R.Taylor and A.C.Bull, Ceramics glaze technology: Oxford Pergamon press, 1986
- (12) W.Jame and A.W.Norris, Thermal expansion coefficient equipment for ceramic tile, Ceramic international, 44 (1987) :34-38.
- (13) L.H.Bullin and K.Green, Crazing of wall tile, J.Am.Ceram.Soc. 25 (11) (1962) :64-70.
- (14) Thermal analysis without limits, www.linseis.com
- (15) J.T.Iones and M.F.Berard, Ceramics industrial processing and testing: Iowa, Iowa state university press, 1993

- (16) F.H.Norton, Refractories, Mcgraw hill inc, 1970
- (17) Thermal analysis trends, www.linseis.com
- (18) S.C.Carniglia and G.L.Barna, Handbook of industrial refractories technology Principles, Types, Properties and Application: New Jersey, Noyes publication, 1992
- (19) Kiln equipment handbook, Ceramic industry, 2000
- (20) Thermodilatometric analysis, www.ortonceramic.com
- (21) F. Singer, W.L. German, Ceramic Glaze: London, Borax Consolidated Limited, (1960)
- (22) J.L.Amoros, A.Gozalbo and V.Fernando, Evolution of glaze porosity in firing. Sintering mechanism and kinetics, Qualicer conference (1996)
- (23) B.E.Yekta and P.Alizadeh, Floor tile glass-ceramic glaze for improvement of glaze surface properties, Journal of the European Ceramic Society, Article in press (2006)
- (24) S.K. Das, K. Dana, N. Singh, R. Sarkar, Shrinkage and strength behaviour of quartzitic and kaolinite clays in wall tile compositions. Applied Clay Science. 29 (2005) : 137-143.
- (25) G.Isgro, C.J.Kleverlaan, H.Wang and A.J.Feilzer, Thermal dimensional behavior of dental ceramics, Biomaterials 25 (2004) :2447-2453.
- (26) J.Ilavsky and C.C.Berndt, Thermal expansion properties of metallic and cermet coating, Surface and coating technology 102 (1998) :19-24.
- (27) N.F.Youssef, M.F.Abadir and M.A.O.Shater, Utilization of soda glass (cullet) in the manufacture of wall and floor tile, Journal of the European Ceramic Society 18 (1998) :1721-1727.
- (28) A.Zanchetta and P.Lefort, Thermal expansion and adhesion of ceramic to metal sealing: case porcelain-Kovar junctions, Journal of the European ceramic society 15 (1995) :233-238.
- (29) R.A. Terpstra, P.P.A.C. Pex, A.H. de Vries, Ceramic processing, London, Chapman & Hall, 1995

- (30) J.S.Reed, Introduction to the Principles of Ceramic Processing, New York, John Wiley & Sons, 1988
- (31) F.J.Torres, E.R. de Sola and J.Alarcon, Mechanism of crystallization of fast fired mullite-based glass-ceramic glazes for floor-tiles, Journal of Non-crystalline solids, Article in press, 2007
- (32) I.A. Metwally, A.Al-Maqrashi, S.Al-Sumry, S.Al-Harthy. Performance improvement of 33kV line-post insulators in harsh environment. Electric Power Systems Research 76 (2006) :778-785.
- (33) J.Garcia-Ten, E.Monfort, P.Gomez and S.Gomer, Influence of calcite content on fluorine compound emissions during ceramic tile firing, Journal of Ceramic processing research. 7 (1) (2006) :75-82.
- (34) W.E.Brownell, Structural clay products: New York Springer-Verlag, 1976
- (35) L.Hupa,R.Bergman, L.Froberg and M.Hupa, Chemical resistance and cleanability of glazed surfaces, Surface science, 584 (2005) :113-115.
- (36) Z.H.Fang, Temperature dependence of volume thermal expansion for NaCl and KCl crystals, Physica B 357 (2005) :433-438.
- (37) Tony Hansen, Understanding thermal expansion in ceramic glazes, www.CeramicMaterials.Info
- (38) L.Hupa,R.Bergman, L.Froberg and M.Hupa, Chemical resistance and cleanability of glazed surfaces, Surface science, 584 (2005) :113-115.
- (39) A.Goleanu, Achieving self-glazed porcelain bodies, Ceramic industry :34-37 Jan 2001
- (40) Tony Hansen, Crazeing in Stoneware Glazes: Treating the Causes, Not the Symptoms, www.CeramicMaterials.Info
- (41) R.A.Islam, Y.C.Chan and M.F.Islam, Structure-property relationship in high-tension ceramic insulator fired at high temperature, Materials science and engineering B106 (2004) :132-140.
- (42) J.T.Jones and M.F.Berard, Ceramics industrial processing and testing: Iowa, Iowa state, 1993

- (43) G.W.Phelps, S.G.Maguire and R.K.Wood, Rheology and Rheometry of clay-water system, Rutgers University, 1996
- (44) Dennis Dinger, Rheology for ceramist, Dinger Ceramic Consulting Service, 2002
- (45) R.Adnan Islam, Y.C. Chan, Md. Fakhru Islam, Structure-property relationship in high-tension ceramic insulator fired at high temperature. Materials Science and Engineering, B106 (2004) :132-140.
- (46) S.W.Twiggs, J.R.Mackert, A.L.Oxford and P.E.Lockwood, Isothermal phase transformations of porcelain, Dental materials 21 (2005) :580-585
- (47) H.Schneider,K.Okada and J.A.Pask,Mullite and Mullite Ceramic, John Wiley& Sons, England, 1994
- (48) F. Singer, W.L. German, Ceramic Glazes, London, Borax Consolidated Limited, 1960
- (49) R. Newcomb, Jr., Ceramic Whitewares, New York, Pitman Publishing Corporation, 1947
- (50) R.M. German, Liquid Phase Sintering, New York and London, Plenum press, 1985
- (51) T.Manfredini, G.C.Pellacani and M.Romagnoli, Porcelainized stoneware tiles, Am ceram. Soc. Bull 74 (1995) :76-79.
- (52) J.S.T. Looms, Insulators for High Voltages, London, Peter Peregrinus, 1990
- (53) O. Isik Ece, Z. Nakagawa. Bending strength of porcelains. Ceramic International 28 (2002) :131-140.
- (54) L.Heller, The thermal transformation of pyrophyllite to mullite , Am.mineral, 47 (1962) :156-157.
- (55) K.S.Mazdiyasi and L.M.Brown, Synthesis and mechanical properties of stoichiometric aluminum silicate (mullite), J.Am.Ceram.Soc. 55 (11) (1972) :548-552.
- (56) M.Bulens, A.Leonard, and B.Delman, Spectroscopic investigation of the kaolinite-mullite sequence, J.Am.Ceram.Soc. 61 (1978) :81-84.
- (57) K.Hamano, S.Okada, H.Nakajima, and F.Okuda, Preparation of mullite ceramic

- from kaolinite and aluminium hydroxide, Abstract of the annual meeting of the ceramic society of Japan, paper no 2F05, 1988
- (58) M.Bulens, A.Leonard, and B.Delman, Spectroscopic investigation of the kaolinite-mullite sequence, J.Am.Ceram.Soc. 61 (1978) :81-84.
- (59) S.Kanzaki and H.Tabata, Sintering and mechanical properties of stoichiometric mullite, J.Am.ceram.Soc. 68 (1) (1985) :c-6-c-7.
- (60) P.Torres, R.S.Manjate, S.Quaresma and J.M.F.Ferreira, Development of ceramic floor tile compositions base on quartzite and granite sludges, Journal of the European Ceramic Society, Article in press (2007)
- (61) M.Dondi, G.Ercolani, M.Marsigli, C.Melandri and C.Mingazzini, The chemical composition of porcelain stoneware tiles and its influence on microstructure and mechanical properties, Interceram. 48 (2) (1999) :75-83.
- (62) T.I.Mah and K.S.Mazdiyasi, Mechanical Properties of Mullite, J.Am.Ceram.Soc. 66(10) (1983) :699-703.
- (63) M.Dondi, M.Raimondo and C.Zanelli, Sintering mechanisms of porcelain stoneware tiles, Journal of the European ceramic society. 17 (1996) :212-219.
- (64) P.C.Dokko, J.A.Pask and K.S.Mazdiyasi, High-Temperature Mechanical Properties of Mullite Under Compression, J.Am.Ceram.Soc. 60(3) (1997) :150-154.
- (65) W.E.Lee, C.J.McConville and T.Tarvorpanich, Mullite formation in clays and clay-derived vitreous ceramics, Journal of the European ceramic society, Article in press (2007)
- (66) J.M. Amigo, F.J.Serrano, M.A. Kojdecki, J.Bastida, V.Esteve, M.M. Reventos, F. Marti. X-ray diffraction microstructure analysis of mullite, quartz and corundum in porcelain insulator. Journal of the European Ceramic Society. 25 (2005) :1479-1486.
- (67) S.J.G.Sousa and J.N.F.Holanda. Development of red wall tiles by the dry process using Brazilian raw materials. Ceramic International 31 (2005) :215-222.



APPENDICES

สถาบันวิทยบริการ
จุฬาลงกรณ์มหาวิทยาลัย

Appendix 1

Particle size Stone ware Average



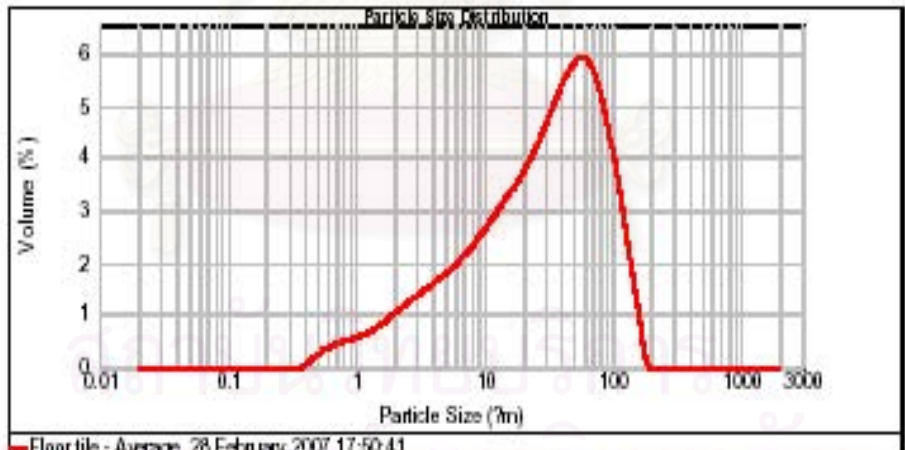
Result Analysis Report

Sample Name: Floor tile - Average **SOP Name:** **Measured:** 28 February 2007 17:50:41
Sample Source & type: **Measured by:** User **Analysed:** 28 February 2007 17:50:42
Sample bulk lot ref: **Result Source:** Averaged

Particle Name: china clay (nl) **Accessory Name:** Hydro 2000 MU (A) **Analysis model:** General purpose **Sensitivity:** Normal
Particle RI: 1.577 **Absorption:** 0.1 **Size range:** 0.020 to 2000.000 um **Obscuration:** 11.69 %
Dispersant Name: Water **Dispersant RI:** 1.330 **Weighted Residual:** 1.195 % **Result Emulation:** Off

Concentration: 0.0141 % Vol **Span :** 2.959 **Uniformity:** 0.927 **Result units:** Volume
Specific Surface Area: 0.724 m²/g **Surface Weighted Mean D[3.2]:** 8.291 um **Vol. Weighted Mean D[4.3]:** 40.578 um

d(0.1): 3.381 um **d(0.5):** 30.565 um **d(0.9):** 93.825 um



Bin #	Bin Range (µm)	Volume (%)	Bin #	Bin Range (µm)	Volume (%)	Bin #	Bin Range (µm)	Volume (%)	Bin #	Bin Range (µm)	Volume (%)	Bin #	Bin Range (µm)	Volume (%)
000	0.00	0.00	015	0.80	0.00	100	0.38	0.00	1142	2.65	12820	2.37	125300	0.00
001	0.05	0.00	020	1.00	0.00	124	0.44	0.00	1510	2.80	13020	1.35	145400	0.00
002	0.075	0.00	025	1.25	0.00	145	0.64	0.00	1570	2.85	13400	1.35	150500	0.00
003	0.10	0.00	030	1.50	0.00	160	0.73	0.00	1730	3.05	14100	0.95	155600	0.00
004	0.125	0.00	035	1.75	0.00	175	0.84	0.00	1900	3.25	14800	0.80	160700	0.00
005	0.15	0.00	040	2.00	0.00	195	0.95	0.00	2090	3.45	15500	0.60	165800	0.00
006	0.175	0.00	045	2.25	0.00	215	1.06	0.00	2290	3.65	16200	0.40	170900	0.00
007	0.20	0.00	050	2.50	0.00	235	1.17	0.00	2500	3.85	16900	0.20	176000	0.00
008	0.225	0.00	055	2.75	0.00	255	1.27	0.00	2720	4.05	17600	0.00	181100	0.00
009	0.25	0.00	060	3.00	0.00	275	1.37	0.00	2950	4.25	18300	0.00	186200	0.00
010	0.275	0.00	065	3.25	0.00	295	1.47	0.00	3190	4.45	19000	0.00	191300	0.00
011	0.30	0.00	070	3.50	0.00	315	1.57	0.00	3440	4.65	19700	0.00	196400	0.00
012	0.325	0.00	075	3.75	0.00	335	1.67	0.00	3700	4.85	20400	0.00	201500	0.00
013	0.35	0.00	080	4.00	0.00	355	1.77	0.00	3970	5.05	21100	0.00	206600	0.00
014	0.375	0.00	085	4.25	0.00	375	1.87	0.00	4250	5.25	21800	0.00	211700	0.00
015	0.40	0.00	090	4.50	0.00	395	1.97	0.00	4540	5.45	22500	0.00	216800	0.00
016	0.425	0.00	095	4.75	0.00	415	2.07	0.00	4840	5.65	23200	0.00	221900	0.00
017	0.45	0.00	100	5.00	0.00	435	2.17	0.00	5150	5.85	23900	0.00	227000	0.00
018	0.475	0.00	105	5.25	0.00	455	2.27	0.00	5470	6.05	24600	0.00	232100	0.00
019	0.50	0.00	110	5.50	0.00	475	2.37	0.00	5800	6.25	25300	0.00	237200	0.00
020	0.525	0.00	115	5.75	0.00	495	2.47	0.00	6140	6.45	26000	0.00	242300	0.00
021	0.55	0.00	120	6.00	0.00	515	2.57	0.00	6490	6.65	26700	0.00	247400	0.00
022	0.575	0.00	125	6.25	0.00	535	2.67	0.00	6850	6.85	27400	0.00	252500	0.00
023	0.60	0.00	130	6.50	0.00	555	2.77	0.00	7220	7.05	28100	0.00	257600	0.00
024	0.625	0.00	135	6.75	0.00	575	2.87	0.00	7600	7.25	28800	0.00	262700	0.00
025	0.65	0.00	140	7.00	0.00	595	2.97	0.00	7990	7.45	29500	0.00	267800	0.00
026	0.675	0.00	145	7.25	0.00	615	3.07	0.00	8390	7.65	30200	0.00	272900	0.00
027	0.70	0.00	150	7.50	0.00	635	3.17	0.00	8800	7.85	30900	0.00	278000	0.00
028	0.725	0.00	155	7.75	0.00	655	3.27	0.00	9220	8.05	31600	0.00	283100	0.00
029	0.75	0.00	160	8.00	0.00	675	3.37	0.00	9650	8.25	32300	0.00	288200	0.00
030	0.775	0.00	165	8.25	0.00	695	3.47	0.00	10090	8.45	33000	0.00	293300	0.00
031	0.80	0.00	170	8.50	0.00	715	3.57	0.00	10540	8.65	33700	0.00	298400	0.00
032	0.825	0.00	175	8.75	0.00	735	3.67	0.00	11000	8.85	34400	0.00	303500	0.00
033	0.85	0.00	180	9.00	0.00	755	3.77	0.00	11470	9.05	35100	0.00	308600	0.00
034	0.875	0.00	185	9.25	0.00	775	3.87	0.00	11950	9.25	35800	0.00	313700	0.00
035	0.90	0.00	190	9.50	0.00	795	3.97	0.00	12440	9.45	36500	0.00	318800	0.00
036	0.925	0.00	195	9.75	0.00	815	4.07	0.00	12940	9.65	37200	0.00	323900	0.00
037	1.00	0.00	200	10.00	0.00	835	4.17	0.00	13450	9.85	37900	0.00	329000	0.00
038	1.125	0.00	210	11.25	0.00	895	4.37	0.00	14470	10.25	39300	0.00	339200	0.00
039	1.25	0.00	220	12.50	0.00	955	4.57	0.00	15510	10.65	40700	0.00	349400	0.00
040	1.375	0.00	230	13.75	0.00	1015	4.77	0.00	16570	11.05	42100	0.00	359600	0.00
041	1.50	0.00	240	15.00	0.00	1075	4.97	0.00	17650	11.45	43500	0.00	369800	0.00
042	1.625	0.00	250	16.25	0.00	1135	5.17	0.00	18750	11.85	44900	0.00	380000	0.00
043	1.75	0.00	260	17.50	0.00	1195	5.37	0.00	19870	12.25	46300	0.00	390200	0.00
044	1.875	0.00	270	18.75	0.00	1255	5.57	0.00	21010	12.65	47700	0.00	400400	0.00
045	2.00	0.00	280	20.00	0.00	1315	5.77	0.00	22170	13.05	49100	0.00	410600	0.00
046	2.125	0.00	290	21.25	0.00	1375	5.97	0.00	23350	13.45	50500	0.00	420800	0.00
047	2.25	0.00	300	22.50	0.00	1435	6.17	0.00	24550	13.85	51900	0.00	431000	0.00
048	2.375	0.00	310	23.75	0.00	1495	6.37	0.00	25770	14.25	53300	0.00	441200	0.00
049	2.50	0.00	320	25.00	0.00	1555	6.57	0.00	27010	14.65	54700	0.00	451400	0.00
050	2.625	0.00	330	26.25	0.00	1615	6.77	0.00	28270	15.05	56100	0.00	461600	0.00
051	2.75	0.00	340	27.50	0.00	1675	6.97	0.00	29550	15.45	57500	0.00	471800	0.00
052	2.875	0.00	350	28.75	0.00	1735	7.17	0.00	30850	15.85	58900	0.00	482000	0.00
053	3.00	0.00	360	30.00	0.00	1795	7.37	0.00	32170	16.25	60300	0.00	492200	0.00
054	3.125	0.00	370	31.25	0.00	1855	7.57	0.00	33510	16.65	61700	0.00	502400	0.00
055	3.25	0.00	380	32.50	0.00	1915	7.77	0.00	34870	17.05	63100	0.00	512600	0.00
056	3.375	0.00	390	33.75	0.00	1975	7.97	0.00	36250	17.45	64500	0.00	522800	0.00
057	3.50	0.00	400	35.00	0.00	2035	8.17	0.00	37650	17.85	65900	0.00	533000	0.00
058	3.625	0.00	410	36.25	0.00	2095	8.37	0.00	39070	18.25	67300	0.00	543200	0.00
059	3.75	0.00	420	37.50	0.00	2155	8.57	0.00	40510	18.65	68700	0.00	553400	0.00
060	3.875	0.00	430	38.75	0.00	2215	8.77	0.00	41970	19.05	70100	0.00	563600	0.00
061	4.00	0.00	440	40.00	0.00	2275	8.97	0.00	43450	19.45	71500	0.00	573800	0.00
062	4.125	0.00	450	41.25	0.00	2335	9.17	0.00	44950	19.85	72900	0.00	584000	0.00
063	4.25	0.00	460	42.50	0.00	2395	9.37	0.00	46470	20.25	74300	0.00	594200	0.00
064	4.375	0.00	470	43.75	0.00	2455	9.57	0.00	48010	20.65	75700	0.00	604400	0.00
065	4.50	0.00	480	45.00	0.00	2515	9.77	0.00	49570	21.05	77100	0.00	614600	0.00
066	4.625	0.00	490	46.25	0.00	2575	9.97	0.00	51150	21.45	78500	0.00	624800	0.00
067	4.75	0.00	500	47.50	0.00	2635	10.17	0.00	52750	21.85	79900	0.00	635000	0.00
068	4.875	0.00	510	48.75	0.00	2695	10.37	0.00	54370	22.25	81300	0.00	645200	0.00
069	5.00	0.00	520	50.00	0.00	2755	10.57	0.00	56010	22.65	82700	0.00	655400	0.00
070	5.125	0.00	530	51.25	0.00	2815	10.77	0.00	57670	23.05	84100	0.00	665600	0.00
071	5.25	0.00	540	52.50	0.00	2875	10.97	0.00	59350	23.45	85500	0.00	675800	0.00
072	5.375	0.00	550	53.75	0.00	2935	11.17	0.00	61050	23.85	86900	0.00	686000	0.00
073	5.50	0.00	560	55.00	0.00	2995	11.37	0.00	62770	24.25	88300	0.00	696200	0.00
074	5.625	0.00	570	56.25	0.00	3055	11.57	0.00	64510	24.65	89700	0.00	706400	0.00
075	5.75	0.00	580	57.50	0.00	3115	11.77	0.00	66270	25.05	91100	0.00	716600	0.00
076	5.875	0.00	590	58.75	0.00	3175	11.97	0.00	68050	25.45	92500	0.00	726800	0.00
077	6.00	0.00	600	60.00	0.00	3235	12.17	0.00	69850	25.85	93900	0.00	737000	0.00
078														

Particle size Earthen ware Average



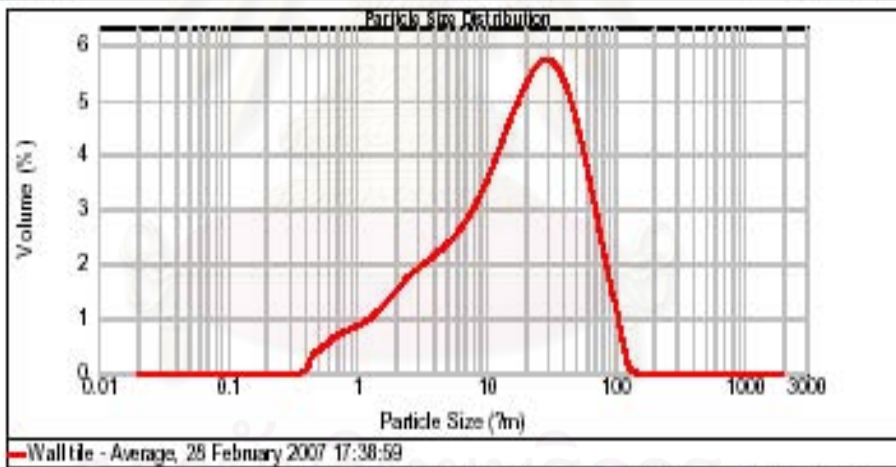
Result Analysis Report

Sample Name: Wall tile - Average
SOP Name:
Measured: 28 February 2007 17:38:59
Sample Source & type:
Measured by: User
Analysed: 28 February 2007 17:39:00
Sample bulk lot ref:
Result Source: Averaged

Particle Name: china clay (H)
Accessory Name: Hydro 2000MU (A)
Analysis model: General purpose
Sensitivity: Normal
Particle RI: 1.577
Absorption: 0.1
Size range: 0.020 to 2000.000 μ m
Obscuration: 13.72 %
Dispersant Name: Water
Dispersant RI: 1.330
Weighted Residual: 1.119 %
Result Emulation: Off

Concentration: 0.0121 % Vol
Span : 3.059
Uniformity: 0.951
Result units: Volume
Specific Surface Area: 0.999 m²/g
Surface Weighted Mean D[3,2]: 6.005 μ m
Vol. Weighted Mean D[4,3]: 25.163 μ m

d(0.1): 2.332 μ m **d(0.5):** 18.417 μ m **d(0.9):** 58.666 μ m



Particle Size (µm)	Volume (%)	Particle Size (µm)	Volume (%)	Particle Size (µm)	Volume (%)	Particle Size (µm)	Volume (%)
0.03	0.00	0.15	0.00	1.00	0.05	11.40	3.81
0.04	0.00	0.20	0.00	1.20	0.06	13.10	3.95
0.05	0.00	0.25	0.00	1.40	0.06	15.10	4.10
0.06	0.00	0.30	0.00	1.60	0.07	17.40	4.25
0.07	0.00	0.35	0.00	1.80	0.07	20.00	4.40
0.08	0.00	0.40	0.00	2.00	0.08	22.90	4.55
0.09	0.00	0.45	0.00	2.20	0.08	26.10	4.70
0.10	0.00	0.50	0.00	2.40	0.09	29.60	4.85
0.12	0.00	0.55	0.00	2.60	0.09	33.40	5.00
0.15	0.00	0.60	0.00	2.80	0.10	37.50	5.15
0.18	0.00	0.65	0.00	3.00	0.10	41.90	5.30
0.20	0.00	0.70	0.00	3.20	0.11	46.60	5.45
0.25	0.00	0.75	0.00	3.40	0.11	51.60	5.60
0.30	0.00	0.80	0.00	3.60	0.12	56.90	5.75
0.35	0.00	0.85	0.00	3.80	0.12	62.50	5.90
0.40	0.00	0.90	0.00	4.00	0.13	68.40	6.05
0.45	0.00	0.95	0.00	4.20	0.13	74.60	6.20
0.50	0.00	1.00	0.00	4.40	0.14	81.10	6.35
0.55	0.00	1.05	0.00	4.60	0.14	87.90	6.50
0.60	0.00	1.10	0.00	4.80	0.15	95.00	6.65
0.65	0.00	1.15	0.00	5.00	0.15	102.40	6.80
0.70	0.00	1.20	0.00	5.20	0.16	110.10	6.95
0.75	0.00	1.25	0.00	5.40	0.16	118.10	7.10
0.80	0.00	1.30	0.00	5.60	0.17	126.40	7.25
0.85	0.00	1.35	0.00	5.80	0.17	135.00	7.40
0.90	0.00	1.40	0.00	6.00	0.18	143.90	7.55
0.95	0.00	1.45	0.00	6.20	0.18	153.10	7.70
1.00	0.00	1.50	0.00	6.40	0.19	162.60	7.85
1.10	0.00	1.55	0.00	6.60	0.19	172.40	8.00
1.20	0.00	1.60	0.00	6.80	0.20	182.50	8.15
1.30	0.00	1.65	0.00	7.00	0.20	192.90	8.30
1.40	0.00	1.70	0.00	7.20	0.21	203.60	8.45
1.50	0.00	1.75	0.00	7.40	0.21	214.60	8.60
1.60	0.00	1.80	0.00	7.60	0.22	225.90	8.75
1.70	0.00	1.85	0.00	7.80	0.22	237.50	8.90
1.80	0.00	1.90	0.00	8.00	0.23	249.40	9.05
1.90	0.00	1.95	0.00	8.20	0.23	261.60	9.20
2.00	0.00	2.00	0.00	8.40	0.24	274.10	9.35
2.20	0.00	2.10	0.00	8.60	0.24	286.90	9.50
2.40	0.00	2.20	0.00	8.80	0.25	299.90	9.65
2.60	0.00	2.30	0.00	9.00	0.25	313.20	9.80
2.80	0.00	2.40	0.00	9.20	0.26	326.80	9.95
3.00	0.00	2.50	0.00	9.40	0.26	340.70	10.10
3.20	0.00	2.60	0.00	9.60	0.27	354.90	10.25
3.40	0.00	2.70	0.00	9.80	0.27	369.40	10.40
3.60	0.00	2.80	0.00	10.00	0.28	384.20	10.55
3.80	0.00	2.90	0.00	10.20	0.28	399.30	10.70
4.00	0.00	3.00	0.00	10.40	0.29	414.70	10.85
4.20	0.00	3.10	0.00	10.60	0.29	430.40	11.00
4.40	0.00	3.20	0.00	10.80	0.30	446.40	11.15
4.60	0.00	3.30	0.00	11.00	0.30	462.70	11.30
4.80	0.00	3.40	0.00	11.20	0.31	479.30	11.45
5.00	0.00	3.50	0.00	11.40	0.31	496.20	11.60
5.20	0.00	3.60	0.00	11.60	0.32	513.40	11.75
5.40	0.00	3.70	0.00	11.80	0.32	530.90	11.90
5.60	0.00	3.80	0.00	12.00	0.33	548.70	12.05
5.80	0.00	3.90	0.00	12.20	0.33	566.80	12.20
6.00	0.00	4.00	0.00	12.40	0.34	585.20	12.35
6.20	0.00	4.10	0.00	12.60	0.34	603.90	12.50
6.40	0.00	4.20	0.00	12.80	0.35	622.90	12.65
6.60	0.00	4.30	0.00	13.00	0.35	642.20	12.80
6.80	0.00	4.40	0.00	13.20	0.36	661.80	12.95
7.00	0.00	4.50	0.00	13.40	0.36	681.70	13.10
7.20	0.00	4.60	0.00	13.60	0.37	701.90	13.25
7.40	0.00	4.70	0.00	13.80	0.37	722.40	13.40
7.60	0.00	4.80	0.00	14.00	0.38	743.20	13.55
7.80	0.00	4.90	0.00	14.20	0.38	764.30	13.70
8.00	0.00	5.00	0.00	14.40	0.39	785.70	13.85
8.20	0.00	5.10	0.00	14.60	0.39	807.40	14.00
8.40	0.00	5.20	0.00	14.80	0.40	829.40	14.15
8.60	0.00	5.30	0.00	15.00	0.40	851.70	14.30
8.80	0.00	5.40	0.00	15.20	0.41	874.30	14.45
9.00	0.00	5.50	0.00	15.40	0.41	897.20	14.60
9.20	0.00	5.60	0.00	15.60	0.42	920.40	14.75
9.40	0.00	5.70	0.00	15.80	0.42	943.90	14.90
9.60	0.00	5.80	0.00	16.00	0.43	967.70	15.05
9.80	0.00	5.90	0.00	16.20	0.43	991.80	15.20
10.00	0.00	6.00	0.00	16.40	0.44	1016.20	15.35
10.20	0.00	6.10	0.00	16.60	0.44	1040.90	15.50
10.40	0.00	6.20	0.00	16.80	0.45	1065.90	15.65
10.60	0.00	6.30	0.00	17.00	0.45	1091.20	15.80
10.80	0.00	6.40	0.00	17.20	0.46	1116.80	15.95
11.00	0.00	6.50	0.00	17.40	0.46	1142.70	16.10
11.20	0.00	6.60	0.00	17.60	0.47	1168.90	16.25
11.40	0.00	6.70	0.00	17.80	0.47	1195.40	16.40
11.60	0.00	6.80	0.00	18.00	0.48	1222.20	16.55
11.80	0.00	6.90	0.00	18.20	0.48	1249.30	16.70
12.00	0.00	7.00	0.00	18.40	0.49	1276.70	16.85
12.20	0.00	7.10	0.00	18.60	0.49	1304.40	17.00
12.40	0.00	7.20	0.00	18.80	0.50	1332.40	17.15
12.60	0.00	7.30	0.00	19.00	0.50	1360.70	17.30
12.80	0.00	7.40	0.00	19.20	0.51	1389.30	17.45
13.00	0.00	7.50	0.00	19.40	0.51	1418.20	17.60
13.20	0.00	7.60	0.00	19.60	0.52	1447.40	17.75
13.40	0.00	7.70	0.00	19.80	0.52	1476.90	17.90
13.60	0.00	7.80	0.00	20.00	0.53	1506.70	18.05
13.80	0.00	7.90	0.00	20.20	0.53	1536.80	18.20
14.00	0.00	8.00	0.00	20.40	0.54	1567.20	18.35
14.20	0.00	8.10	0.00	20.60	0.54	1597.90	18.50
14.40	0.00	8.20	0.00	20.80	0.55	1628.90	18.65
14.60	0.00	8.30	0.00	21.00	0.55	1660.20	18.80
14.80	0.00	8.40	0.00	21.20	0.56	1691.80	18.95
15.00	0.00	8.50	0.00	21.40	0.56	1723.70	19.10
15.20	0.00	8.60	0.00	21.60	0.57	1755.90	19.25
15.40	0.00	8.70	0.00	21.80	0.57	1788.40	19.40
15.60	0.00	8.80	0.00	22.00	0.58	1821.20	19.55
15.80	0.00	8.90	0.00	22.20	0.58	1854.30	19.70
16.00	0.00	9.00	0.00	22.40	0.59	1887.70	19.85
16.20	0.00	9.10	0.00	22.60	0.59	1921.40	20.00
16.40	0.00	9.20	0.00	22.80	0.60	1955.40	20.15
16.60	0.00	9.30	0.00	23.00	0.60	1989.70	20.30
16.80	0.00	9.40	0.00	23.20	0.61	2024.30	20.45
17.00	0.00	9.50	0.00	23.40	0.61	2059.20	20.60
17.20	0.00	9.60	0.00	23.60	0.62	2094.40	20.75
17.40	0.00	9.70	0.00	23.80	0.62	2129.90	20.90
17.60	0.00	9.80	0.00	24.00	0.63	2165.70	21.05
17.80	0.00	9.90	0.00	24.20	0.63	2201.80	21.20
18.00	0.00	10.00	0.00	24.40	0.64	2238.20	21.35
18.20	0.00	10.10	0.00	24.60	0.64	2274.90	21.50
18.40	0.00	10.20	0.00	24.80	0.65	2311.90	21.65
18.60	0.00	10.30	0.00	25.00	0.65	2349.20	21.80
18.80	0.00	10.40	0.00	25.20	0.66	2386.80	21.95
19.00	0.00	10.50	0.00	25.40	0.66	2424.70	22.10
19.20	0.00	10.60	0.00	25.60	0.67	2462.90	22.25
19.40	0.00	10.70	0.00	25.80	0.67	2501.40	22.40
19.60	0.00	10.80	0.00	26.00	0.68	2540.20	22.55
19.80	0.00	10.90	0.00	26.20	0.68	2579.30	22.70
20.00	0.00	11.00	0.00	26.40	0.69	2618.70	22.85
20.20	0.00	11.10	0.00	26.60	0.69	2658.40	23.00
20.40	0.00	11.20	0.00	26.80	0.70	2698.40	23.15
20.60	0.00	11.30	0.00	27.00	0.70	2738.70	23.30
20.80	0.00	11.40	0.00	27.20	0.71	2779.30	23.45
21.00	0.00	11.50	0.00	27.40	0.71	2820.20	23.60
21.20	0.00	11.60	0.00	27.60	0.72	2861.40	23.75
21.40	0.00	11.70	0.00	27.80	0.72	2902.90	23.90
21.60	0.00	11.80	0.00	28.00	0.73	2944.70	24.05
21.80	0.00	11.90	0.00	28.20	0.73	2986.80	24.20
22.00	0.00	12.00	0.00	28.40	0.7		

Particle size Porcelain Average



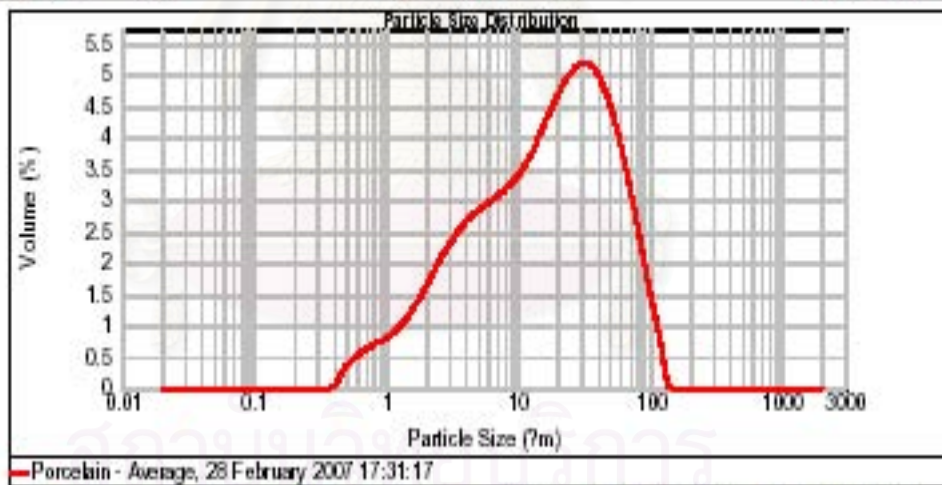
Result Analysis Report

Sample Name: Porcelain - Average
 Sample Source & type:
 Sample bulk lot ref:
 SOP Name:
 Measured by: User
 Result Source: Averaged
 Measured: 28 February 2007 17:31:17
 Analysed: 28 February 2007 17:31:18

Particle Name: china clay (H)
 Particle RI: 1.577
 Dispersant Name: Water
 Accessory Name: Hydro 2000MU (A)
 Absorption: 0.1
 Dispersant RI: 1.330
 Analysis model: General purpose
 Size range: 0.020 to 2000.000 um
 Weighted Residual: 1.032 %
 Sensitivity: Normal
 Obscuration: 12.79 %
 Result Emulation: Off

Concentration: 0.0109 %Vol
 Specific Surface Area: 1.02 m²/g
 Span: 3.434
 Surface Weighted Mean D[3,2]: 5.898 um
 Uniformity: 1.07
 Vol. Weighted Mean D[4,3]: 25.398 um
 Result units: Volume

d(0.1): 2.335 um d(0.5): 17.250 um d(0.9): 61.564 um



Bin	Volume (%)	Bin	Volume (%)	Bin	Volume (%)	Bin	Volume (%)	Bin	Volume (%)	Bin	Volume (%)
0.00	0.00	0.125	0.00	1.00	0.00	11.40	3.37	128.20	0.00	1250.00	0.00
0.01	0.00	0.150	0.00	1.25	0.00	13.10	3.58	138.05	0.00	1405.90	0.00
0.02	0.00	0.175	0.00	1.50	0.00	14.80	3.89	148.89	0.00	1512.80	0.00
0.03	0.00	0.200	0.00	1.75	0.00	16.50	4.20	159.78	0.00	1619.70	0.00
0.04	0.00	0.225	0.00	2.00	0.00	18.20	4.51	170.67	0.00	1726.60	0.00
0.05	0.00	0.250	0.00	2.25	0.00	19.90	4.82	181.56	0.00	1833.50	0.00
0.06	0.00	0.275	0.00	2.50	0.00	21.60	5.13	192.45	0.00	1940.40	0.00
0.07	0.00	0.300	0.00	2.75	0.00	23.30	5.44	203.34	0.00	2047.30	0.00
0.08	0.00	0.325	0.00	3.00	0.00	25.00	5.75	214.23	0.00	2154.20	0.00
0.09	0.00	0.350	0.00	3.25	0.00	26.70	6.06	225.12	0.00	2261.10	0.00
0.10	0.00	0.375	0.00	3.50	0.00	28.40	6.37	236.01	0.00	2368.00	0.00
0.12	0.00	0.400	0.00	3.75	0.00	30.10	6.68	246.90	0.00	2474.90	0.00
0.15	0.00	0.425	0.00	4.00	0.00	31.80	6.99	257.79	0.00	2581.80	0.00
0.17	0.00	0.450	0.00	4.25	0.00	33.50	7.30	268.68	0.00	2688.70	0.00
0.20	0.00	0.475	0.00	4.50	0.00	35.20	7.61	279.57	0.00	2795.60	0.00
0.25	0.00	0.500	0.00	4.75	0.00	36.90	7.92	290.46	0.00	2902.50	0.00
0.30	0.00	0.525	0.00	5.00	0.00	38.60	8.23	301.35	0.00	3009.40	0.00
0.35	0.00	0.550	0.00	5.25	0.00	40.30	8.54	312.24	0.00	3116.30	0.00
0.40	0.00	0.575	0.00	5.50	0.00	42.00	8.85	323.13	0.00	3223.20	0.00
0.45	0.00	0.600	0.00	5.75	0.00	43.70	9.16	334.02	0.00	3330.10	0.00
0.50	0.00	0.625	0.00	6.00	0.00	45.40	9.47	344.91	0.00	3437.00	0.00
0.55	0.00	0.650	0.00	6.25	0.00	47.10	9.78	355.80	0.00	3543.90	0.00
0.60	0.00	0.675	0.00	6.50	0.00	48.80	10.09	366.69	0.00	3650.80	0.00
0.65	0.00	0.700	0.00	6.75	0.00	50.50	10.40	377.58	0.00	3757.70	0.00
0.70	0.00	0.725	0.00	7.00	0.00	52.20	10.71	388.47	0.00	3864.60	0.00
0.75	0.00	0.750	0.00	7.25	0.00	53.90	11.02	399.36	0.00	3971.50	0.00
0.80	0.00	0.775	0.00	7.50	0.00	55.60	11.33	410.25	0.00	4078.40	0.00
0.85	0.00	0.800	0.00	7.75	0.00	57.30	11.64	421.14	0.00	4185.30	0.00
0.90	0.00	0.825	0.00	8.00	0.00	59.00	11.95	432.03	0.00	4292.20	0.00
0.95	0.00	0.850	0.00	8.25	0.00	60.70	12.26	442.92	0.00	4399.10	0.00
1.00	0.00	0.875	0.00	8.50	0.00	62.40	12.57	453.81	0.00	4506.00	0.00
1.12	0.00	0.900	0.00	8.75	0.00	64.10	12.88	464.70	0.00	4612.90	0.00
1.25	0.00	0.925	0.00	9.00	0.00	65.80	13.19	475.59	0.00	4719.80	0.00
1.40	0.00	0.950	0.00	9.25	0.00	67.50	13.50	486.48	0.00	4826.70	0.00
1.55	0.00	0.975	0.00	9.50	0.00	69.20	13.81	497.37	0.00	4933.60	0.00
1.70	0.00	1.000	0.00	9.75	0.00	70.90	14.12	508.26	0.00	5040.50	0.00
1.85	0.00	1.025	0.00	10.00	0.00	72.60	14.43	519.15	0.00	5147.40	0.00
2.00	0.00	1.050	0.00	10.25	0.00	74.30	14.74	530.04	0.00	5254.30	0.00
2.20	0.00	1.075	0.00	10.50	0.00	76.00	15.05	540.93	0.00	5361.20	0.00
2.40	0.00	1.100	0.00	10.75	0.00	77.70	15.36	551.82	0.00	5468.10	0.00
2.60	0.00	1.125	0.00	11.00	0.00	79.40	15.67	562.71	0.00	5575.00	0.00
2.80	0.00	1.150	0.00	11.25	0.00	81.10	15.98	573.60	0.00	5681.90	0.00
3.00	0.00	1.175	0.00	11.50	0.00	82.80	16.29	584.49	0.00	5788.80	0.00
3.20	0.00	1.200	0.00	11.75	0.00	84.50	16.60	595.38	0.00	5895.70	0.00
3.40	0.00	1.225	0.00	12.00	0.00	86.20	16.91	606.27	0.00	6002.60	0.00
3.60	0.00	1.250	0.00	12.25	0.00	87.90	17.22	617.16	0.00	6109.50	0.00
3.80	0.00	1.275	0.00	12.50	0.00	89.60	17.53	628.05	0.00	6216.40	0.00
4.00	0.00	1.300	0.00	12.75	0.00	91.30	17.84	638.94	0.00	6323.30	0.00
4.20	0.00	1.325	0.00	13.00	0.00	93.00	18.15	649.83	0.00	6430.20	0.00
4.40	0.00	1.350	0.00	13.25	0.00	94.70	18.46	660.72	0.00	6537.10	0.00
4.60	0.00	1.375	0.00	13.50	0.00	96.40	18.77	671.61	0.00	6644.00	0.00
4.80	0.00	1.400	0.00	13.75	0.00	98.10	19.08	682.50	0.00	6750.90	0.00
5.00	0.00	1.425	0.00	14.00	0.00	99.80	19.39	693.39	0.00	6857.80	0.00
5.20	0.00	1.450	0.00	14.25	0.00	101.50	19.70	704.28	0.00	6964.70	0.00
5.40	0.00	1.475	0.00	14.50	0.00	103.20	20.01	715.17	0.00	7071.60	0.00
5.60	0.00	1.500	0.00	14.75	0.00	104.90	20.32	726.06	0.00	7178.50	0.00
5.80	0.00	1.525	0.00	15.00	0.00	106.60	20.63	736.95	0.00	7285.40	0.00
6.00	0.00	1.550	0.00	15.25	0.00	108.30	20.94	747.84	0.00	7392.30	0.00
6.20	0.00	1.575	0.00	15.50	0.00	110.00	21.25	758.73	0.00	7499.20	0.00
6.40	0.00	1.600	0.00	15.75	0.00	111.70	21.56	769.62	0.00	7606.10	0.00
6.60	0.00	1.625	0.00	16.00	0.00	113.40	21.87	780.51	0.00	7713.00	0.00
6.80	0.00	1.650	0.00	16.25	0.00	115.10	22.18	791.40	0.00	7819.90	0.00
7.00	0.00	1.675	0.00	16.50	0.00	116.80	22.49	802.29	0.00	7926.80	0.00
7.20	0.00	1.700	0.00	16.75	0.00	118.50	22.80	813.18	0.00	8033.70	0.00
7.40	0.00	1.725	0.00	17.00	0.00	120.20	23.11	824.07	0.00	8140.60	0.00
7.60	0.00	1.750	0.00	17.25	0.00	121.90	23.42	834.96	0.00	8247.50	0.00
7.80	0.00	1.775	0.00	17.50	0.00	123.60	23.73	845.85	0.00	8354.40	0.00
8.00	0.00	1.800	0.00	17.75	0.00	125.30	24.04	856.74	0.00	8461.30	0.00
8.20	0.00	1.825	0.00	18.00	0.00	127.00	24.35	867.63	0.00	8568.20	0.00
8.40	0.00	1.850	0.00	18.25	0.00	128.70	24.66	878.52	0.00	8675.10	0.00
8.60	0.00	1.875	0.00	18.50	0.00	130.40	24.97	889.41	0.00	8782.00	0.00
8.80	0.00	1.900	0.00	18.75	0.00	132.10	25.28	900.30	0.00	8888.90	0.00
9.00	0.00	1.925	0.00	19.00	0.00	133.80	25.59	911.19	0.00	8995.80	0.00
9.20	0.00	1.950	0.00	19.25	0.00	135.50	25.90	922.08	0.00	9102.70	0.00
9.40	0.00	1.975	0.00	19.50	0.00	137.20	26.21	932.97	0.00	9209.60	0.00
9.60	0.00	2.000	0.00	19.75	0.00	138.90	26.52	943.86	0.00	9316.50	0.00
9.80	0.00	2.025	0.00	20.00	0.00	140.60	26.83	954.75	0.00	9423.40	0.00
10.00	0.00	2.050	0.00	20.25	0.00	142.30	27.14	965.64	0.00	9530.30	0.00
10.20	0.00	2.075	0.00	20.50	0.00	144.00	27.45	976.53	0.00	9637.20	0.00
10.40	0.00	2.100	0.00	20.75	0.00	145.70	27.76	987.42	0.00	9744.10	0.00
10.60	0.00	2.125	0.00	21.00	0.00	147.40	28.07	998.31	0.00	9851.00	0.00
10.80	0.00	2.150	0.00	21.25	0.00	149.10	28.38	1009.20	0.00	9957.90	0.00
11.00	0.00	2.175	0.00	21.50	0.00	150.80	28.69	1020.09	0.00	10064.80	0.00
11.20	0.00	2.200	0.00	21.75	0.00	152.50	29.00	1030.98	0.00	10171.70	0.00
11.40	0.00	2.225	0.00	22.00	0.00	154.20	29.31	1041.87	0.00	10278.60	0.00
11.60	0.00	2.250	0.00	22.25	0.00	155.90	29.62	1052.76	0.00	10385.50	0.00
11.80	0.00	2.275	0.00	22.50	0.00	157.60	29.93	1063.65	0.00	10492.40	0.00
12.00	0.00	2.300	0.00	22.75	0.00	159.30	30.24	1074.54	0.00	10599.30	0.00
12.20	0.00	2.325	0.00	23.00	0.00	161.00	30.55	1085.43	0.00	10706.20	0.00
12.40	0.00	2.350	0.00	23.25	0.00	162.70	30.86	1096.32	0.00	10813.10	0.00
12.60	0.00	2.375	0.00	23.50	0.00	164.40	31.17	1107.21	0.00	10920.00	0.00
12.80	0.00	2.400	0.00	23.75	0.00	166.10	31.48	1118.10	0.00	11026.90	0.00
13.00	0.00	2.425	0.00	24.00	0.00	167.80	31.79	1128.99	0.00		

Particle size Terracotta sample3



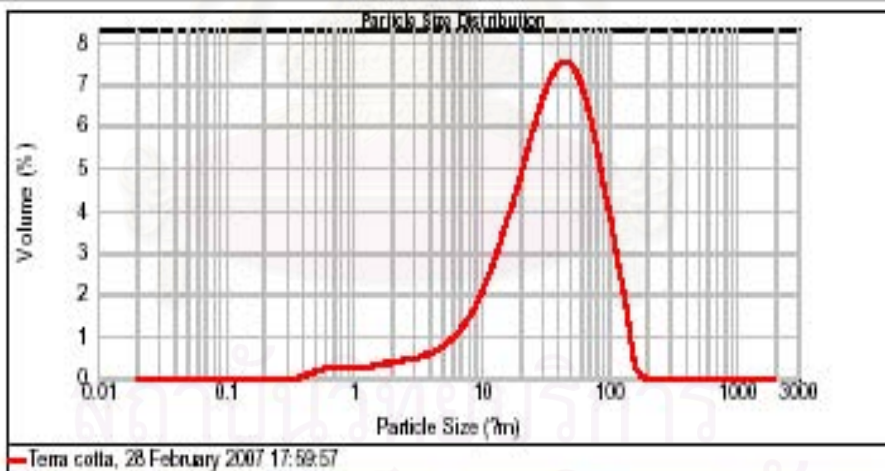
Result Analysis Report

Sample Name: Terra cotta
 SOP Name:
 Measured: 28 February 2007 17:59:57
 Sample Source & type:
 Measured by: User
 Analysed: 28 February 2007 17:59:58
 Sample bulk lot ref:
 Result Source: Measurement

Particle Name: china clay (nl)
 Accessory Name: Hydro 2000MU (A)
 Analysis model: General purpose
 Sensitivity: Normal
 Particle RI: 1.577
 Absorption: 0.1
 Size range: 0.020 to 2000.000 um
 Obscuration: 13.35 %
 Dispersant Name: Water
 Dispersant RI: 1.330
 Weighted Residual: 1.029 %
 Result Emulation: Off

Concentration: 0.0277 % Vol
 Span : 2.202
 Uniformity: 0.673
 Result units: Volume
 Specific Surface Area: 0.434 m²/g
 Surface Weighted Mean D[3,2]: 13.814 um
 Vol. Weighted Mean D[4,3]: 43.488 um

d(0.1): 8.988 um d(0.5): 36.342 um d(0.9): 89.020 um



Bin #	Bin Range (µm)	Volume (%)	Bin #	Bin Range (µm)	Volume (%)	Bin #	Bin Range (µm)	Volume (%)	Bin #	Bin Range (µm)	Volume (%)
000	0.00	0.00	100	1.00	0.26	1142	2.00	1.28	128	12.00	0.00
001	0.00	0.00	120	1.20	0.26	1145	2.00	1.30	132	12.00	0.00
005	0.00	0.00	140	1.40	0.26	1148	2.00	1.32	136	12.00	0.00
005	0.00	0.00	160	1.60	0.26	1152	2.00	1.34	140	12.00	0.00
007	0.00	0.00	180	1.80	0.26	1155	2.00	1.36	144	12.00	0.00
000	0.00	0.00	200	2.00	0.26	1158	2.00	1.38	148	12.00	0.00
002	0.00	0.00	220	2.20	0.26	1162	2.00	1.40	152	12.00	0.00
003	0.00	0.00	240	2.40	0.26	1165	2.00	1.42	156	12.00	0.00
000	0.00	0.00	260	2.60	0.26	1168	2.00	1.44	160	12.00	0.00
002	0.00	0.00	280	2.80	0.26	1172	2.00	1.46	164	12.00	0.00
000	0.00	0.00	300	3.00	0.26	1175	2.00	1.48	168	12.00	0.00
002	0.00	0.00	320	3.20	0.26	1178	2.00	1.50	172	12.00	0.00
000	0.00	0.00	340	3.40	0.26	1182	2.00	1.52	176	12.00	0.00
000	0.00	0.00	360	3.60	0.26	1185	2.00	1.54	180	12.00	0.00
000	0.00	0.00	380	3.80	0.26	1188	2.00	1.56	184	12.00	0.00
000	0.00	0.00	400	4.00	0.26	1192	2.00	1.58	188	12.00	0.00
000	0.00	0.00	420	4.20	0.26	1195	2.00	1.60	192	12.00	0.00
000	0.00	0.00	440	4.40	0.26	1198	2.00	1.62	196	12.00	0.00
000	0.00	0.00	460	4.60	0.26	1202	2.00	1.64	200	12.00	0.00
000	0.00	0.00	480	4.80	0.26	1205	2.00	1.66	204	12.00	0.00
000	0.00	0.00	500	5.00	0.26	1208	2.00	1.68	208	12.00	0.00
000	0.00	0.00	520	5.20	0.26	1212	2.00	1.70	212	12.00	0.00
000	0.00	0.00	540	5.40	0.26	1215	2.00	1.72	216	12.00	0.00
000	0.00	0.00	560	5.60	0.26	1218	2.00	1.74	220	12.00	0.00
000	0.00	0.00	580	5.80	0.26	1222	2.00	1.76	224	12.00	0.00
000	0.00	0.00	600	6.00	0.26	1225	2.00	1.78	228	12.00	0.00
000	0.00	0.00	620	6.20	0.26	1228	2.00	1.80	232	12.00	0.00
000	0.00	0.00	640	6.40	0.26	1232	2.00	1.82	236	12.00	0.00
000	0.00	0.00	660	6.60	0.26	1235	2.00	1.84	240	12.00	0.00
000	0.00	0.00	680	6.80	0.26	1238	2.00	1.86	244	12.00	0.00
000	0.00	0.00	700	7.00	0.26	1242	2.00	1.88	248	12.00	0.00
000	0.00	0.00	720	7.20	0.26	1245	2.00	1.90	252	12.00	0.00
000	0.00	0.00	740	7.40	0.26	1248	2.00	1.92	256	12.00	0.00
000	0.00	0.00	760	7.60	0.26	1252	2.00	1.94	260	12.00	0.00
000	0.00	0.00	780	7.80	0.26	1255	2.00	1.96	264	12.00	0.00
000	0.00	0.00	800	8.00	0.26	1258	2.00	1.98	268	12.00	0.00
000	0.00	0.00	820	8.20	0.26	1262	2.00	2.00	272	12.00	0.00
000	0.00	0.00	840	8.40	0.26	1265	2.00	2.02	276	12.00	0.00
000	0.00	0.00	860	8.60	0.26	1268	2.00	2.04	280	12.00	0.00
000	0.00	0.00	880	8.80	0.26	1272	2.00	2.06	284	12.00	0.00
000	0.00	0.00	900	9.00	0.26	1275	2.00	2.08	288	12.00	0.00
000	0.00	0.00	920	9.20	0.26	1278	2.00	2.10	292	12.00	0.00
000	0.00	0.00	940	9.40	0.26	1282	2.00	2.12	296	12.00	0.00
000	0.00	0.00	960	9.60	0.26	1285	2.00	2.14	300	12.00	0.00
000	0.00	0.00	980	9.80	0.26	1288	2.00	2.16	304	12.00	0.00
000	0.00	0.00	1000	10.00	0.26	1292	2.00	2.18	308	12.00	0.00

Operator notes:

Particle size Terracotta Average



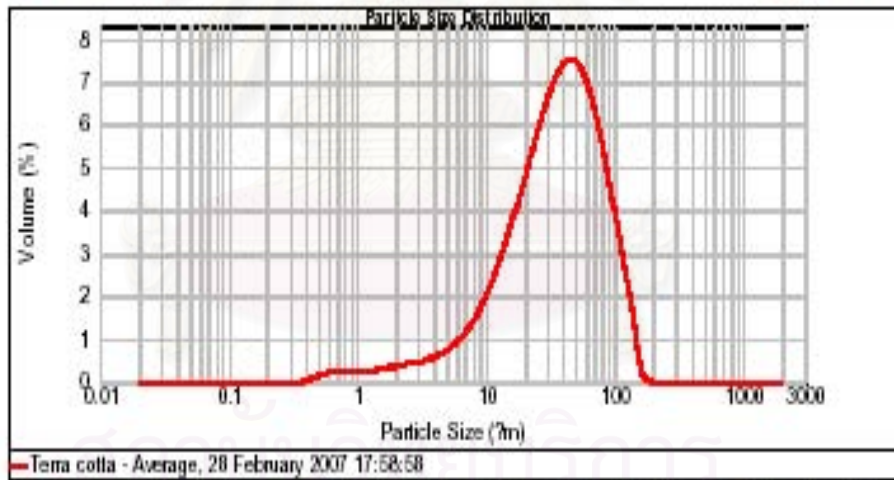
Result Analysis Report

Sample Name: Terra cotta - Average SOP Name: Measured: 28 February 2007 17:58:58
 Sample Source & type: Measured by: User Analysed: 28 February 2007 17:58:59
 Sample bulk lot ref: Result Source: Averaged

Particle Name: china clay (nl) Accessory Name: Hydro 2000MU (A) Analysis model: General purpose Sensitivity: Normal
 Particle RI: 1.577 Absorption: 0.1 Size range: 0.020 to 2000.000 um Obscuration: 13.33 %
 Dispersant Name: Water Dispersant RI: 1.330 Weighted Residual: 1.018 % Result Emulation: Off

Concentration: 0.0276 % Vol Span : 2.204 Uniformity: 0.674 Result units: Volume
 Specific Surface Area: 0.436 m²/g Surface Weighted Mean D[3,2]: 13.771 um Vol. Weighted Mean D[4,3]: 43.375 um

d[0.1]: 8.947 um d[0.5]: 36.246 um d[0.9]: 88.832 um



Bin #	Bin Range (µm)	Volume (%)	Bin #	Bin Range (µm)	Volume (%)	Bin #	Bin Range (µm)	Volume (%)	Bin #	Bin Range (µm)	Volume (%)	Bin #	Bin Range (µm)	Volume (%)	Bin #	Bin Range (µm)	Volume (%)
000	0.00	0.00	016	0.80	0.00	100	1.00	0.26	1142	2.00	1.00	12820	1.00	0.00	12840	0.00	
001	0.00	0.00	017	0.90	0.00	110	1.10	0.26	1143	2.10	1.00	12850	0.75	0.00	12860	0.00	
002	0.00	0.00	018	1.00	0.00	105	1.05	0.26	1144	2.20	1.00	12870	0.00	0.00	12880	0.00	
003	0.00	0.00	019	1.10	0.00	100	1.00	0.26	1145	2.30	1.00	12880	0.00	0.00	12890	0.00	
004	0.00	0.00	020	1.20	0.00	95	1.05	0.26	1146	2.40	1.00	12900	0.00	0.00	12910	0.00	
005	0.00	0.00	021	1.30	0.00	90	1.10	0.26	1147	2.50	1.00	12920	0.00	0.00	12930	0.00	
006	0.00	0.00	022	1.40	0.00	85	1.15	0.26	1148	2.60	1.00	12940	0.00	0.00	12950	0.00	
007	0.00	0.00	023	1.50	0.00	80	1.20	0.26	1149	2.70	1.00	12960	0.00	0.00	12970	0.00	
008	0.00	0.00	024	1.60	0.00	75	1.25	0.26	1150	2.80	1.00	12980	0.00	0.00	12990	0.00	
009	0.00	0.00	025	1.70	0.00	70	1.30	0.26	1151	2.90	1.00	13000	0.00	0.00	13010	0.00	
010	0.00	0.00	026	1.80	0.00	65	1.35	0.26	1152	3.00	1.00	13020	0.00	0.00	13030	0.00	
011	0.00	0.00	027	1.90	0.00	60	1.40	0.26	1153	3.10	1.00	13040	0.00	0.00	13050	0.00	
012	0.00	0.00	028	2.00	0.00	55	1.45	0.26	1154	3.20	1.00	13060	0.00	0.00	13070	0.00	
013	0.00	0.00	029	2.10	0.00	50	1.50	0.26	1155	3.30	1.00	13080	0.00	0.00	13090	0.00	
014	0.00	0.00	030	2.20	0.00	45	1.55	0.26	1156	3.40	1.00	13100	0.00	0.00	13110	0.00	
015	0.00	0.00	031	2.30	0.00	40	1.60	0.26	1157	3.50	1.00	13120	0.00	0.00	13130	0.00	
016	0.00	0.00	032	2.40	0.00	35	1.65	0.26	1158	3.60	1.00	13140	0.00	0.00	13150	0.00	
017	0.00	0.00	033	2.50	0.00	30	1.70	0.26	1159	3.70	1.00	13160	0.00	0.00	13170	0.00	
018	0.00	0.00	034	2.60	0.00	25	1.75	0.26	1160	3.80	1.00	13180	0.00	0.00	13190	0.00	
019	0.00	0.00	035	2.70	0.00	20	1.80	0.26	1161	3.90	1.00	13200	0.00	0.00	13210	0.00	
020	0.00	0.00	036	2.80	0.00	15	1.85	0.26	1162	4.00	1.00	13220	0.00	0.00	13230	0.00	
021	0.00	0.00	037	2.90	0.00	10	1.90	0.26	1163	4.10	1.00	13240	0.00	0.00	13250	0.00	
022	0.00	0.00	038	3.00	0.00	5	1.95	0.26	1164	4.20	1.00	13260	0.00	0.00	13270	0.00	
023	0.00	0.00	039	3.10	0.00	0	2.00	0.26	1165	4.30	1.00	13280	0.00	0.00	13290	0.00	
024	0.00	0.00	040	3.20	0.00	0	2.05	0.26	1166	4.40	1.00	13300	0.00	0.00	13310	0.00	
025	0.00	0.00	041	3.30	0.00	0	2.10	0.26	1167	4.50	1.00	13320	0.00	0.00	13330	0.00	
026	0.00	0.00	042	3.40	0.00	0	2.15	0.26	1168	4.60	1.00	13340	0.00	0.00	13350	0.00	
027	0.00	0.00	043	3.50	0.00	0	2.20	0.26	1169	4.70	1.00	13360	0.00	0.00	13370	0.00	
028	0.00	0.00	044	3.60	0.00	0	2.25	0.26	1170	4.80	1.00	13380	0.00	0.00	13390	0.00	
029	0.00	0.00	045	3.70	0.00	0	2.30	0.26	1171	4.90	1.00	13400	0.00	0.00	13410	0.00	
030	0.00	0.00	046	3.80	0.00	0	2.35	0.26	1172	5.00	1.00	13420	0.00	0.00	13430	0.00	
031	0.00	0.00	047	3.90	0.00	0	2.40	0.26	1173	5.10	1.00	13440	0.00	0.00	13450	0.00	
032	0.00	0.00	048	4.00	0.00	0	2.45	0.26	1174	5.20	1.00	13460	0.00	0.00	13470	0.00	
033	0.00	0.00	049	4.10	0.00	0	2.50	0.26	1175	5.30	1.00	13480	0.00	0.00	13490	0.00	
034	0.00	0.00	050	4.20	0.00	0	2.55	0.26	1176	5.40	1.00	13500	0.00	0.00	13510	0.00	
035	0.00	0.00	051	4.30	0.00	0	2.60	0.26	1177	5.50	1.00	13520	0.00	0.00	13530	0.00	
036	0.00	0.00	052	4.40	0.00	0	2.65	0.26	1178	5.60	1.00	13540	0.00	0.00	13550	0.00	
037	0.00	0.00	053	4.50	0.00	0	2.70	0.26	1179	5.70	1.00	13560	0.00	0.00	13570	0.00	
038	0.00	0.00	054	4.60	0.00	0	2.75	0.26	1180	5.80	1.00	13580	0.00	0.00	13590	0.00	
039	0.00	0.00	055	4.70	0.00	0	2.80	0.26	1181	5.90	1.00	13600	0.00	0.00	13610	0.00	
040	0.00	0.00	056	4.80	0.00	0	2.85	0.26	1182	6.00	1.00	13620	0.00	0.00	13630	0.00	
041	0.00	0.00	057	4.90	0.00	0	2.90	0.26	1183	6.10	1.00	13640	0.00	0.00	13650	0.00	
042	0.00	0.00	058	5.00	0.00	0	2.95	0.26	1184	6.20	1.00	13660	0.00	0.00	13670	0.00	
043	0.00	0.00	059	5.10	0.00	0	3.00	0.26	1185	6.30	1.00	13680	0.00	0.00	13690	0.00	
044	0.00	0.00	060	5.20	0.00	0	3.05	0.26	1186	6.40	1.00	13700	0.00	0.00	13710	0.00	
045	0.00	0.00	061	5.30	0.00	0	3.10	0.26	1187	6.50	1.00	13720	0.00	0.00	13730	0.00	
046	0.00	0.00	062	5.40	0.00	0	3.15	0.26	1188	6.60	1.00	13740	0.00	0.00	13750	0.00	
047	0.00	0.00	063	5.50	0.00	0	3.20	0.26	1189	6.70	1.00	13760	0.00	0.00	13770	0.00	
048	0.00	0.00	064	5.60	0.00	0	3.25	0.26	1190	6.80	1.00	13780	0.00	0.00	13790	0.00	
049	0.00	0.00	065	5.70	0.00	0	3.30	0.26	1191	6.90	1.00	13800	0.00	0.00	13810	0.00	
050	0.00	0.00	066	5.80	0.00	0	3.35	0.26	1192	7.00	1.00	13820	0.00	0.00	13830	0.00	
051	0.00	0.00	067	5.90	0.00	0	3.40	0.26	1193	7.10	1.00	13840	0.00	0.00	13850	0.00	
052	0.00	0.00	068	6.00	0.00	0	3.45	0.26	1194	7.20	1.00	13860	0.00	0.00	13870	0.00	
053	0.00	0.00	069	6.10	0.00	0	3.50	0.26	1195	7.30	1.00	13880	0.00	0.00	13890	0.00	
054	0.00	0.00	070	6.20	0.00	0	3.55	0.26	1196	7.40	1.00	13900	0.00	0.00	13910	0.00	
055	0.00	0.00	071	6.30	0.00	0	3.60	0.26	1197	7.50	1.00	13920	0.00	0.00	13930	0.00	
056	0.00	0.00	072	6.40	0.00	0	3.65	0.26	1198	7.60	1.00	13940	0.00	0.00	13950	0.00	
057	0.00	0.00	073	6.50	0.00	0	3.70	0.26	1199	7.70	1.00	13960	0.00	0.00	13970	0.00	
058	0.00	0.00	074	6.60	0.00	0	3.75	0.26	1200	7.80	1.00	13980	0.00	0.00	13990	0.00	
059	0.00	0.00	075	6.70	0.00	0	3.80	0.26	1201	7.90	1.00	14000	0.00	0.00	14010	0.00	
060	0.00	0.00	076	6.80	0.00	0	3.85	0.26	1202	8.00	1.00	14020	0.00	0.00	14030	0.00	
061	0.00	0.00	077	6.90	0.00	0	3.90	0.26	1203	8.10	1.00	14040	0.00	0.00	14050	0.00	
062	0.00	0.00	078	7.00	0.00	0	3.95	0.26	1204	8.20	1.00	14060	0.00	0.00	14070	0.00	
063	0.00	0.00	079	7.10	0.00	0	4.00	0.26	1205	8.30	1.00	14080	0.00	0.00	14090	0.00	
064	0.00	0.00	080	7.20	0.00	0	4.05	0.26	1206	8.40	1.00	14100	0.00	0.00	14110	0.00	
065	0.00	0.00	081	7.30	0.00	0	4.10	0.26	1207	8.50	1.00	14120	0.00	0.00	14130	0.00	
066	0.00	0.00	082	7.40	0.00	0	4.15	0.26	1208	8.60	1.00	14140	0.00	0.00	14150	0.00	
067	0.00	0.00	083	7.50	0.00	0	4.20	0.26	1209	8.70	1.00	14160	0.00	0.00	14170	0.00	
068	0.00	0.00	084	7.60	0.00	0	4.25	0.26	1210	8.80	1.00	14180	0.00	0.00	14190	0.00	
069	0.00	0.00	085	7.70	0.00	0	4.30	0.26	1211	8.90	1.00	14200	0.00	0.00	14210	0.00	
070	0.00	0.00	086	7.80	0.00	0	4.35	0.26	1212	9.00	1.00	14220	0.00	0.00	14230	0.00	
071	0.00	0.00	087	7.90	0.00	0	4.40	0.26	1213	9.10	1.00	14240	0.00	0.00	14250	0.00	
072	0.00	0.00	088	8.00	0.00	0	4.45	0.26	1214	9.20	1.00						

Particle size Vitreous china Average



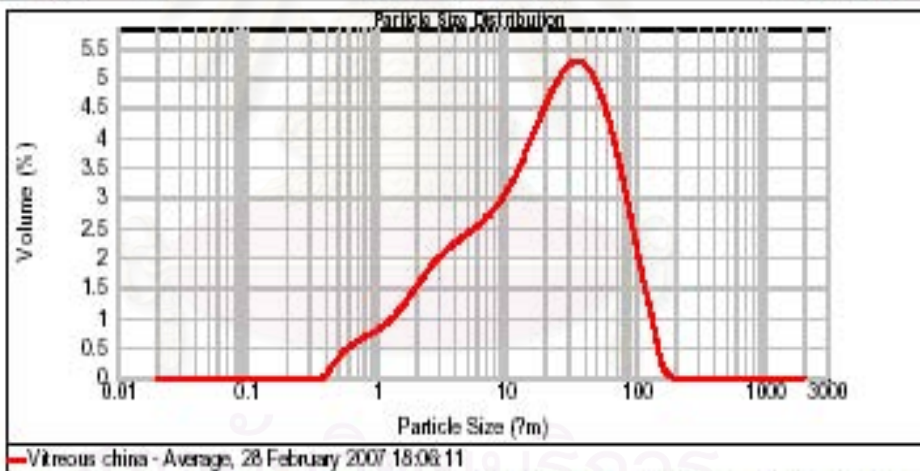
Result Analysis Report

Sample Name: Vitreous china - Average SOP Name: Measured: 28 February 2007 18:08:11
 Sample Source & type: Measured by: User Analysed: 28 February 2007 18:08:12
 Sample bulk lot ref: Result Source: Averaged

Particle Name: china clay (nl) Accessory Name: Hydro 2000MU (A) Analysis model: General purpose Sensitivity: Normal
 Particle RI: 1.577 Absorption: 0.1 Size range: 0.020 to 2000.000 μ m Obscuration: 14.47 %
 Dispersant Name: Water Dispersant RI: 1.330 Weighted Residual: 1.802 % Result Emulation: Off

Concentration: 0.0135 % Vol Span: 3.304 Uniformity: 1.05 Result units: Volume
 Specific Surface Area: 0.939 m²/g Surface Weighted Mean D[3,2]: 6.387 μ m Vol. Weighted Mean D[4,3]: 29.999 μ m

d[0.1]: 2.456 μ m d[0.5]: 20.600 μ m d[0.9]: 72.368 μ m



Bin #	Bin Range (µm)	Volume (%)	Bin #	Bin Range (µm)	Volume (%)	Bin #	Bin Range (µm)	Volume (%)	Bin #	Bin Range (µm)	Volume (%)	Bin #	Bin Range (µm)	Volume (%)
000	0.00	0.00	100	1.20	0.80	1142	2.10	12820	1.00	12820	0.00	12820	0.00	
001	0.02	0.00	120	1.45	0.81	1145	2.30	13025	1.00	14640	0.00	14640	0.00	
002	0.03	0.00	145	1.69	1.00	1170	2.50	13240	0.00	16260	0.00	16260	0.00	
003	0.05	0.00	169	1.90	1.20	1200	2.80	13470	0.00	17900	0.00	17900	0.00	
004	0.07	0.00	195	2.10	1.30	1230	3.00	13720	0.00	19570	0.00	19570	0.00	
005	0.09	0.00	219	2.30	1.50	1260	3.20	14000	0.00	21280	0.00	21280	0.00	
006	0.12	0.00	242	2.50	1.60	1290	3.40	14300	0.00	23030	0.00	23030	0.00	
007	0.15	0.00	264	2.69	1.80	1320	3.60	14620	0.00	24820	0.00	24820	0.00	
008	0.19	0.00	284	2.89	1.80	1350	3.80	15000	0.00	26650	0.00	26650	0.00	
009	0.24	0.00	302	3.00	2.00	1380	4.00	15400	0.00	28530	0.00	28530	0.00	
010	0.30	0.00	318	3.20	2.00	1410	4.20	15800	0.00	30460	0.00	30460	0.00	
011	0.37	0.00	331	3.40	2.00	1440	4.40	16200	0.00	32450	0.00	32450	0.00	
012	0.45	0.00	343	3.60	2.00	1470	4.60	16600	0.00	34490	0.00	34490	0.00	
013	0.54	0.00	353	3.80	2.00	1500	4.80	17000	0.00	36590	0.00	36590	0.00	
014	0.64	0.00	361	4.00	2.00	1530	5.00	17400	0.00	38750	0.00	38750	0.00	
015	0.76	0.00	367	4.20	2.00	1560	5.20	17800	0.00	40980	0.00	40980	0.00	
016	0.89	0.00	371	4.40	2.00	1590	5.40	18200	0.00	43290	0.00	43290	0.00	
017	1.03	0.00	373	4.60	2.00	1620	5.60	18600	0.00	45680	0.00	45680	0.00	
018	1.19	0.00	373	4.80	2.00	1650	5.80	19000	0.00	48150	0.00	48150	0.00	
019	1.36	0.00	371	5.00	2.00	1680	6.00	19400	0.00	50700	0.00	50700	0.00	
020	1.54	0.00	367	5.20	2.00	1710	6.20	19800	0.00	53330	0.00	53330	0.00	
021	1.74	0.00	361	5.40	2.00	1740	6.40	20200	0.00	56050	0.00	56050	0.00	
022	1.95	0.00	353	5.60	2.00	1770	6.60	20600	0.00	58860	0.00	58860	0.00	
023	2.18	0.00	343	5.80	2.00	1800	6.80	21000	0.00	61760	0.00	61760	0.00	
024	2.43	0.00	331	6.00	2.00	1830	7.00	21400	0.00	64750	0.00	64750	0.00	
025	2.70	0.00	318	6.20	2.00	1860	7.20	21800	0.00	67830	0.00	67830	0.00	
026	3.00	0.00	302	6.40	2.00	1890	7.40	22200	0.00	71000	0.00	71000	0.00	
027	3.32	0.00	284	6.60	2.00	1920	7.60	22600	0.00	74260	0.00	74260	0.00	
028	3.67	0.00	264	6.80	2.00	1950	7.80	23000	0.00	77700	0.00	77700	0.00	
029	4.05	0.00	242	7.00	2.00	1980	8.00	23400	0.00	81330	0.00	81330	0.00	
030	4.47	0.00	219	7.20	2.00	2010	8.20	23800	0.00	85150	0.00	85150	0.00	
031	4.93	0.00	195	7.40	2.00	2040	8.40	24200	0.00	89170	0.00	89170	0.00	
032	5.43	0.00	169	7.60	2.00	2070	8.60	24600	0.00	93390	0.00	93390	0.00	
033	5.97	0.00	145	7.80	2.00	2100	8.80	25000	0.00	97820	0.00	97820	0.00	
034	6.56	0.00	120	8.00	2.00	2130	9.00	25400	0.00	102470	0.00	102470	0.00	
035	7.19	0.00	100	8.20	2.00	2160	9.20	25800	0.00	107340	0.00	107340	0.00	
036	7.87	0.00	82	8.40	2.00	2190	9.40	26200	0.00	112440	0.00	112440	0.00	
037	8.60	0.00	67	8.60	2.00	2220	9.60	26600	0.00	117770	0.00	117770	0.00	
038	9.38	0.00	55	8.80	2.00	2250	9.80	27000	0.00	123340	0.00	123340	0.00	
039	10.22	0.00	45	9.00	2.00	2280	10.00	27400	0.00	129160	0.00	129160	0.00	
040	11.12	0.00	37	9.20	2.00	2310	10.20	27800	0.00	135240	0.00	135240	0.00	
041	12.08	0.00	30	9.40	2.00	2340	10.40	28200	0.00	141590	0.00	141590	0.00	
042	13.11	0.00	24	9.60	2.00	2370	10.60	28600	0.00	148220	0.00	148220	0.00	
043	14.21	0.00	19	9.80	2.00	2400	10.80	29000	0.00	155140	0.00	155140	0.00	
044	15.39	0.00	15	10.00	2.00	2430	11.00	29400	0.00	162360	0.00	162360	0.00	
045	16.65	0.00	12	10.20	2.00	2460	11.20	29800	0.00	170000	0.00	170000	0.00	
046	18.00	0.00	9	10.40	2.00	2490	11.40	30200	0.00	178170	0.00	178170	0.00	
047	19.44	0.00	7	10.60	2.00	2520	11.60	30600	0.00	186890	0.00	186890	0.00	
048	20.98	0.00	5	10.80	2.00	2550	11.80	31000	0.00	196180	0.00	196180	0.00	
049	22.63	0.00	4	11.00	2.00	2580	12.00	31400	0.00	206060	0.00	206060	0.00	
050	24.39	0.00	3	11.20	2.00	2610	12.20	31800	0.00	216560	0.00	216560	0.00	
051	26.28	0.00	2	11.40	2.00	2640	12.40	32200	0.00	227700	0.00	227700	0.00	
052	28.30	0.00	1	11.60	2.00	2670	12.60	32600	0.00	239510	0.00	239510	0.00	
053	30.46	0.00	0	11.80	2.00	2700	12.80	33000	0.00	252030	0.00	252030	0.00	
054	32.77	0.00	0	12.00	2.00	2730	13.00	33400	0.00	265300	0.00	265300	0.00	
055	35.24	0.00	0	12.20	2.00	2760	13.20	33800	0.00	279360	0.00	279360	0.00	
056	37.88	0.00	0	12.40	2.00	2790	13.40	34200	0.00	294250	0.00	294250	0.00	
057	40.69	0.00	0	12.60	2.00	2820	13.60	34600	0.00	310000	0.00	310000	0.00	
058	43.68	0.00	0	12.80	2.00	2850	13.80	35000	0.00	326650	0.00	326650	0.00	
059	46.86	0.00	0	13.00	2.00	2880	14.00	35400	0.00	344250	0.00	344250	0.00	
060	50.24	0.00	0	13.20	2.00	2910	14.20	35800	0.00	362840	0.00	362840	0.00	
061	53.83	0.00	0	13.40	2.00	2940	14.40	36200	0.00	382470	0.00	382470	0.00	
062	57.64	0.00	0	13.60	2.00	2970	14.60	36600	0.00	403200	0.00	403200	0.00	
063	61.68	0.00	0	13.80	2.00	3000	14.80	37000	0.00	425090	0.00	425090	0.00	
064	66.06	0.00	0	14.00	2.00	3030	15.00	37400	0.00	448200	0.00	448200	0.00	
065	70.79	0.00	0	14.20	2.00	3060	15.20	37800	0.00	472590	0.00	472590	0.00	
066	75.88	0.00	0	14.40	2.00	3090	15.40	38200	0.00	498330	0.00	498330	0.00	
067	81.34	0.00	0	14.60	2.00	3120	15.60	38600	0.00	525500	0.00	525500	0.00	
068	87.18	0.00	0	14.80	2.00	3150	15.80	39000	0.00	554190	0.00	554190	0.00	
069	93.41	0.00	0	15.00	2.00	3180	16.00	39400	0.00	584490	0.00	584490	0.00	
070	100.05	0.00	0	15.20	2.00	3210	16.20	39800	0.00	616500	0.00	616500	0.00	
071	107.11	0.00	0	15.40	2.00	3240	16.40	40200	0.00	650330	0.00	650330	0.00	
072	114.61	0.00	0	15.60	2.00	3270	16.60	40600	0.00	686000	0.00	686000	0.00	
073	122.56	0.00	0	15.80	2.00	3300	16.80	41000	0.00	723640	0.00	723640	0.00	
074	130.98	0.00	0	16.00	2.00	3330	17.00	41400	0.00	763300	0.00	763300	0.00	
075	139.88	0.00	0	16.20	2.00	3360	17.20	41800	0.00	805030	0.00	805030	0.00	
076	149.28	0.00	0	16.40	2.00	3390	17.40	42200	0.00	848900	0.00	848900	0.00	
077	159.20	0.00	0	16.60	2.00	3420	17.60	42600	0.00	895000	0.00	895000	0.00	
078	169.76	0.00	0	16.80	2.00	3450	17.80	43000	0.00	943400	0.00	943400	0.00	
079	180.98	0.00	0	17.00	2.00	3480	18.00	43400	0.00	994200	0.00	994200	0.00	
080	192.88	0.00	0	17.20	2.00	3510	18.20	43800	0.00	1047600	0.00	1047600	0.00	
081	205.48	0.00	0	17.40	2.00	3540	18.40	44200	0.00	1103800	0.00	1103800	0.00	
082	218.81	0.00	0	17.60	2.00	3570	18.60	44600	0.00	1163000	0.00	1163000	0.00	
083	232.89	0.00	0	17.80	2.00	3600	18.80	45000	0.00	1225400	0.00	1225400	0.00	
084	24													

Appendix2

Modulus of rupture of Vitreous china body

Slip casting firing temperature 1150 °C

Formula	P(kg)	L(cm)	b(cm)	d(cm)	MOR(kg/cm ²)
S401	202	4.5	1.79	1.5	306.11
S402	203	4.5	1.77	1.48	306.09
S403	205	4.5	1.77	1.49	308.54
S404	205	4.5	1.78	1.49	307.45
S405	200	4.5	1.79	1.5	304.43
S501	185	4.5	1.75	1.46	295
S502	180	4.5	1.75	1.46	294.45
S503	186	4.5	1.74	1.47	292.34
S504	179	4.5	1.73	1.47	288.11
S505	183	4.5	1.73	1.46	290.12
S601	161	4.5	1.7	1.44	280.98
S602	165	4.5	1.7	1.44	283.32
S603	164	4.5	1.71	1.45	282.54
S604	169	4.5	1.7	1.44	288.56
S605	162	4.5	1.7	1.45	280.21

สถาบันวิทยบริการ
จุฬาลงกรณ์มหาวิทยาลัย

Slip casting firing temperature 1200 °C

Formula	P(kg)	L(cm)	b(cm)	d(cm)	MOR(kg/cm ²)
S401	250	4.5	1.77	1.43	466.23
S402	240	4.5	1.76	1.42	455.32
S403	245	4.5	1.77	1.43	458.14
S404	261	4.5	1.77	1.44	472.11
S405	255	4.5	1.77	1.44	455.32
S501	240	4.5	1.75	1.41	428.43
S502	243	4.5	1.75	1.41	431.45
S503	242	4.5	1.74	1.41	430.28
S504	240	4.5	1.73	1.41	422.61
S505	238	4.5	1.73	1.42	410.12
S601	225	4.5	1.7	1.4	371.23
S602	213	4.5	1.7	1.4	344.56
S603	224	4.5	1.71	1.39	369.43
S604	216	4.5	1.7	1.39	349.23
S605	220	4.5	1.7	1.39	356.23

สถาบันวิทยบริการ
จุฬาลงกรณ์มหาวิทยาลัย

Slip casting firing temperature 1250 °C

Formula	P(kg)	L(cm)	b(cm)	d(cm)	MOR(kg/cm ²)
S401	309	4.5	1.74	1.5	622.32
S402	306	4.5	1.73	1.48	624.54
S403	310	4.5	1.74	1.49	625.31
S404	315	4.5	1.73	1.49	640.23
S405	305	4.5	1.72	1.5	618.11
S501	301	4.5	1.71	1.46	601.01
S502	300	4.5	1.71	1.46	598.32
S503	298	4.5	1.71	1.47	584.32
S504	299	4.5	1.72	1.47	585.45
S505	301	4.5	1.72	1.46	599.31
S601	267	4.5	1.7	1.44	457.65
S602	265	4.5	1.7	1.44	455.54
S603	276	4.5	1.71	1.45	465.43
S604	267	4.5	1.7	1.44	462.34
S605	282	4.5	1.7	1.45	477.23

Extrude firing temperature 1150 °C

Formula	P(kg)	L(cm)	d(cm)	MOR(kg/cm ²)
SEx1	172	6.5	2.23	256.78
SEx2	170	6.5	2.2	261.21
SEx3	169	6.5	2.21	257.54
SEx4	171	6.5	2.24	254.43
SEx5	167	6.5	2.23	252.34

Extrude firing temperature 1200 °C

Formula	P(kg)	L(cm)	d(cm)	MOR(kg/cm ²)
SEx1	263	6.5	2.15	438.38
SEx2	262	6.5	2.13	441.23
SEx3	260	6.5	2.16	433.45
SEx4	265	6.5	2.16	442.12
SEx5	261	6.5	2.15	431.43

Extrude firing temperature 1250 °C

Formula	P(kg)	L(cm)	d(cm)	MOR(kg/cm ²)
SEx1	275	6.5	2.11	535.32
SEx2	278	6.5	2.11	541.23
SEx3	279	6.5	2.12	540.11
SEx4	281	6.5	2.11	544.34
SEx5	269	6.5	2.12	534.43

สถาบันวิทยบริการ
จุฬาลงกรณ์มหาวิทยาลัย

Pressing firing temperature 1150 °C

Formula	P(kg)	L(cm)	b(cm)	d(cm)	MOR(kg/cm ²)
P501	87	6.5	4.74	0.7	193.34
P502	85	6.5	4.73	0.71	195.43
P503	86	6.5	4.73	0.71	194.43
P504	89	6.5	4.74	0.69	198.32
P505	84	6.5	4.74	0.7	192.12
P1001	93	6.5	4.84	0.68	225.11
P1002	95	6.5	4.82	0.68	223.21
P1003	91	6.5	4.83	0.67	225.34
P1004	89	6.5	4.82	0.68	222.67
P1005	90	6.5	4.82	0.67	227.76
P1501	98	6.5	4.97	0.67	378.43
P1502	99	6.5	4.98	0.66	375.67
P1503	102	6.5	4.97	0.66	377.76
P1504	100	6.5	4.98	0.67	374.32
P1505	99	6.5	4.97	0.66	373.45

สถาบันวิทยบริการ
จุฬาลงกรณ์มหาวิทยาลัย

Pressing firing temperature 1200 °C

Formula	P(kg)	L(cm)	b(cm)	d(cm)	MOR(kg/cm ²)
P501	37	6.5	4.52	0.46	397.76
P502	38	6.5	4.53	0.45	398.65
P503	35	6.5	4.55	0.46	397.65
P504	35	6.5	4.54	0.46	399.78
P505	36	6.5	4.53	0.45	399.02
P1001	55	6.5	4.52	0.46	567.11
P1002	54	6.5	4.53	0.45	566.43
P1003	60	6.5	4.55	0.46	571.11
P1004	61	6.5	4.54	0.45	559.2
P1005	52	6.5	4.53	0.46	558.75
P1501	55	6.5	4.64	0.43	567.76
P1502	56	6.5	4.62	0.44	573.43
P1503	57	6.5	4.62	0.43	576.55
P1504	55	6.5	4.61	0.42	571.23
P1505	56	6.5	4.63	0.42	574.32

สถาบันวิทยบริการ
จุฬาลงกรณ์มหาวิทยาลัย

Pressing firing temperature 1250 °C

Formula	P(kg)	L(cm)	b(cm)	d(cm)	MOR(kg/cm ²)
P501	37	6.5	4.52	0.46	475.55
P502	38	6.5	4.53	0.45	476.54
P503	35	6.5	4.55	0.46	475.43
P504	35	6.5	4.54	0.46	477.89
P505	36	6.5	4.53	0.45	477.98
P1001	55	6.5	4.52	0.46	570.34
P1002	54	6.5	4.53	0.45	571.33
P1003	60	6.5	4.55	0.46	565.67
P1004	61	6.5	4.54	0.45	564.54
P1005	52	6.5	4.53	0.46	566.32
P1501	55	6.5	4.64	0.43	573.43
P1502	56	6.5	4.62	0.44	573.78
P1503	57	6.5	4.62	0.43	577.43
P1504	55	6.5	4.61	0.42	575.65
P1505	56	6.5	4.63	0.42	574.32

สถาบันวิทยบริการ
จุฬาลงกรณ์มหาวิทยาลัย

Modulus of rupture of Porcelain body

Slip casting firing temperature 1150 °C

Formula	P(kg)	L(cm)	b(cm)	d(cm)	MOR(kg/cm ²)
S401	250	4.5	1.77	1.43	433.56
S402	240	4.5	1.76	1.42	440.21
S403	245	4.5	1.77	1.43	440.43
S404	261	4.5	1.77	1.44	438.54
S405	255	4.5	1.77	1.44	436.65
S501	240	4.5	1.75	1.41	367.76
S502	243	4.5	1.75	1.41	368.87
S503	242	4.5	1.74	1.41	370.43
S504	240	4.5	1.73	1.41	365.65
S505	238	4.5	1.73	1.42	368.76
S601	225	4.5	1.7	1.4	355.54
S602	213	4.5	1.7	1.4	354.32
S603	224	4.5	1.71	1.39	354.21
S604	216	4.5	1.7	1.39	355.65
S605	220	4.5	1.7	1.39	356.23

สถาบันวิทยบริการ
จุฬาลงกรณ์มหาวิทยาลัย

Slip casting firing temperature 1200 °C

Formula	P(kg)	L(cm)	b(cm)	d(cm)	MOR(kg/cm ²)
S401	291	4.5	1.77	1.43	515.54
S402	293	4.5	1.76	1.42	523.32
S403	292	4.5	1.77	1.43	524.45
S404	294	4.5	1.77	1.44	521.23
S405	293	4.5	1.77	1.44	521.11
S501	282	4.5	1.75	1.41	506.65
S502	281	4.5	1.75	1.41	507.65
S503	279	4.5	1.74	1.41	508.61
S504	277	4.5	1.73	1.41	503.45
S505	279	4.5	1.73	1.42	504.31
S601	265	4.5	1.7	1.4	476.65
S602	263	4.5	1.7	1.4	475.54
S603	259	4.5	1.71	1.39	478.94
S604	263	4.5	1.7	1.39	478.12
S605	261	4.5	1.7	1.39	481.21

สถาบันวิทยบริการ
จุฬาลงกรณ์มหาวิทยาลัย

Slip casting firing temperature 1250 °C

Formula	P(kg)	L(cm)	b(cm)	d(cm)	MOR(kg/cm ²)
S401	291	4.5	1.77	1.4	709.15
S402	293	4.5	1.76	1.4	711.32
S403	292	4.5	1.77	1.4	706.54
S404	294	4.5	1.77	1.39	704.34
S405	293	4.5	1.77	1.4	707.43
S501	282	4.5	1.75	1.41	688.34
S502	281	4.5	1.75	1.41	689.54
S503	279	4.5	1.74	1.41	678.65
S504	277	4.5	1.73	1.41	677.64
S505	279	4.5	1.73	1.42	680.33
S601	265	4.5	1.7	1.4	593.32
S602	263	4.5	1.7	1.4	590.11
S603	259	4.5	1.71	1.39	587.65
S604	263	4.5	1.7	1.39	586.76
S605	261	4.5	1.7	1.39	589.43

Extrude firing temperature 1150 °C

Formula	P(kg)	L(cm)	d(cm)	MOR(kg/cm ²)
PEx1	187	6.5	2.23	451.11
PEx2	185	6.5	2.2	455.65
PEx3	189	6.5	2.21	456.54
PEx4	188	6.5	2.24	452.13
PEx5	184	6.5	2.23	450.11

Extrude firing temperature 1200 °C

Formula	P(kg)	L(cm)	d(cm)	MOR(kg/cm ²)
PEx1	201	6.5	2.2	755.43
PEx2	200	6.5	2.2	756.87
PEx3	199	6.5	2.21	759.78
PEx4	197	6.5	2.2	749.43
PEx5	203	6.5	2.19	755.11

Extrude firing temperature 1250 °C

Formula	P(kg)	L(cm)	d(cm)	MOR(kg/cm ²)
PEx1	202	6.5	2.19	751.21
PEx2	200	6.5	2.19	752.34
PEx3	189	6.5	2.2	747.65
PEx4	188	6.5	2.2	749.61
PEx5	199	6.5	2.19	751.12

สถาบันวิทยบริการ
จุฬาลงกรณ์มหาวิทยาลัย

Pressing firing temperature 1150 °C

Formula	P(kg)	L(cm)	b(cm)	d(cm)	MOR(kg/cm ²)
P501	87	6.5	4.74	0.7	181.23
P502	85	6.5	4.73	0.71	179.34
P503	86	6.5	4.73	0.71	182.45
P504	89	6.5	4.74	0.69	183.43
P505	84	6.5	4.74	0.7	177.59
P1001	93	6.5	4.84	0.68	257.78
P1002	95	6.5	4.82	0.68	259.89
P1003	91	6.5	4.83	0.67	254.43
P1004	89	6.5	4.82	0.68	252.11
P1005	90	6.5	4.82	0.67	255.76
P1501	98	6.5	4.97	0.67	442.11
P1502	99	6.5	4.98	0.66	443.54
P1503	102	6.5	4.97	0.66	438.87
P1504	100	6.5	4.98	0.67	439.76
P1505	99	6.5	4.97	0.66	440.42

สถาบันวิทยบริการ
จุฬาลงกรณ์มหาวิทยาลัย

Pressing firing temperature 1200 °C

Formula	P(kg)	L(cm)	b(cm)	d(cm)	MOR(kg/cm ²)
P501	92	6.5	4.74	0.7	304.54
P502	91	6.5	4.73	0.71	305.54
P503	90	6.5	4.73	0.71	301.23
P504	89	6.5	4.74	0.69	306.54
P505	92	6.5	4.74	0.7	307.55
P1001	93	6.5	4.84	0.65	641.22
P1002	95	6.5	4.82	0.65	643.23
P1003	91	6.5	4.83	0.65	643.21
P1004	89	6.5	4.82	0.66	638.76
P1005	90	6.5	4.82	0.65	639.87
P1501	98	6.5	4.97	0.65	746.54
P1502	99	6.5	4.98	0.63	743.43
P1503	102	6.5	4.97	0.63	734.55
P1504	100	6.5	4.98	0.63	732.11
P1505	99	6.5	4.97	0.63	739.76

สถาบันวิทยบริการ
จุฬาลงกรณ์มหาวิทยาลัย

Pressing firing temperature 1250 °C

Formula	P(kg)	L(cm)	b(cm)	d(cm)	MOR(kg/cm ²)
P501	87	6.5	4.74	0.7	731.11
P502	85	6.5	4.73	0.71	734.32
P503	86	6.5	4.73	0.71	731.45
P504	89	6.5	4.74	0.69	727.87
P505	84	6.5	4.74	0.7	729.87
P1001	93	6.5	4.84	0.68	741.23
P1002	95	6.5	4.82	0.68	743.43
P1003	91	6.5	4.83	0.67	730.34
P1004	89	6.5	4.82	0.68	735.45
P1005	90	6.5	4.82	0.67	740.54
P1501	98	6.5	4.97	0.67	739.55
P1502	99	6.5	4.98	0.66	734.54
P1503	102	6.5	4.97	0.66	738.87
P1504	100	6.5	4.98	0.67	743.32
P1505	99	6.5	4.97	0.66	741.23

สถาบันวิทยบริการ
จุฬาลงกรณ์มหาวิทยาลัย

Modulus of rupture of Stone ware body

Slip casting firing temperature 1100 °C

Formula	P(kg)	L(cm)	b(cm)	d(cm)	MOR(kg/cm ²)
S401	168	4.5	1.77	1.43	249.21
S402	170	4.5	1.76	1.42	248.67
S403	165	4.5	1.77	1.43	250.87
S404	167	4.5	1.77	1.44	251.21
S405	164	4.5	1.77	1.44	250.43
S501	160	4.5	1.75	1.41	221.12
S502	157	4.5	1.75	1.41	221.34
S503	155	4.5	1.74	1.41	223.54
S504	157	4.5	1.73	1.41	225.43
S505	154	4.5	1.73	1.42	224.67
S601	146	4.5	1.7	1.4	217.78
S602	147	4.5	1.7	1.4	216.74
S603	146	4.5	1.71	1.39	219.79
S604	148	4.5	1.7	1.39	220.11
S605	146	4.5	1.7	1.39	218.54

สถาบันวิทยบริการ
จุฬาลงกรณ์มหาวิทยาลัย

Slip casting firing temperature 1150 °C

Formula	P(kg)	L(cm)	b(cm)	d(cm)	MOR(kg/cm ²)
S401	187	4.5	1.77	1.43	477.56
S402	188	4.5	1.76	1.42	479.78
S403	178	4.5	1.77	1.43	475.64
S404	179	4.5	1.77	1.44	473.43
S405	181	4.5	1.77	1.44	481.23
S501	160	4.5	1.75	1.41	315.67
S502	157	4.5	1.75	1.41	316.78
S503	155	4.5	1.74	1.41	318.74
S504	157	4.5	1.73	1.41	315.4
S505	154	4.5	1.73	1.42	316.98
S601	146	4.5	1.7	1.4	217.78
S602	147	4.5	1.7	1.4	216.74
S603	146	4.5	1.71	1.39	212.34
S604	148	4.5	1.7	1.39	214.32
S605	146	4.5	1.7	1.39	215.43

สถาบันวิทยบริการ
จุฬาลงกรณ์มหาวิทยาลัย

Slip casting firing temperature 1200 °C

Formula	P(kg)	L(cm)	b(cm)	d(cm)	MOR(kg/cm ²)
S401	21	4.5	2.01	1.67	15.55
S402	19	4.5	2	1.65	16.76
S403	20	4.5	1.99	1.67	16.78
S404	16	4.5	2	1.65	15.43
S405	17	4.5	1.98	1.65	14.65
S501	18	4.5	1.99	1.65	15.76
S502	19	4.5	1.99	1.76	16.78
S503	20	4.5	2	1.68	16.54
S504	16	4.5	2.01	1.67	15.43
S505	17	4.5	2.02	1.7	16.11
S601	18	4.5	1.99	1.67	17.76
S602	19	4.5	1.99	1.68	17.65
S603	21	4.5	1.98	1.67	15.78
S604	18	4.5	2	1.7	16.11
S605	19	4.5	2	1.69	16.54

Extrude firing temperature 1100 °C

Formula	P(kg)	L(cm)	d(cm)	MOR(kg/cm ²)
FEx1	187	6.5	2.23	373.21
FEx2	185	6.5	2.2	370.12
FEx3	189	6.5	2.21	375.43
FEx4	188	6.5	2.24	373.11
FEx5	184	6.5	2.23	372.12

Extrude firing temperature 1150 °C

Formula	P(kg)	L(cm)	d(cm)	MOR(kg/cm ²)
FEx1	185	6.5	2.23	364.43
FEx2	185	6.5	2.21	365.56
FEx3	189	6.5	2.2	371.12
FEx4	188	6.5	2.24	357.76
FEx5	184	6.5	2.23	364.34

Extrude firing temperature 1200 °C

Formula	P(kg)	L(cm)	d(cm)	MOR(kg/cm ²)
FEx1	21	6.5	2.66	16.76
FEx2	23	6.5	2.64	17.87
FEx3	18	6.5	2.65	18.76
FEx4	19	6.5	2.63	15.69
FEx5	20	6.5	2.67	16.89

สถาบันวิทยบริการ
จุฬาลงกรณ์มหาวิทยาลัย

Modulus of rupture of Earthen ware body

Slip casting firing temperature 1050 °C

Formula	P(kg)	L(cm)	b(cm)	d(cm)	MOR(kg/cm ²)
S401	120	4.5	1.97	1.43	105.65
S402	121	4.5	1.98	1.42	107.67
S403	123	4.5	1.95	1.43	105.34
S404	121	4.5	1.97	1.44	108.76
S405	123	4.5	1.97	1.44	107.12
S501	114	4.5	1.95	1.41	88.78
S502	112	4.5	1.96	1.41	88.34
S503	113	4.5	1.95	1.41	87.34
S504	116	4.5	1.96	1.41	85.64
S505	111	4.5	1.96	1.42	85.41
S601	94	4.5	1.97	1.4	52.23
S602	98	4.5	1.95	1.4	51.87
S603	95	4.5	1.95	1.39	49.89
S604	91	4.5	1.95	1.39	49.73
S605	94	4.5	1.96	1.39	50.21

สถาบันวิทยบริการ
จุฬาลงกรณ์มหาวิทยาลัย

Slip casting firing temperature 1100 °C

Formula	P(kg)	L(cm)	b(cm)	d(cm)	MOR(kg/cm ²)
S401	120	4.5	1.97	1.43	128.23
S402	121	4.5	1.98	1.42	124.54
S403	123	4.5	1.95	1.43	125.65
S404	121	4.5	1.97	1.44	132.11
S405	123	4.5	1.97	1.44	127.89
S501	114	4.5	1.95	1.41	121.22
S502	112	4.5	1.96	1.41	122.12
S503	113	4.5	1.95	1.41	117.78
S504	116	4.5	1.96	1.41	118.98
S505	111	4.5	1.96	1.42	119.65
S601	94	4.5	1.97	1.4	113.45
S602	98	4.5	1.95	1.4	115.43
S603	95	4.5	1.95	1.39	112.56
S604	91	4.5	1.95	1.39	117.65
S605	94	4.5	1.96	1.39	116.54

สถาบันวิทยบริการ
จุฬาลงกรณ์มหาวิทยาลัย

Slip casting firing temperature 1150 °C

Formula	P(kg)	L(cm)	b(cm)	d(cm)	MOR(kg/cm ²)
S401	120	4.5	1.97	1.43	218.87
S402	121	4.5	1.98	1.42	217.65
S403	123	4.5	1.95	1.43	216.54
S404	121	4.5	1.97	1.44	215.45
S405	123	4.5	1.97	1.44	213.43
S501	114	4.5	1.95	1.41	134.54
S502	112	4.5	1.96	1.41	126.76
S503	113	4.5	1.95	1.41	128.78
S504	116	4.5	1.96	1.41	129.76
S505	111	4.5	1.96	1.42	134.32
S601	94	4.5	1.97	1.4	125.56
S602	98	4.5	1.95	1.4	124.34
S603	95	4.5	1.95	1.39	128.98
S604	91	4.5	1.95	1.39	132.43
S605	94	4.5	1.96	1.39	131.04

Extrude firing temperature 1050 °C

Formula	P(kg)	L(cm)	d(cm)	MOR(kg/cm ²)
WEx1	165	6.5	2.23	198.23
WEx2	163	6.5	2.2	199.23
WEx3	168	6.5	2.21	197.14
WEx4	164	6.5	2.24	196.67
WEx5	168	6.5	2.23	198.45

Extrude firing temperature 1100 °C

Formula	P(kg)	L(cm)	d(cm)	MOR(kg/cm ²)
WEx1	165	6.5	2.23	225.34
WEx2	163	6.5	2.2	223.43
WEx3	168	6.5	2.21	227.67
WEx4	164	6.5	2.24	218.67
WEx5	168	6.5	2.23	229.41

Extrude firing temperature 1100 °C

Formula	P(kg)	L(cm)	d(cm)	MOR(kg/cm ²)
WEx1	165	6.5	2.23	244.45
WEx2	163	6.5	2.2	243.21
WEx3	168	6.5	2.21	247.45
WEx4	164	6.5	2.24	236.65
WEx5	168	6.5	2.23	238.92

สถาบันวิทยบริการ
จุฬาลงกรณ์มหาวิทยาลัย

Modulus of rupture of Terracotta body

Pressing firing temperature 950 °C

Formula	P(kg)	L(cm)	b(cm)	d(cm)	MOR(kg/cm ²)
P501	25	6.5	4.74	0.7	31.34
P502	23	6.5	4.73	0.71	32.45
P503	24	6.5	4.73	0.71	30.23
P504	23	6.5	4.74	0.69	26.78
P505	24	6.5	4.74	0.7	34.54
P1001	26	6.5	4.84	0.68	33.45
P1002	23	6.5	4.82	0.68	30.23
P1003	21	6.5	4.83	0.67	28.89
P1004	20	6.5	4.82	0.68	34.54
P1005	23	6.5	4.82	0.67	32.11
P1501	24	6.5	4.97	0.67	33.45
P1502	26	6.5	4.98	0.66	36.65
P1503	24	6.5	4.97	0.66	31.23
P1504	25	6.5	4.98	0.67	36.78
P1505	23	6.5	4.97	0.66	29.76

สถาบันวิทยบริการ
จุฬาลงกรณ์มหาวิทยาลัย

Pressing firing temperature 1000 °C

Formula	P(kg)	L(cm)	b(cm)	d(cm)	MOR(kg/cm ²)
P501	25	6.5	4.74	0.7	37.12
P502	23	6.5	4.73	0.71	34.56
P503	24	6.5	4.73	0.71	41.23
P504	23	6.5	4.74	0.69	35.65
P505	24	6.5	4.74	0.7	32.34
P1001	26	6.5	4.84	0.68	39.87
P1002	23	6.5	4.82	0.68	44.32
P1003	21	6.5	4.83	0.67	45.43
P1004	20	6.5	4.82	0.68	34.56
P1005	23	6.5	4.82	0.67	38.76
P1501	24	6.5	4.97	0.67	41.21
P1502	26	6.5	4.98	0.66	43.53
P1503	24	6.5	4.97	0.66	44.56
P1504	25	6.5	4.98	0.67	46.54
P1505	23	6.5	4.97	0.66	41.23

สถาบันวิทยบริการ
จุฬาลงกรณ์มหาวิทยาลัย

Pressing firing temperature 1050 °C

Formula	P(kg)	L(cm)	b(cm)	d(cm)	MOR(kg/cm ²)
P501	31	6.5	4.74	0.7	54.43
P502	32	6.5	4.73	0.71	52.32
P503	30	6.5	4.73	0.71	53.21
P504	32	6.5	4.74	0.69	56.76
P505	32	6.5	4.74	0.7	46.78
P1001	55	6.5	4.84	0.68	108.78
P1002	45	6.5	4.82	0.68	105.45
P1003	51	6.5	4.83	0.67	107.65
P1004	47	6.5	4.82	0.68	106.43
P1005	49	6.5	4.82	0.67	106.45
P1501	65	6.5	4.97	0.67	128.98
P1502	64	6.5	4.98	0.66	132.42
P1503	67	6.5	4.97	0.66	133.23
P1504	61	6.5	4.98	0.67	130.11
P1505	58	6.5	4.97	0.66	126.78

Extrude firing temperature 950 °C

Formula	P(kg)	L(cm)	d(cm)	MOR(kg/cm ²)
TEx1	134	6.5	2.23	111.23
TEx2	136	6.5	2.2	110.89
TEx3	131	6.5	2.21	109.87
TEx4	131	6.5	2.24	108.65
TEx5	132	6.5	2.23	109.99

Extrude firing temperature 1000 °C

Formula	P(kg)	L(cm)	d(cm)	MOR(kg/cm ²)
TEx1	105	6.5	2.23	148.89
TEx2	102	6.5	2.2	154.43
TEx3	104	6.5	2.21	151.23
TEx4	106	6.5	2.24	153.45
TEx5	103	6.5	2.23	151.23

Extrude firing temperature 1000 °C

Formula	P(kg)	L(cm)	d(cm)	MOR(kg/cm ²)
TEx1	112	6.5	2.23	180.54
TEx2	113	6.5	2.2	181.23
TEx3	115	6.5	2.21	176.78
TEx4	111	6.5	2.24	178.9
TEx5	115	6.5	2.23	175.45

สถาบันวิทยบริการ
จุฬาลงกรณ์มหาวิทยาลัย

Appendix3

Bulk density and water absorption

Vitreous china body

Slip casting firing temperature 1150 °C

Formula	w2	w3	w1	w3-w2	Bulk density	%water absorption
S40-1	0.9838	1.6654	1.4392	0.6816	2.06	8.05
S40-2	0.9811	1.6646	1.4385	0.6835	2.05	8.00
S40-3	0.9766	1.6632	1.4371	0.6866	2.05	8.01
S50-1	0.9968	1.6579	1.4580	0.6611	2.02	9.51
S50-2	0.9971	1.6584	1.4585	0.6613	2.02	9.45
S50-3	0.9965	1.6574	1.4566	0.6609	2.02	9.48
S60-1	0.9837	1.6242	1.4376	0.6405	2.00	10.34
S60-2	0.9856	1.6251	1.4379	0.6395	1.99	10.36
S60-3	0.9901	1.6266	1.4388	0.6365	1.99	10.25

Slip casting firing temperature 1200 °C

Formula	w2	w3	w1	w3-w2	Bulk density	%water absorption
S40-1	0.9838	1.6843	1.4543	0.4816	2.22	3.05
S40-2	0.9811	1.6646	1.4385	0.6835	2.22	3.00
S40-3	0.9766	1.6632	1.4371	0.6866	2.22	3.02
S50-1	0.9968	1.6579	1.4580	0.6611	2.17	3.66
S50-2	0.9971	1.6584	1.4585	0.6613	2.19	3.70
S50-3	0.9965	1.6574	1.4566	0.6609	2.18	3.61
S60-1	0.9837	1.6242	1.4376	0.6405	2.16	3.63
S60-2	0.9856	1.6251	1.4379	0.6395	2.15	3.67
S60-3	0.9901	1.6266	1.4388	0.6365	2.16	3.64

Slip casting firing temperature 1250 °C

Formula	w2	w3	w1	w3-w2	Bulk density	%water absorption
S40-1	0.9838	1.6654	1.4392	0.6816	2.40	0.09
S40-2	0.9811	1.6646	1.4385	0.6835	2.42	0.11
S40-3	0.9766	1.6632	1.4371	0.6866	2.41	0.08
S50-1	0.9968	1.6579	1.4580	0.6611	2.38	0.23
S50-2	0.9971	1.6584	1.4585	0.6613	2.38	0.21
S50-3	0.9965	1.6574	1.4566	0.6609	2.37	0.22
S60-1	0.9837	1.6242	1.4376	0.6405	2.33	0.23
S60-2	0.9856	1.6251	1.4379	0.6395	2.33	0.21
S60-3	0.9901	1.6266	1.4388	0.6365	2.33	0.21

Extrude firing temperature 1150 °C

Formula	w2	w3	w1	w3-w2	Bulk density	%water absorption
SEX-1	0.9834	1.6543	1.4392	0.6816	2.05	7.29
SEX-2	0.9854	1.6532	1.4385	0.6835	2.04	7.24
SEX-3	0.9743	1.6543	1.4371	0.6866	2.05	7.22

Extrude firing temperature 1200 °C

Formula	w2	w3	w1	w3-w2	Bulk density	%water absorption
SEX-1	0.9754	1.6543	1.4561	0.6816	2.23	1.79
SEX-2	0.9754	1.6532	1.4558	0.6835	2.23	1.81
SEX-3	0.9752	1.6543	1.4562	0.6866	2.23	1.77

Extrude firing temperature 1250 °C

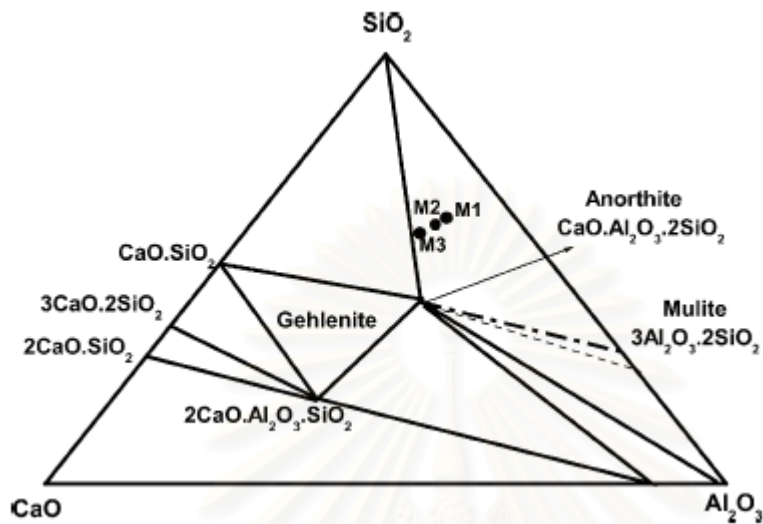
Formula	w2	w3	w1	w3-w2	Bulk density	%water absorption
SEX-1	0.9754	1.6543	1.4561	0.6816	2.39	0.59
SEX-2	0.9754	1.6532	1.4558	0.6835	2.38	0.55
SEX-3	0.9752	1.6543	1.4562	0.6866	2.39	0.61



สถาบันวิทยบริการ
จุฬาลงกรณ์มหาวิทยาลัย

Appendix 6

The ternary phase diagram of SiO_2 - CaO - Al_2O_3



สถาบันวิทยบริการ
จุฬาลงกรณ์มหาวิทยาลัย

VITA

Mr. Kachin Saiintawong was born on the 9th of March 1968, in Bangkok. After graduation with a Bachelor Degree in Ceramic and Materials Science from Faculty of Science, Chulalongkorn University in 1992, he joined Thai Ceramic Company, an incorporated company of Siam Cement Group, until 2001. He graduated in Master Degree course in Ceramic Technology, Faculty of Science, Chulalongkorn University in June 2004.



สถาบันวิทยบริการ
จุฬาลงกรณ์มหาวิทยาลัย